Laser Excitation ESR Studies on Laser Dyes

By

Mikio YAMASHITA

Chapter 1 General Introduction

1-1 Organic Dyes as Laser Materials and in Photochemical Reactions

Since the first successful operation of a laser was achieved in a pink ruby crystal by Maiman in 1960[1], many kinds of lasers have been developed by making use of insulating solids, semiconductors, liquids, and gases, which are based on a great many basic spectroscopic-studies in physics and chemistry over the years. Lasers have now been demonstrated with peak powers exceeding terawatts, average powers in excess of 60 kilowatts, pulse durations less than one picosecond, frequency stabilities in the one part in 10^{14} range, efficiencies in exess of 60 percent, and operating wavelengths from the submillimeter waves down into the vacuum ultra-violet range[2]. The applications of the lasers extend over the interdiscipline among many branches of science and technology including nuclear fusion, isotopic separation, photochemistry, nonlinear optics, information transmission and processing, spectroscopy, and biophysics.

The dye lasers, which were first obtained as a class of liquid lasers in 1966, always have fairly complex organic molecules as their active species[3]. Unlike the other laser substances, they have the chemical aspects that there exist a larger number of commercially available chemicals and one is easily able to synthesize new special dyes. In addition, the organic dyes have much wider fluorescence bands in the visible region and the lifetime of the upper level is 10^4 to 10^6 times shorter than typical metastable upper level lifetimes of the other fixed-frequency laser materials. The broad fluorescence band enables coherent light to be generated over wide range of frequencies. The tunable light sources of high spectral brightness are presently available for many research and spectroscopy utilization requiring selective optical excitation[4].

However, the usefulness of the dye lasers, particularlly the continuous wave, plastic, and nonflowing-system dye lasers, is limitted by the relatively low efficiency and chemical-stability which are due to the spectroscopic and photochemical properties in dye molecules themselves, respectively. For example, the accumulation of the molecules in the metastable lowest triplet state (T_1 state) plays a major role in determing the efficiency of the dye

laser[5]. The photodegradation (which is also called photobleaching or photodeterioration) of laser dyes under optical excitation increases rapidly the threshold energy of the laser oscillation and shortens seriously the lifetime of the laser[6]. As will be described in the sections 3-1 and 4-1, several efforts have been made to overcome those disadvantages. Now that a few thousands of commercial dyes were screened[7] and the synthesis of new special dyes is planned, the rules for the selection or synthesis of useful laser dyes should be found out. However, spectroscopic and photochemical investigation on organic dyes available for the purpose was scarcely performed so far. It is now necessary to gain some insight into the relation between the molecular structure and the relaxation or the photodegradation mechanisms of organic dyes excited by a high-intensity flashlamp or a laser.

Since about ten years before the first laser appeared, many studies on organic dyes have been performed in photochemistry and biophysics, by using optical spectroscopy, ESR, and flash photolysis techniques[8)~10]. Optical absorption by organic dyes is caused not only by a series of physical effects but also by a series of chemical effects where an excited state is more reactive than the normally occupied ground state. For example, the excitation energy can be converted into chemical energy by dissociation, intramolecular rearrangement, reduction or oxidation processes with neighbor molecules, or any other photochemical reactions. In addition, the absorbed energy may be transferred to another molecule which is excited by this energy-transfer process and is ready for photophysical and photochemical reactions such as photosensitization, quenching, or photocatalysis. These effects essential to many forms of life are often encountered in nature. For example there should be mentioned the process of vision in the eye, the process of assimilation in plants (photosynthesis), the processes that involve damage in biological metabolism and genetic information by radiation, the dye-sensitized phototendering and photodegradation of textiles, and photography. From these examples we see that many important processes can be initiated by the illuminations of dyes.

By the study of the photochemistry of dyes in solution our knowledge of the photochemical behavior of dyes has considerably increased. Above all, it should be noted that in the primary steps of these processes in many photochemical reactions of organic compounds in solution the formation of the T_1 state with a long lifetime is decisive[11),12]. But it should not be overlooked that the complexity of the systems and the different variables affecting the reaction process have brought about many difficulties for the elucidation of a detailed mechanism of the reactions. Therefore, a good knowledge is needed on the physical properties of the excited states, especially the T_1 state, of the dye molecules including quantitative information concerning the rate constants of a number of processes involved. Among them, the determination of a singlet-to-triplet intesystem crossing rate constant K_{ST} is the key to evaluation of many of the other rate constants for the complex photochemical processes of the substance, but it is difficult because of the so-called dark process[13].

1-2 Properties of Laser Dyes

1-2-1 Molecular Structure

Today several hundreds of dyes are reported as laser active materials[14]. Their organic dyes are broadly divided into the five classes by the structure, that is, polymethine (or cyanine), oxazine, xanthene and acridine, coumarin, and scintillator classes, which oscillate in the wavelength region from 720 to 1175 nm, from 615 to 750 nm, from 461 to 656 nm, from 391 to 567 nm, and from 330 to 437 nm, respectively. The molecular structure of the typical dye belonging to each class is shown in **Fig. 1-1**[14)~16)]. Our discussion in this thesis is confined to xanthene and acridine class of dyes whice are the most widely employed as laser materials among them at the present time. This class of organic dyes is characterized by rings with one or more carbon atoms replaced by oxygen or nitrogen atoms, which are called as a chromophore, and are classified into rhodamine, fluorescein, and acridine types by the number of their oxygen or nitrogen atoms, as shown in **Fig. 1-2**. In addition, the aromatic heterocyclic compounds have the so-called auxochromic

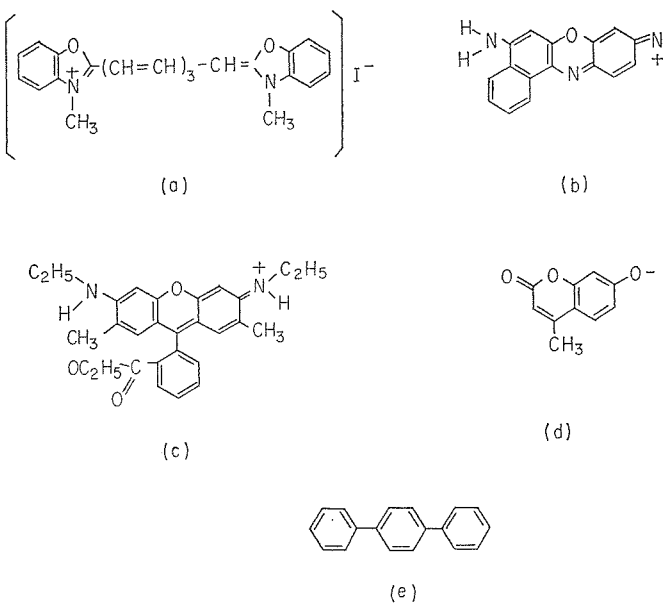

Fig. 1-1 Molecular structure of typical laser dyes belonging to different classes.
(a) polymethine (or cyanine) class of 3, 3-dimethyloxatricarbocyanine iodide.
(b) oxazine class of cresyl violet (oxazine 9).
(c) xanthene and acridine class of rhodamine 6 G.
(d) coumarin class of 4-methlumbelliferone (coumarin 4).
(e) scintillator class of p-terphenyl.

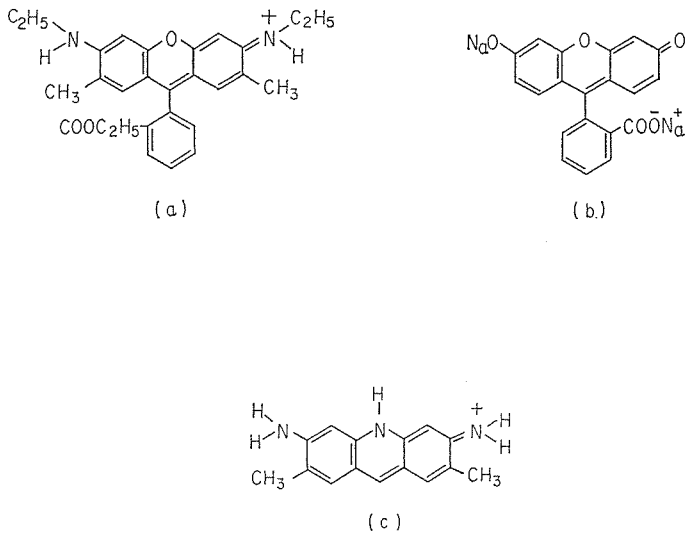

Fig. 1-2 Molecular structure of typical laser dyes belonging to xanthene and acridine class.
(a) rhodamine type (type R) of rhodamine 6G (R6G).
(b) fluorescein type (type F) of fluorescein disodium salt (FDS).
(c) acridine type (type A) of acridine yellow (AY).

groups such as methyl, ethyl, amino, or phenyl attached to the rings at various positions, and their total molecular weight is ranging from 200 to 500. A strong absorption in the visible region, characterizing organic dyes, is found only in organic compounds which contain an extended system of conjugated bonds, i. e., alternating single and double bonds. The absorption by organic molecules takes place along a preferred direction within the molecular flame. The absorbing electronic transition moment, whose direction determines the polarization of the absorption band, corresponds to each electronic absorption band. In other words, the substitution with the auxochrome intensifies all the absorption bands that have their corresponding transition moments located in the direction of the substituent (hyperchromic effect) and cause a red shift (bathochromic effect)[17].

1-2-2 Energy Levels

All lasing organic molecules have a similar characteristic set of energy levels. The energy levels of organic dyes can be understood on a semiquantitative basis if we take a highly simplified quantum-mechanical model such as the free-electron gas model[18),19]. Since most stable compounds have an even number of electrons n in the ground state of the dye molecules, which in the model is the state with the $n/2$ lowest levels filled, the spins of two electrons occupying the same level are necessarily antiparallel, as required by the Pauli exclusion principle. When the molecule become electronically excited, however, the spin orientation of the excited electron is not restricted by the Pauli principle, so that the exited states with antiparallel spin (singlet state) and parallel spin (triplet state) exist. As illustrated in **Fig. 1-3**, S_0 is the singlet ground state and S_1 and S_2 are singlet

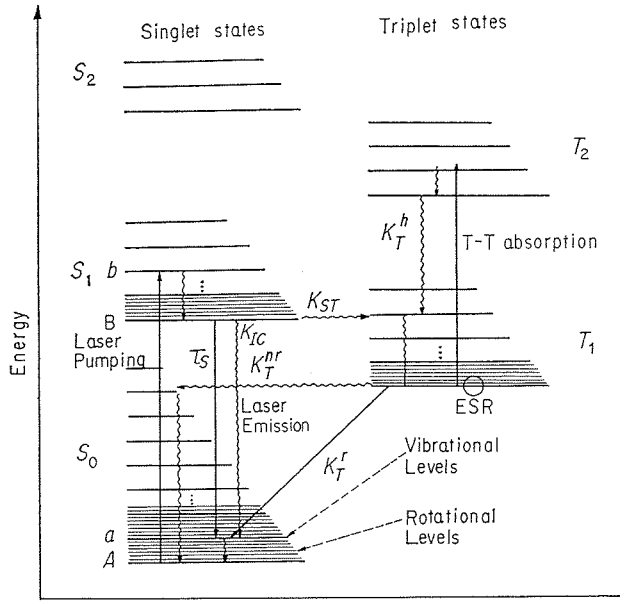

Fig. 1-3 Schematic energy-level diagram of a typical organic laser-dye molecule.

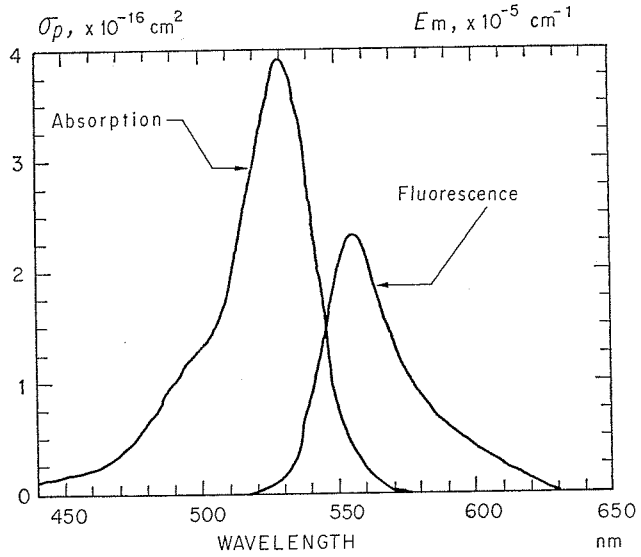

Fig. 1-4 Singlet-state absorption and fluorescence spectra of R6G, measured from a 10^{-4} M solution of the dye. The emission spectrum is normalized so that $\int_0^\infty Em(\lambda)d\lambda = 0.83 = q$[29].

excited electronic states, whereas T_1 and T_2 represent triplet excited electronic states.

The ground and excited states of a molecule are also characterized by quantized vibrational and rotational levels. The average vibrational-level separation of dye molecules

lies in the range 1200～1600 cm^{-1} [20),22)]. Usually, for the compounds, the 0, 0 band of the electronic absorption transition $S_1 \leftarrow S_0$ is the most intense, and the fluorescence is a good mirror image of the $S_1 \leftarrow S_0$ absorption spectrum as shown in **Fig. 1-4**[21)]. Franck-Condon considerations which are made in the section 3-3-2, therefore, indicate that the potential energy curves of S_1 and S_0 states are of similar shapes. The large size and mass of an organic lasing molecule means the rotational levels are very closely spaced, with an energy separation of less than 1/100 of the vibrational levels. The thermal energy fluctuations of the solvent molecules at 77 K are about kT or 60 cm^{-1}, which smear the rotational levels into a continuum and account for the smmoothness of the broad absorption and emmission bands of a laser dye molecule.

The lowest energy excited electronic state of such compounds is usually a triplet state because the differenue in the sign of the linear combination of the space part of the two one-electron wavefunctions gives rise to a value for the energy of the triplet state which is lower than that for the singlet state of the same electron configuration, as required by the Hund's multiplicity rule. The S_1-T_1 split of laser dyes is relatively small and lies in the range 1400～4500 cm^{-1} [20),22)], which is associated with the large molecular size of most dyes and the spatial restriction of one electron primarily to the left side of the molecule and the other electron primarily to the right side.

Under the molecular-orbital aproximation[22)], the hamiltonian of organic compounds is a sum of effective one-electron energy operators. Molecular orbitals differ from atomic orbitals only in that they have a multicenter nature, and five types of molecular orbitals are related to the organic compounds. There are pi-bonding (π), pi-antibonding (π^*), nonbonding (n), sigma-bonding (σ), and sigma-antibonding (σ^*) orbitals. Single bonds between two atoms involve σ orbitals and the electrons located in such orbitals are called σ-electrons. These electrons are strongly bonding and essentially localized. Consequently, σ-electrons require greater excitation energy than π-electrons which occupy the π or multiple-bond orbitals. For each σ and π orbital there correspond σ^* and π^* antibonding orbitals, respectively. Certain heteroatoms (e.g., oxygen, nitrogen) introduce the possibility of n orbitals which are essentially localized on one particular atom and have no antibonding counterpart.

In this section we briefly describe only the π and π^* orbitals that are especially relevant to laser dyes, The π and π^* orbitals are delocalized over two or more nuclei. The π orbitals are usually pictured as some combination of p atomic orbitals as, for example, the carbonyl group shown in **Fig. 1-5**[13)]. Corresponding to each π orbital there is a π^* orbital which has a node between the carbon and oxygen atoms, as shown in Fig. 1-5. The relatively greater electronegativity of oxygen versus carbon causes the mobile π-electrons to undergo a considerable displacement from carbon to oxygen. In contrast, the π^* orbit has charge displacement from oxygen to carbon. Both the π and π^* orbitals possess a plane of antisymmetry which coincides with the molecular plane.

The electronic state of organic molecules such as xanthene and acridine dyes, which are typical dye laser media and are investigated in this thesis, is described as that of a

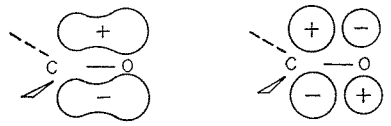

Fig. 1-5 Form of a π orbital (left) and a π^* orbital (right) of a carbonyl compound[13].

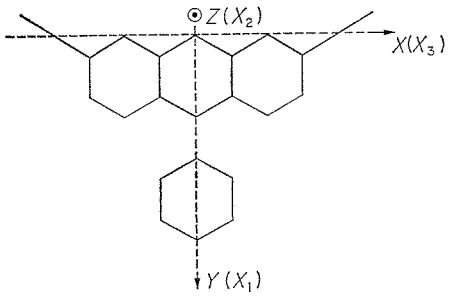

Fig. 1-6 Orientation of the chromophore group in xanthene and acridine dyes contributing to the different canonical peaks in the frequency-derivative ESR absorption lines. The Z axis is perpendicular the chromophoric plane.

system of 7 pairs of π-electrons in the chromophore in the free-electron model[19]. These dyes in the S_0 state have nearly C_{2V} symmetry. The S_0 state of π-electrons belongs to the totally symmetric representation $^1A_1$, whereas the S_1 and T_1 states belong to $^1B_2$ and $^3\Gamma_{\pi\pi^*}$, respectively[22),23]. In the compounds, the electrons which are responsible for the $S_0 \rightarrow S_1$ absorption transition have their largest extension along the long axis (X axis) in the chromophoric plane in **Fig. 1-6.**

1-2-3 Electronic Transition Processes

The photophysical transition processes that can occur in an isolated dye in dilute solution under optical excitation are divided into the following categories[10], which are illustrated in Fig. 1-3.

(i) $S_0 \rightarrow S_1$ absorption: The long-wavelength absorption band of dyes is attributed to the transition from the electronic ground state S_0 to the first excited singlet state S_1, which is spin-allowed. The transition moment for this process is typically very large, thus giving rise to an absorption band with an oscillator strength of the order of unity, corresponding to the absorption cross section $\sigma \cong 10^{-16}\,\mathrm{cm}^2$.

(ii) $S_1 \rightarrow S_0$ emission: The radiative transition $S_1 \rightarrow S_0$ between states of the same spin-multiplicity is responsible for the spontaneous emission known as fluorescence and for the stimulated emission in dye lasers. Because of the large transition moment the radiative lifetime τ_S is of the order of nanoseconds, and hence the gain of a dye laser exceeds

that of solid-state lasers by several orders of magnitude.

(iii) $S_1 \rightarrow S_0$ radiationless transition: The nonradiative direct decay of $S_1 \rightarrow S_0$ transition known as internal conversion is mostly responsible for the loss of fluorescence and stimulated emission in laser dyes. Therefore, the transition rate K_{IC} is one loss-factor that determines the operating efficiency of the laser. Depending on the dye molecular-structure and the properties of the solvent, the relaxation rate vavies by many orders of magnitudes.

(iv) $S_1 \rightarrow T_1$ radiationless transition: Molecules in the S_1 state also decay by a nonradiative process to the T_1 state, which is described as intersystem crossing and competes with the normal fluorescence and the stimulated emission. This process proceeds at a rate designated by the intersystem crossing rate constant K_{ST}, which cannot be easily measured. But we will present a novel method for measuring the rate of a typical laser dye in the section 3-4[24),25)]. This transition also lowers the efficiency of the laser.

(v) $T_1 \rightarrow S_0$ emission: The radiative process from the T_1 state to the S_0 state is of much longer duration than the fluorescence because it is a spin-forbidden transition, and it is called phosphorescence.

(vi) $T_1 \rightarrow S_0$ radiationless transition: The nonradiative process from the T_1 state to the S_0 state competes with the normal phosphorescence. In many cases the rate $K_T{}^{nr}$ is much larger than the above-mentioned phosphorescent rate $K_T{}^{r}$.

The value of the triplet-state lifetime, which is the reciprocal of the sum of the rates $K_T{}^{r}$ and $K_T{}^{nr}$, is very large and is ranging from milliseconds to a few seconds for organic molecules. These relaxation mechanisms related to the T_1 state of laser dyes will be discussed in the chapter 3[26),27)]. In dye lasers the population accumulation in the triplet state is generally quite detrimental since the below-mentioned T-T absorption at the laser wavelength presents a loss to the system as well as depleting the molecules available for laser action.

(vii) $T_1 \rightarrow T_2$ absorption: The absorption transition from the T_1 state having the long lifetime to higher excited triplet states T_2 is spin-allowed, and the molecules excited to the higher triplet state relax very fast to the T_1 state ($K_T{}^{h} \cong 10^{12}$ sec^{-1}).

1-2-4 The Role of the First Excited Triplet State (T_1 state) under Laser Action

When the dye laser is pumped with an intense light source such as flashlamps or lasers, the dye molecules are excited to some higher vibrational level in the S_1 state in Fig. 1-3 (A→b), from which they relax within picoseconds to the lowest vibronic level of the S_1 state (b→B). Laser stimulated emission results from the S_1 state to a highlying vibrational-rotational level of the ground S_0 state (B→a)[28)]. Therefore, dye lasers are the so-called four-levels laser system. The wavelength shift due to the energy difference between the absorbed photon and the emitted proton is essential to the lasing process, since the dye thereby becomes transparent to the fluorescence radiation. But, there are many nonradiative processes from the S_1 state that can complete effectively with the light emission and thus reduce the fluorescence and stimulated emission efficiency. These nonradiative processes are grouped into those that cause a direct realxation to the ground

S_0 state (internal conversion loss) and those that are responsible for intersystem crossing to the T_1 state (intersystem crossing loss). In addition, because of the relatively long lifetime of the T_1 state the dye molecule accumulates during the pumping process in the T_1 state, which often has considerable absorption for the laser light (optical losses due to a T-T absorption)[5),29),30)]. Thus not only are some of the dye molecules taken away from the lasing process but also they cause an additional loss in the laser owing to the T-T absorption. In particular, the optical losses due to absorption of laser cavity photons can be great enough to severely diminish lasing intensity, or prevent lasing altogether. Thus, the T_1 state of dye molecules is detrimental to laser action[13)]. In order to avoid or reduce these losses, two different techniques have been till now applied to the dye laser system. The first is to use a very rapid pumping source with a risetime shorter than $1/K_{ST}$ and thereby to get the laser pulse out of the system before the population of the T_1 state climbs to unacceptable levels, since the population builds up with time of $1/K_{ST}$ from zero initially[32),33)]. The second is by having suitable additive molecules (triplet-state quenchers) in solution with the lasing dye, which allows the dye molecules to return rapidly to the ground state due to an energy-transfer from the molecules in the T_1 state to the acceptor (quencher) molecules[34),35)]. For a cycrooctatetraene (COT) which is a typical quencher in an ethanolic R6G solution, the mechanism of the energy transfer will be discussed in the section 3-5[24)].

Finally, we should like to mention about photochemical stability as another property relevant to laser dyes. An ethanolic xanthene-dye laser of nonflowing system has the lifetime of only 41 msec when it is pumped by a cw Ar ion laser at intensities required for laser threshold[36)]. That is, the absorption coefficient decreases, the fluorescence is quenched, and the laser-threshold energy rapidly increases[6),37),38)]. The reason is that the laser dye solution is photochemically degraded by the pumping laser light. However, the photodegradation mechanism is not yet disclosed. On the other hand, in the field of photochemistry it is known that most of photochemical reactions in organic dye solutions proceed after passing through the T_1 state because of the long lifetime and the biradical property[8),11~13)]. Therefore, we surmise that in the photochemical reaction of the laser dye solution under optical excitation at high intensity the T_1 state also plays a direct role, which will be verified in the chapter 4 by using a first laser irradiated ESR technique[39),40)].

1-3 Outline of the Present Work

In this first laser excitation ESR study we are concerned with the first excited triplet state (T_1 state) of laser dyes, and, in particular, with the magnetic properties[26),41)], the relaxation processes including quenching by additive molecules[24~27)], and the photodegadation mechanisms[39),40)]. A novel method for determining directly an intersystem crossing rate which is very important for the evaluation of the operating efficiency of dye laser and of the rate constants for the complex photochemical processes, is established. Furthermore, two kinds of different photodegradation processes depending on the wavelengths of

the pumping laser light are systematically disclosed in the dye laser solution.

In Chapter 2, with the description of the advantages of the laser excited ESR technique the ESR absorption in the randomly oriented triplet-state of organic molecules is theoretically described on the basis of two π-electron spin-spin dipole interaction[42,43], and the linearly polarized excitation beam effect on the ESR signal intensity is treated[44,45]. For randomly oriented xanthene and acridine laser dye molecules in the T_1 state, several triplet ESR spectra are observed and the magnetophotoselection experiments are performed at 77 K. The results enable us to to determine principal values of a π-electron spin-spin interaction tensor, resonance magnetic fields, zero-field splitting (ZFS) parameters, and the polarization of π-electron distribution in the T_1 state, and consequently to relate these values to the dye molecular structure.

In Chapter 3, we introduce not only rate-equations for the population of the T_1 state under laser excitation but also theories on the intersystem crossing transition and the triplet-to-singlet radiative and nonradiative transitions, which are due to the spin-orbit interaction of π-electrons in organic molecules[10,22,46~48]. In addition, Perrin's model of triplet-triplet energy transfer is given[49]. The intersystem crossing rate is determined by connection of the rate-equation analysis with the experimentally obtained optical saturation curve of dye molecules in the T_1 state. The effects of the molecular structure of xanthene and acridine dyes, the temperature of the dye solution, and the solvent phase (glass, crystal, and plastic) on triplet-state lifetimes which are determined from the decay of the ESR signals are discussed in comparison with the above-mentioned theoretical results on the electronic transitions.

Chapter 4 is devoted to investigate photodegradation mechanisms in an R6G laser dye solution, by detecting free radicals induced by laser irradiation with wavelengths of UV (3511+3638 Å) or visible (5145 Å) beams. Detailed studies are made on the dependence of the radical concentration on the irradiation time and power, the effects of molecular structures of xanthene and acridine laser dyes and solvents on the producing processes of radicals, and the role of dye molecules in the T_1 state. On the basis of those results the laser-induced reaction sequences in the cases of UV and visible laser irradiations are proposed, which are quite different from each other. Furthermore, the rate equation analysis for the photodegradation processes is presented by means of the reaction sequences, and the number of degradation molecules per absorbed photon is calculated from the decrease of dye molecules in the T_1 state after photodegradation.

In final Chapter 5, our findings concerning with magnetic, optical, and photochemical properties of xanthene and acridine laser dyes obtained by a new laser excited ESR technique are summarized in cennection with the molecular structures. Future areas of this study including the investigation on important molecules in biophysics, such as chlorophyll, proteines, and nucleic acids[9,50], are suggested as applications of the present technique.

Chapter 2 Laser Excited Triplet State ESR

The purpose of this chapter is to determine principal values of a π-electron spin-spin interaction tensor, resonance magnetic fields, zero-field splitting (ZFS) parameters, and the polarization of the π-electron distribution in the excited molecular structure, and to relate these values to the molecular structure for xanthene and acridine laser-dye molecules in the first excited triplet state (T_1 state). At first, the advantages of a laser excited ESR technique, which is applied to the triplet-state of organic molecules for the first time by us, are described. The theoretical description of ESR absorption is given on the basis of two π-electrons spin-spin dipole interaction in the randomly oriented triplet-states, and the linear-polarized excitation beam effect on the ESR signal intensity of molecules having the anisotropic electronic transition moment is treated. The $\Delta M_S = \pm 2$, $\Delta M_S = \pm 1$, and two-photon absorption ESR signals in rhodamine (type R), fluorescein (type F), and acridine (type A) laser dyes during Ar ion laser excitation are observed. Comparison of the experimental results with the triplet-state spectroscopic theory enables us to obtain principal values X_i of the spin interaction tensor, resonance fields $F(H, h\nu)$, and ZFS parameters D^*, D, and E of their dyes. And the relation between dye molecular structures and their values or triplet spectra is discussed. Furthermore, the result of the magnetophotoselection in the $\Delta M_S = \pm 1$ ESR signals of a few dyes presents the relation between the principal axes of the spin interaction tensor and the molecular structural symmetric axes, and allows to determine components of polarization of the dipole transition moment of the first singlet excited optical absorption.

2-1 Advantages of a Laser Excitation Method

Electron spin resonance (ESR) experiments on aromatic molecules in the T_1 state during mercury lamp excitation were successfully first performed by Hutchison and Mangum[51] in 1958 for the phosphorescent naphthalene diluted and oriented in a single crystal of durence at 77 K, in order to show that the phosphorescent state is paramagnetic. Soon afterwards (1959), van der Waals and de Groot[52] pointed out that another absorption line ($H_{\min}$ line) corresponding to the forbidden $\Delta M_S = \pm 2$ transition in the limit of a strong magnetic field could also be observed in rigid glassy solution of some triplet-state aromatic molecules having higher symmetric structure. Furthermore, they analyzed quantum-mechanically the randomly oriented triplet-state ESR spectra of the higher symmetric molecules using the electron spin-spin interaction tensor and indicated that the zero-field splitting (ZFS) parameter D characterizing the tensor was experimentally obtained from the observation of the $H_{\min}$ line. In 1962, Yarger, Wasserman, and Cramer[53] observed some very weak $\Delta M_S = \pm 1$ transitions as well as the more intense $\Delta M_S = \pm 2$ transition of the randomly oriented triplet-state aromatic morecules dissolved in rigid

glasses. Furthermore, by Kottis and Lefebvre (1963), van der Waals' treatment was extended to molecules having less than ternary symmetry, and the resonance fields and lineshapes of their absorption lines in a rigid silution were in detail discussed[42)43)]. In the case of lower symmetry, it was found that , the ZFS parameters D and E and their root-mean-square $D^*=\sqrt{D^2+3E^2}$ were obtained from some absorption lines corresponding to $\Delta M_S=\pm 1$ transition and the $H_{\min}$ line, respectively. In those days, the two-quantum transition was also observed in the triplet-state ESR spectrum in the phenanthrene rigid glassy solution[54)]. With those experimental and analytical developments, the ZFS parameters were theoretically evaluated from a knowledge of the proper molecular-orbital triplet-state spatial wavefunction by several computational methods for rather simple molecules and were compaired with the experimental values[55)].

As for the magnetophotoselection method, on the basis of the results of application of the lineshape analysis during polarized light pumping to $\Delta M_S=\pm 1$ transitions due to a regular array of molecules in the randomly oriented triplet-state, it was initially proposed by Kottis and Lefebvre[44)] (1964) that the ESR signal intensity varies with the angle between the electric field of the light and the static magnetic field under some conditions. The magnetophotoselection experiments were carried out and quantitatively discussed to determine the polarization of first singlet electronic dipole transitions, to assign ESR signals and to make clear the triplet-triplet energy trasfer mechanism for high triplet-yield molecules by Elsayed, Siegel and their coworkers[56,45,57)].

After that, the ESR method during mercury light pumping has been appied successfully to many chemical and biochemical studies in which triplet state molecules play important roles.

The use of ESR techniques for triplet states enabled us to investigate as follows[22)].

(1) The ESR signal intensity is directly proportional to the concentration of triplet-state molecules. Therefore, the lifetime of the triplet state can be determined from the decay characteristics of the signal intensity after the cut-off of irradiation.

(2) The obtained ZFS parameters of one compound rarely coincide with those of another. Consequently, the ESR method becomes an effective analytic tool for distinguishing between different components of mixtures in studies of intermolocular triplet-triplet transfer phenomena. The polarization of π=electron distribution in the triplet state can be also discussed on the basis of the values of the ZFS parameters. Furthermore, comparison of the experimental value with the theoretical values of the parameters constitutes sensitive tests of approximate triplet-state molecular wavefunctions.

(3) Even in randomly oriented samples, only those triplet-state molecules which are in the cannonical orientations are observed. This orientation selectivity under polarized light excitation gives rise to the information on the assignment of triplet ESR signals, the polarization of populating electronic dipole transitions, and energy transfer phenomena in rigid glassy media.

(4) Triplet states which do not phosphoresce are detectable.

However, these investigations on the physical properties related to the triplet state

have been limitted to only molecules of relatively high triplet-yield because of the weak intensity of mercury lamp light as a pumping source rather than the detectable sensitivity of an ESR spectrometer.

A laser as an intense pumping source has been first applied by us to the first excited triplet state ESR study[41]. The method using the ESR technique during laser excitation has the following advantages in comparison with the usual method using the mercury lamp for observation of only strong ESR signals such as of $\Delta M_S = \pm 2$ transitions in some laser dyes, which was reported[58] right after our first paper on triplet-state ESR of a typical laser dye during laser excitation had been published[41].

(1) The population of T_1 state shows a remarkable increase owing to the high intensity of pumping laser light : (2) The depolarization of electronic absorption band of dye molecules hardly occurs owing to the very narrow spectral width of pumping laser beam : (3) Free radicals of the sample solution are hardly produced because the pumping light is a single beam in the visible region. These merits enable us to perform the observation on weak triplet ESR signals such as of $\Delta M_S = \pm 1$ transitions and the experiments on magnetophotoselection for molecules of low triplet-yield[26], which are presented in the section 2-3 and 2-4 of this chapter, to estimate the singlet-to-triplet intersystem crossing rate constant of high luminescent molecules by obtaining optical saturatin curves for the molecules in the T_1 state[24], which will be presented in the next chapter, and to make clear the pumping wavelength effect on the photo -degradiaton or -chemical reaction mechanism of laser dyes[40], which will be discussed in the chapter 4. Furthermore, during laser excitation, the behaviors of triplet-state molecules are able to be analyzed by using simple rate equations.

In the next section, we describe quantum-mechanically the energy splittings of a triplet state due to two π-electron spin-spin interaction in an organic molecule, and obtain the ESR absorption pattern in the randomly oriented triplet-states such as triplet-dyes in an ethanol solution, using the interaction hamiltonian including the applied magnetic field effect[22,46,59]. At the end of the section, we derive the equation determining the components along the molecular symmetric axes of the optical absorption transition moment from the intensity variation of some of their ESR signals with the direction of the linear-polarized pumping light[45]. In the following sections the experimental technique for application of the laser excitation method to laser dyes is described, and the experimental results and interpretation for the triplet-state ESR spectra and their magnetophotoselections in laser dye solutions are given.

2-2 Theory on Triplet State ESR Spectroscopy

2-2-1 The effect of spin-spin dipole interaction on zero-field splitting (ZFS) parameters

We consider the effect of π-electron spin interaction in organic molecules in the absence of an external magnetic field. The spin forces cause the total π-electronic spin of the

molecule to be coupled to an axis that is related to the molecular structure. We may see this coupling symbolically as a quantization of the spin with respect to the molecular axis, and associate the magnitude of the coupling with a magnetic field that is directed along this molecular axis. For aromatic molecules the order of magnitude of this built-in magnetic field may be taken as 2000 G[46]. In the case that the external field $\vec{H}$ and the spin forces are both present, if H is much smaller than 2000 G the triplet-energy-levels are determined by the spin interactions, and if H is much larger than 2000 G the effect of the spin interactions becomes negligible. However, since in ESR experiments at x-band H is usually taken from 1000 to 5000 G, the quantizations due to H and to the spin interactions compete with one another on an almost equal basis and the energies of the triplet-levels depend strongly on the angle between $\vec{H}$ and the molecular axis.

Now, we will consider the more exact description of the energy splittings of a triplet state due to spin interactions. An electronic part of the molecular hamiltonian $\mathscr{H}^e$ is approximately written as

$$\mathscr{H}^e=\mathscr{H}_0{}^e+\mathscr{H}_{ss} \tag{2-1}$$

where the zero-order spin-independent hamiltoniam $\mathscr{H}_0{}^e$, which represents kinetic energy of electrons and Coulomb's energies between electrons and nuclei and between electrons themselves of many atoms composing the molecule, is in general described by using the Born-Oppenheimer, the molecular-orbital, and the π-electron approximations[22]. A perturbation term $\mathscr{H}_{ss}$ represents the spin dipole-dipole interaction between the magnetic moment due to one π-eleectron spin and the magnetic field produced by another π-electron spin magnetic dipole. In the case of organic molecules, the zero-field separation is mainly due to the spin-spin interaction rather than the spin-orbit interaction, and the g-factor is isotropic. The operator $\mathscr{H}_0{}^e$ has a set of eigenvalues and eigenfunctions given by

$$\mathscr{H}_0{}^e\Psi_i{}^e=E_i{}^e\Psi_i{}^e \tag{2-2}$$

If we impose the restriction that the eigenfunctions are antisymmetry with respect to all two-electron permutations and are eigenfunctions of the total spin operators $\vec{S}^2$ and S_Z, and that the number of electrons is even, we obtain a zero-order set of singlet eigenfunctions ${}^1\Psi_m{}^e$ with corresponding energies $E_{l,m}{}^e$, a set of triplet eigenfunctions ${}^3\Psi_{kMS}{}^e$ ($M_S=\pm1.0$) with corresponding energies $E_{3,k}{}^e$, etc.. Since the closed-shell electrons do not contribute to dipole-dipole interactions, we reduce the many-electron function ${}^3\Psi_{kMS}{}^e$ $(1,\cdots\cdots,n)$ to its relevant two-electron $(1,2)$ part:

$${}^3\Psi_{kMS}{}^e(1,2,3,\cdots\cdots,n)\supset\Phi_k(1,2)\theta_{SMS}(1,2)\,;\ M_S=\pm1,0\,;\ S=1, \tag{2-3}$$

where Φ_k is a functuion of spatial coordinates only and θ_{SMS} is a function of spin coordinates only. The possible MO functions φ_i which are described by linear conbination of carbon $2p_z$ atomic orbitals and the spin functions are

$$\Phi_k(1,2)=(1/2)^{1/2}[\varphi_a(1)\varphi_b(2)-\varphi_b(1)\varphi_a(2)] \tag{2-4}$$

$$\theta_{11}(1,2)=\alpha(1)\alpha(2)$$
$$\theta_{10}(1,2)=(1/2)^{1/2}[\alpha(1)\beta(2)+\beta(1)\alpha(2)]. \tag{2-5}$$
$$\theta_{1-1}(1,2)=\beta(1)\beta(2)$$

The explicit form of the operator $\mathscr{H}_{ss}$ is given by[60]

$$\mathscr{H}_{ss}=g^2\beta^2[r_{12}^2(\vec{s}_1\cdot\vec{s}_2)-3(\vec{r}_{12}\cdot\vec{s}_1)(\vec{r}_{12}\cdot\vec{s}_2)]r_{12}^{-5}$$
$$=\sum_{p,q}\Lambda_{pq}s_{1p}s_{2p}\ ;\ (p,\ q=x,\ y,\ z), \tag{2-6}$$

where

$$\Lambda_{pp}=g^2\beta^2(r_{12}^2-3p_{12}^2)r_{12}^{-5}$$
$$\Lambda_{pq}=-3g^2\beta^2(p_{12}q_{12})r_{12}^{-5}, \tag{2-7}$$

and $\vec{s}_i$ is the vector spin operator of electron i in units of $\hbar$, $\vec{r}_{ij}$ is the interelectronic vector, g is the g-factor, and β is the Bohr mageton. It is convenient to rearrange $\mathscr{H}_{ss}$ so that spatial and spin parts are separated. The ZFS of the triplet state ${}^3\Psi_k^e$ is evaluated from the roots of the secular determinant

$$|H_{ij}-W\delta_{ij}|=0,\quad ij=M_S, \tag{2-8}$$

where

$$H_{ij}\equiv<{}^3\Psi_{ki}^e|\mathscr{H}_{ss}|{}^3\Psi_{kj}^e>$$
$$=\sum_{p,q}<\Phi_k|\Lambda_{pq}|\Phi_k><\theta_{1i}|s_{1p}s_{2q}|\theta_{1j}>$$
$$=<\theta_{1i}|\sum_{p,q}\Omega_{pq}s_{1p}s_{2q}|\theta_{1j}>$$
$$\equiv<\theta_{1i}|\mathscr{H}_s|\theta_{1j}>, \tag{2-9}$$

and W is eigenvalues of this hamiltonian $\mathscr{H}_s$. The spatial parts $\Omega_{pq}\equiv<\Phi_k|\Lambda_{pq}|\Phi_k>$ do not depend on the M_S value i or j. Since a new form of the spin hamiltonian

$$\mathscr{H}_s\equiv\sum_{p,q}\Omega_{pq}s_{1p}s_{2q} \tag{2-10}$$

is an Hermite matrix, an appropriate choice of coordinate axes (X_1, X_2, and X_3 axes) for the molecule enables one to set $\Omega_{pq}=0$ when $p\neq q$. In the case of lower symmetry such as dye molecules, however, determination of the axes is by no means straight-forward; they are experimentally accessible from studies of magnetophotoselection techniques. From $\Omega_{X_1X_1}+\Omega_{X_2X_2}+\Omega_{X_3X_3}=0$, we obtain

$$\mathscr{H}_s=\frac{1}{2}(\Omega_{X_1X_1}-\Omega_{X_2X_2})(s_{1X_1}s_{2X_1}-s_{1X_2}s_{2X_2})$$
$$+\frac{1}{2}\Omega_{X_3X_3}(3s_{1X_3}s_{2X_3}-\vec{s}_1\cdot\vec{s}_2). \tag{2-10'}$$

Usage of the total spin operators $S_p=s_{1p}+s_{2p}(p=X_1, X_2, X_3)$ or $\vec{S}=\vec{s}_1+\vec{s}_2$ reduces the spin hamiltonian of Eq. (2-10) to the following form

$$\mathcal{H}_s=\frac{3}{4}\Omega_{X_3X_3}\left[S_{X_3}^2-\frac{1}{3}\vec{S}^2\right]+\frac{1}{4}(\Omega_{X_1X_1}-\Omega_{X_2X_2})(S_{X_1}^2-S_{X_2}^2)$$

$$=D\left[S_{X_3}^2-\frac{1}{3}\vec{S}^2\right]+E\left[S_{X_1}^2-S_{X_2}^2\right]. \tag{2-11}$$

Instead of Eq. (2-5) if we adopt spin functions which have the spin quantized along the X_1-, X_2-, and X_3-axes:

$$T_{X_1}=\left(\frac{1}{2}\right)^{1/2}(\theta_{1-1}-\theta_{11})=\left(\frac{1}{2}\right)^{1/2}(\beta(1)\beta(2)-\alpha(1)\alpha(2)),$$

$$T_{X2}=\left(-\frac{1}{2}\right)^{1/2}(\theta_{1-1}+\theta_{11})=i\left(\frac{1}{2}\right)^{1/2}(\beta(1)\beta(2)+\alpha(1)\alpha(2)), \tag{2-5′}$$

$$T_{X_3}=\theta_{10}=\left(\frac{1}{2}\right)^{1/2}(\alpha(1)\beta(2)+\beta(1)\alpha(2)),$$

and another form of the spin hamiltonian $\mathcal{H}_s$ is obtained[61]

$$\mathcal{H}_s=-(X_1S_{X_1}^2+X_2S_{X_2}^2+X_3S_{X_3}^2). \tag{2-11′}$$

The identifications relating Eqs. (2-11) and (2-11′) are

$$X_1\equiv\frac{D}{3}-E,\quad X_2\equiv\frac{D}{3}+E,\quad X_3\equiv-\frac{2}{3}D, \tag{2-12 a}$$

$$X_1+X_2+X_3\equiv 0. \tag{2-12 b}$$

This X_i description diagonalize the hamiltonian and X_1, X_2, and X_3 are the principal values of the hamiltonian tensor.

The ZFS parameters D and E have dimensions of energy and are obtained as

$$D=\frac{3}{4}\Omega_{X_3X_3}=\frac{3g^2\beta^2}{4}<\Phi_k\left|\frac{r_{12}^2-3z_{12}^2}{r_{12}^5}\right|\Phi_k>,$$

$$E=\frac{1}{4}(\Omega_{X_1X_1}-\Omega_{X_2X_2})=\frac{3g^2\beta^2}{4}<\Phi_k\left|\frac{y_{12}^2-x_{12}^2}{r_{12}^5}\right|\Phi_k>, \tag{2-13}$$

where D is related to the average of the inverse cube of the distance between the two π-electrons, $<1/r_{ij}^3>$, and is sensitive to the average separation of these electrons. Consequently, D is used as a probe to analyze the spatial distribution of the triplet-electrons. As the space available to the two electrons increases in size, D should decrease. The parameter E is related to the distribution symmetry of two π-electrons along the symmetry axes perpendicusar to the molecular plane. If two horizontal axes are equivalent (the molecular symmetry is higher than C_3), it is seen from Eq. (2-13) that $E=0$. Furthermore, the parameters D and E describe the separation of the three energy levels in the triplet state in the absence of an external magnetic field. These levels are given by the roots of the secular determinant of Eq. (2-11) as

$$W_3=-\frac{2}{3}D,$$

$$W_{1,2}=\frac{1}{3}D\pm E. \tag{2-14}$$

As shown in **Fig. 2-2**, D is the difference between the W_3-level and the mean of the

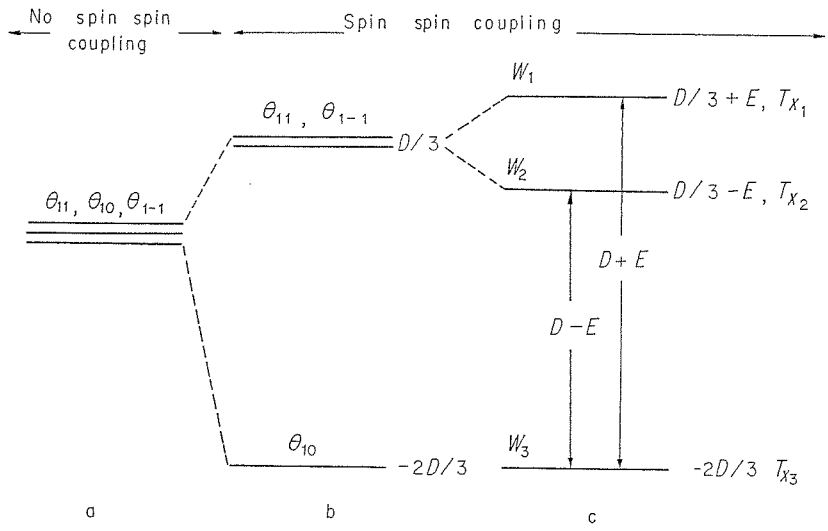

Fig. 2-1 An illustration of zero-field splitting. Column a - spherical symmetry molecule : column b - cylindrical (or axial) symmetry molecule : column c - orthorhombic C_{2v}, D_{2h} and D_2 symmetry molecule. The energies are quoted for $D>0$ and $E>0$[22].

other two. The latter pair is separated by energy $2E$.

2-2-2 ESR absorption lines in randomly oriented triplet states

In the presence of an external magnetic field $\vec{H}$, the spin hamiltonian of Eqs. (2-11) or (2-11′) is modified to

$$\mathcal{H}_s=\beta\vec{H}\cdot\hat{g}\cdot\vec{S}-(X_1S_{X_1}^2+X_2S_{X_2}^2+X_3S_{X_3}^2)$$
$$=\beta\vec{H}\cdot\hat{g}\cdot\vec{S}+D\left[S_{X_3}^2-\frac{1}{3}\vec{S}^2\right]+E[S_{X_1}^2-S_{X_2}^2], \qquad (2\text{-}15)$$

where $\hat{g}$ is the g-facter tensor. Since we can neglect the spin-orbit interaction for organic molecules, we assume that the g-factor is isotropic. Using the spinfunction of Eq. (2-5′), we obtain the following secular determinant[42,43] :

$$\begin{vmatrix} X_1-W & -ig\beta Hn & ig\beta Hm \\ ig\beta Hn & X_2-W & -ig\beta Hl \\ -ig\beta Hm & ig\beta Hl & X_3-W \end{vmatrix}=0, \qquad (2\text{-}16)$$

where l, m, and n are the direction consines of $\vec{H}$ with respect to the molecular principal X_1-, X_2-, and X_3-axes. The secular determinant provides three energy levels W_i and, consequently, three energy level differences for a given molecular orientation. Since these energy differences are field-dependent, we find an appropriate magnetic field strength where one of the energy differences becomes equal to the microwave energy quantum $h\nu$. In other words, for a given molecular orientation, there are three different magnetic field strengths where magnetic resonance occurs. Such resonance conditions are given by

$$(X_1\cos^2\phi+X_2\sin^2\phi)\sin^2\theta+X_3\cos^2\theta$$
$$=(g\beta H)^{-2}\{X_1X_2X_3\mp\sqrt{3}^{-3}[(h\nu)^2+X_1X_2+X_1X_3+X_2X_3$$
$$-(g\beta H)^2][(2g\beta H)^2-(h\nu)^2-4(X_1X_2+X_1X_3+X_2X_3)]^{1/2}\}. \quad (2\text{-}17)$$

This equation is rewritten in functional form as

$$f(\theta,\phi)=F(H,h\nu), \quad (2\text{-}18)$$

which describes the resonant magnetic field H, in terms of a given microwave frequency ν, a given molecular orientation θ and ϕ in **Fig. 2-2**, and molecular parameters of g and X_i (or D and E). Apart from the question of transition probabilities, we also find those magnetic fields where the anisotropy of absorption is not sensitive to small changes in the angles θ and/or ϕ. These conditions are found by differentiating Eq. (2-18) by θ, ϕ, and H: they are

$$df=F'(H,h\nu)dH\ ;\quad dH=df/F'(H,h\nu), \quad (2\text{-}19)$$

where

$$df=\frac{\partial f}{\partial\theta}d\theta+\frac{\partial f}{\partial\phi}d\phi,$$
$$F'(H,h\nu)=\partial F(H,h\nu)/\partial H. \quad (2\text{-}20)$$

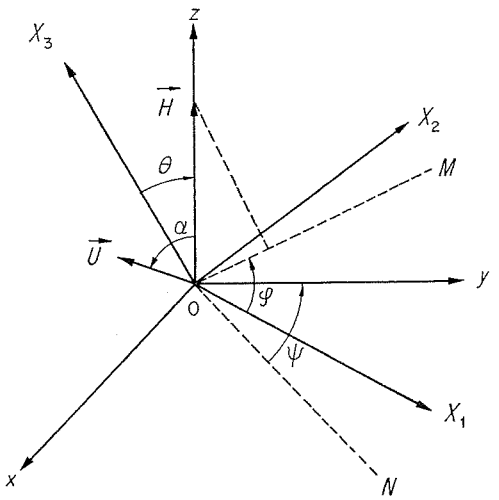

Fig. 2-2 Reference systems, $Oxyz$ and $OX_1X_2X_3$ are the coordinate systems in the laboratory based on the static magnetic field $\vec{H}$ and in the molecule based on the molecular principal axes, respectively. ON is the intersection between the xOy and X_1OX_2 planes, OM the projection of Oz in the X_1OX_2 plane. $\vec{U}$ is unitary vector in the xOz plane, along the direction of the oscillating field $\vec{H}_{rf}$, $\vec{H}$ is the static magnetic field, α the angle between the two fields[42].

Inspection of Eq. (2-19) indicates that these conditions exist as follows:

(i) when $F'(H, h\nu)$ goes to infinity; or

(ii) when $df \cong 0$, whereas $F'(H, h\nu) \neq 0$

The differentiation leads to the following results:

from condition (i)

$$(2g\beta H)^2-(h\nu)^2-4(X_1X_2+X_1X_3+X_2X_3)=0, \tag{2-21}$$

and from condition (ii)

$$\theta \cong 0, \text{ for any } \phi \ (X_3 \text{ axis}), \text{ and}$$

$$\theta \cong \pi/2, \text{ for } \phi=0 \ (X_1 \text{ axis}) \text{ or } \phi \cong \pi/2 \ (X_2 \text{ axis}). \tag{2-22}$$

The result of Eq. (2-21) is equivalent to

$$H_{\min}=(2g\beta)^{-1}[(h\nu)^2+4(X_1X_2+X_1X_3+X_2X_3)]^{1/2}$$

$$=(2g\beta)^{-1}\{(h\nu)^2-\frac{4}{3}(D^2+3E^2)\}^{1/2}$$

$$\equiv(2g\beta)^{-1}\{(h\nu)^2-\frac{4}{3}D^{*2}\}^{1/2}, \tag{2-23 a}$$

providing that $(h\nu)^2/4 > -(X_1X_2+X_1X_3+X_2X_3)$ or $(D^2+3E^2)/3$, where we call

$$D^*=(D^2+3E^2)^{1/2}, \tag{2-23 b}$$

the root-mean-square of ZFS parameters D and E. The lowest magnetic field satisfying Eq. (2-21) is given by $H_{\min}$, where the absorption is expected for a paticular set of parameters including $h\nu$. The transitions observed at $H_{\min}$ correspond to the forbidden transitions between two Zeeman levels which are not adjacent at high magnetic fields. Consequently, these transitions are often referred to as $\Delta M_S=\pm 2$ transitions.

The results of Eq. (2-22) are easily correlated with the cannonical orientations which refer to magnetic field alignments such that $\vec{H}$ is parallel to one of the three principal molecular axes of the interaction tensor. Since each cannonical orientation induces three enery differences, in addition to the peak at $H_{\min}$ we may observe at most nine peaks (3 energy differences×3 orientations) in the rigid glassy solution. Three of these and the other six appear in the regions corresponding to the $\Delta M_S=\pm 2$ and the $\Delta M_S=\pm 1$ transitions in the strong field quantization limit, respectively. Taking into account the transition probabilies between the Zeeman levels for these cannonical orientations, we find that when the microwave-frequency oscillating magnetic field $\vec{H}_{rf}$ is perpendicular to the static field $\vec{H}$ such as the case of the experimental arrangement to be reported in the section 3 of this chapter only the $\Delta M_S=\pm 1$ transitions appear. That is, from Eq. (2-22) the following six $\Delta M_S=\pm 1$ transition for cannonical orientations become allowed when $\vec{H}_{rf} \perp \vec{H}$, in addition to a $\vec{H}_{\min}$ line.

$$H_{X_1}{}^{L}=(2g\beta)^{-1}[(2h\nu-3|X_1|)^2-(X_2-X_3)^2]^{1/2}, \tag{2-24 a}$$

$$H_{X_1}{}^{H}=(2g\beta)^{-1}[(2h\nu+3|X_1|)^2-(X_2-X_3)^2]^{1/2}. \tag{2-24 b}$$

The expressions for $H_{X_2}{}^L$ or $H_{X_2}{}^H$ and $H_{X_3}{}^L$ or $H_{X_3}{}^H$ are obtained from cyclic permutation of X_1, X_2 and X_3 in Eqs. (2-24 a, b). By the use of Eqs. (2-12) and (2-24), the principal values and the ZFS parameters are evaluated in terms of the $\Delta M_S=\pm 1$ resonance fields for cannonical orientations

$$|X_i|=(g^2\beta^2/6h\nu)[(H_{X_i}{}^H)^2-(H_{X_i}{}^L)^2], \tag{2-25}$$

under the condition that the the principal values satisfy the inequalities

$$X_1, X_2>0, \quad X_3<0, \quad X_1<X_2<|X_3|. \tag{2-26}$$

We can also discuss graphically the resonance field for a given $h\nu$ and a cannonical orientation, using Eqs. (2-18), (2-21), and (2-22). If we construct the function $F(H, h\nu)$ with H as the variable, and if we draw a parallel to the H axis at coordinate equal to the value of $f(\theta, \phi)=X_i$, the abscissas of the intersections give the resonance fiields.

Next, we briefly describe the ESR lineshape analyzed by Kottis and Lefebvre[42,43] under the assumption that the absorption line of a molecuse has a Gaussian shape with a width independent of the molecular orientation. In the analysis, they used the lineshape function with a linewidth parameter λ, taking into account the averaged relative transition probability $\bar{B}(\theta, \phi, \alpha)$ between the two Zeeman levels and the resonance fields $H(\theta, \phi)$ between H and $H+dH$, which depend on the angle between the molecular axes and the static magnetic field. That is,

$$g(H, \alpha)\propto\int_0^{2\pi}d\phi\int_0^{\pi}d\theta\bar{B}(\theta, \phi, \alpha)\exp\left\{\frac{-2[H-H(\theta, \phi)]^2}{\lambda^2}\right\}\sin\theta, \tag{2-27}$$

where α is the angle between the oscillating and the static magnetic fields. The result of the calculation for the $H_{\min}$ line showed that

$$H_{\min}=H_l+0.45\Delta H_l, \tag{2-28}$$

where H_l is the value of the magnetic field corresponding to the low-field maximum of the frequency-derivative spectrum of the $H_{\min}$ line and ΔH_l is the distance from this maximum to the first zero of the signal.

Not only microwave-one-photon absorption such as the $\Delta M_S=\pm 1$ and $\Delta M_S=\pm 2$ transitions ($H_{\min}$ line) mentioned till now, but also another type of absorption line is found near the center of normal $\Delta M_S=\pm 1$ spectra. It has been ascribed to a two-quantum transition between nonadjacent triplet-sublevels. The simultaneous absorption of two quanta of an incident electromagnetic wave may occur whenever there is an intermediate state at a position very close to (but not necessarily exact equal to) the midway point between two energy levels and the energy quantum of the incident microwave is exactly equal to half the energy difference between the latter two levels. Hence, it should be located at the value H_d of the resonance field where two of the three possible roots of Eq. (2-17) coincide. Such coincidence occurs when the term preceded by the $\pm$ sign in Eq. (2-17) vanishes. That is,

$$(g\beta H_d)^2=(h\nu)^2+(X_1X_2+X_2X_3+X_1X_3)$$

$$=(h\nu)^2-\frac{1}{3}D^{*2}, \tag{2-29}$$

if the second factor in Eq. (2-17) is equal to zero we have the case corresponding to the $H_{\min}$ line.

2-2-3 Magnetophotoselection[45]

The method of magnetophotoselection is based on observation of the $\Delta M_S=\pm 1$ transition of a regular array of triplet-molecules embedded in a rigid glass. This regular array is produced by excitation of the random glassy assemble with polarized light.

As mentioned in the previous subsection, the peaks occurring in the $\Delta M_S=\pm 1$ ESR frequency-derivative spectra of randomly oriented triplet molecules are to be interpreted as due to those molecules which have one of the principal axes of their electron spin-spin interaction tensor oriented along or nearly along the static magnetic field. The spectra observed in the neighborhood of such cannonical peaks are therefore essentially due to three quasioriented assemblies of magnetoselected molecules, the other molecules only contributing a nearly continuous background to the absorption. Therefore, if polarized light is used to excite the $S_0\rightarrow S_1$ transition and the polarization of the electric vector $\vec{E}$ of the light is parallel to the direction of the external magnetic field $\vec{H}$, the intensity I_i of the $\Delta M_S=\pm 1$ transition corresponding to any orientation i of the three cannonical orientations is proportional to the number of excited triplet-state molecules $N_i^0(//)$ which have their i-th molecular axis at the angle $\theta_{iH}<\delta$ if the following conditions are satisfied.

(1) The symmetry of the molecule is high enough for the principal axes of the electron spin-spin coupling tensor to be also the direction carrying the electric dipolar transition moments.

(2) The polarized light is used to populate the triplet state via intersystem crossing without depolarization of the electric dipolar moment.

(3) The molecules are sufficiently diluted and in such a rigid solvent as to prevent exciton transfer and reorientation.

By polarization is meant the direction of the optical absorption transition moment with respect to a set of orthogonal molecular structure axes corresponding to the long (X axis) and short (in-plane) (Y axis) and perpendicular (Z axis) axes. For example, the intensity of the absorption components viewed parallely to the three orthogonal crystal axes will be proportional to the squares of the projections of the transition moment vector on these axes. The probability of absorption P_A for any molecule excited with light polarized parallel to $\vec{H}$ is

$$P_A=r_X\cos^2\theta_{XH}+r_Y\cos^2\theta_{YH}+r_Z\cos^2\theta_{ZH},$$
$$r_X+r_Y+r_Z=1, \tag{2-30}$$

where r_i is the component of the polarization of the optical absorption transition moment carried along each axis i and θ_{iH} is the angle between the molecular axis and the magnetic field. According to Siegel and Judeiks, the fraction of molecules ρ_i excited by

polarized light with $\theta_{iH} \leq \delta$ (δ is a small quantity) for a random distribution of originally unexcited molecules is

$$\rho_i = \frac{r_i \int_0^{\delta} \cos^2\theta_{iH} \sin\theta_{iH} d\theta_{iH}}{\int_0^{\pi/2} \cos^2\theta_{iH} \sin\theta_{iH} d\theta_{iH}} \cong \frac{3}{2}\delta^2 r_i, \tag{2-31}$$

and the fraction of all molecules ρ' excited by nonpolarized light with $\theta_{iH} \leq \delta$ is

$$\rho' = \frac{\delta^2}{2}, \tag{2-32}$$

for all three axes. If the incident optical excitation has also a depolarized isotropic component, the excited molecules will have $N_{EX}(p)$ molecules excited by the polarized excitation and $N_{EX}(np)$ molecules excited by the nonpolarized component. Therefore, the number of excited molecules $N_i^{\delta}(//)$ with the observation angles $\delta \geq \theta_{iH}$ when $\vec{E}//\vec{H}$ can be written as

$$\begin{aligned} N_i^{\delta}(//) &= N_{EX}(p)\rho_i + N_{EX}(np)\rho' \\ &= N_{EX}(p)\frac{\delta^2}{2}(3r_i + k_p), \end{aligned} \tag{2-33}$$

where it is assumed that the ratio $N_{EX}(np)/N_{EX}(p) = k_p$ is a constant. When $\vec{E} \perp \vec{H}$, only molecules excited along the other components ($j \neq i$) of the molecular polarization will contribute to $N_i^{\delta}(\perp)$ and

$$\begin{aligned} N_i^{\delta}(\perp) &= N_{EX}(p)\sum_{j \neq i}\rho_j + N_{EX}(np)\rho' \\ &= N_{EX}(p)\frac{\delta^2}{2}(3(1-r_i)/2 + k_p). \end{aligned} \tag{2-34}$$

Under the assumption that photoexcited molecules with the cannonical orientation $\theta_{iH} \leq \delta$ have unit probability of being observed and those with $\theta_{iH} > \delta$ have zero observational probability, the intensity of the ESR transition I_i is proportional to $N_i^{\delta}(//)$ or $N_i^{\delta}(\perp)$ when $E//H$ or $E \perp H$, respectively. Then, an expression for the usual polarization R_i becomes as follows

$$R_i = \frac{N_i^{\delta}(//) - N_i^{\delta}(\perp)}{N_i^{\delta}(//) + N_i^{\delta}(\perp)} = \frac{I_i(//) - I_i(\perp)}{I_i(//) + I_i(\perp)} = \frac{3r_i - 1}{1 + 4/3k_p + r_i}. \tag{2-35}$$

This equation indicates that the results of the magnetophotoselection experiments enable us not only to directly relate the principal axes of the spin-spin interaction tensor to the molecular structure axes and then to assign the triplet ESR signals if we qualitatively know the $S_1 \leftarrow S_0$ transition dipole polarization, but also to quantitatively determine the component of the polarization of the optical dipole transition.

2-3 Experimental Procedures

2-3-1 Experimental Preparations

Samples of dye powder used were commercial products. Rhodamine 6G (R6G), acridine

red (AR), fluorescein disodium salt (=uranin) (FDS) and eosin Y (EY) were obtained from both the Eastman Kodak and the Tokyo Kasei Kogyo Cos., and rhodamine B (RB), dichlorofluorescein (DF) and eosin B (EB) from the former Co., and rhodamine S (RS), acridine orange (AO) and acridine yellow (AY) from the latter Co.. These dyes, with the exception of AO and EB, have been already reported as laser active media[14]. A quantity of the dye, generally about a few ten mg, was weighed on an analytical balance of measurable minimum weight 0.1mg. A solvent was added to a small flask to produce a solution of a proper concentration (1×10^{-5} to 5×10^{-3} M) when the weighted dye powder was added. The ethanol used as a solvent was Kanto Chemical's guaranteed reagent grade, and the methanol and the dimethyl-sulfoxide (DMSO) were Tokyo Kasei's guaranteed and spectrograde, respectively. The dye solution of about 0.2 cc in volume was put into an about 4 mm-o.d. cylindrical quartz tube of about 15 cm in length. After connecting the tube to a vecuum line and immersing it in liquid nitrogen, we removed oxygen by the freeze-pump-thaw technique under about 10^{-5} mmHg pressure and sealed its tube. The transparent lower part of a 500 cc Dewar was made by a 11 mm-o.d. double cylindrical quartz-tube to efficiently pass through pumping laser light with any wavelength from 3000 Å to 7000 Å. The sample tube supported by a stainless pipe was inserted into liquid nitrogen in the Dewar.

2-3-2 Measuring instruments and arrangement

The triplet-state ESR spectra were recorded with a Varian E-4 x-band spectrometer using a model E-234 optical transmission rectangular cavity withe 100 kHz field modulation. The magnetic fieldial regulator resettability and the automatic frequency lock stability of the spectrometer were 0.1 G and one part in 10^6, respectively. The strength of the static magnetic field perpendicular to the microwave field was calibrated against an EPM-15 AD proton NMR gaussmeter made by the Echo Electronic Co. The spectrometer was checked by confirming an exact coincidence between the ZFS parameter's values already known and the values observed with the apparatus under high pressure mercury lamp irradiation for the triplet spectra of anthracene and triphenylene molecules. The liquid nitrogen Dewar where the sample tube had been already set was put into the center holes along the long axis of the rectangular microwave cavity. The direction of the propagation of an Ar ion laser beam, Spectro Physics model 165-03, was perpendicular to the static magnetic field. The glassy dye solution was excited by the unfocused 5145 or 4880-Å laser beams which gave a several hundred milliwatts of power to the sample surface with the power stability of 1 percent. In the experiments on magneto-photoselection, the exciting beam linearly polarized with a given angle was obtained through a rotatable polarizer and a $\lambda/4$ sheet located in front of the vertical polarized laser. The transmittance of the quartz tube without the dye solution, which was inserted into the Dewar containing liquid nitrogen, was measured for the 5145-Å laser beam. The attenuation of the laser excitation power due to air, liquid nitrogen, and the cylindrical quartz sheets of the Dewar vessel and sample tube was about 45 percent, and the beam

diameters at the sample surface was about 3.5 mm for the 5145-Å laser beam.

2-4 Experimental Results and Discussions

2-4-1 Observation on several ESR spectra including double quantum transitions in the T_1 state

When the frequency ν and the cavity input power of the microwave magnetic field were about 9.342 GHz and 10 mW, respectively, the frequency-derivative of a rather strong ESR signal was successfully recorded around 1621 G in the 1×10^{-5} M R6G ethanol solution at 77 K under excitation by the 5145-Å laser beam of 500 mW power as shown in **Fig. 2-3.** The magnitude of the applied 100 kHz magnetic field modulation was about 8 G. For each solvent of methanol, ethanol, and a mixture of ethanol and methanol (5 : 1), the H_{min} line was observed at almost the same value of the magnetic field. Furthermore, under high power (1000 mW) laser excitation with circular polarization and in the high concentration (5×10^{-3} M) solution, the one pair of very weak signals with broad width corresponding to the $\Delta M_S=\pm1$ transition were also observed around 2716 and 3866 G in addition to the H_{min} line. Thus, performed were observations on the $\Delta M_S=\pm2$ (H_{min} line) and $\Delta M_S=\pm1$ ($H_{X_i}{}^L$ or $H_{X_i}{}^H$ lines) spectra in ten dyes of rhodamine (type R), fluorescein (type F), and acridine (type A) during laser excitation at 77 K.

The resonance fields of the observed $\Delta M_S=\pm2$ and $\Delta M_S=\pm1$ signals of the three types of dyes (AR, RS, RB, and R6G belonging to type R, FDS, DF, EY, and EB to type F,

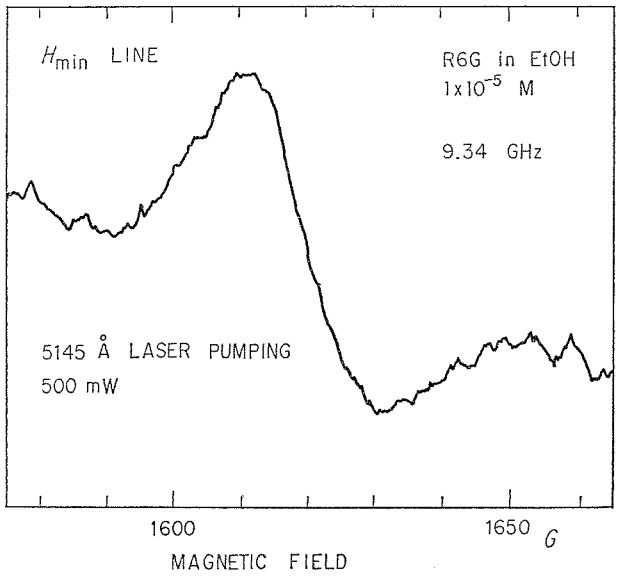

Fig. 2-3 Frequency-derivative spectra of a H_{min} line in 1×10^{-5} M solution of R6G in ethanol at 77 K. The pumping laser power of 5145 Å and the applied microwave power at 9.34 GHz are 500 and 10 mW, respectively.

and AO and AY to type A) are tabulated together with the molecular structure in **Table 2-1.** In the case of type A dyes, unlike the case of the other dyes, the signal intensity of H_{min} lines under the 4880-Å laser pumping beam was higher than the one under the 5145-Å beam. This fact corresponds to each absorption spectrum of the dye solutions at room temperature[21]. The signal intensity in the 1×10^{-5} M R6G-ethanol solution corresponds to approximately 10^{14} molecules in the triplet state under excitation power of 0.3 W/cm² on the basis of very crude comparison with the spectrometer sensitivity. Under

Table 2-1 Molecular structures and resonance fields (gauss) of triplet-dyes in ethanol at 9.230~9.370 GHz and 77K.

	DYES	$\Delta M_S=\pm2$			$\Delta M_S=\pm1$	
		H_l^a	H_0^b	ΔH^c	$H_{X_i}^L$	$H_{X_i}^H$
Type R	AR	1612	1623	21	——	——
	RS	1596	1606	18	2714	3863
	RB	1595	1604	18	2699	3875
	R6G	1611	1621	16	2716	3866
Type F	FDS	1604.4	1608.7	7.7	2632 2675	3987 4031
	DF	1603.8	1608.9	8.5	——	——
	EY	1590	1602	19	——	——
	EB	1589	1599	20	——	——
Type A	AO	1612	1623	22	2680 2756 3230	3392 3909 3992
	AY	1607	1618	26	——	——

a Low-field maximum of $\Delta M_S=\pm2$ signal.
b First zero of $\Delta M_S=\pm2$ signal.
c Peak-to-peak width of $\Delta M_S=\pm2$ signal.

condition of the same concentration and pumping power, the intensities of H_{min} lines of FDS and AO were about 5 times as large as those of the other dyes. This is due to the reasons that the intersystem crossing rate of FDS and the triplet-state lifetime of AO are fairly large in comparison with those of the other dyes. All the $\Delta M_S = \pm 2$ ESR spectra of the molecules examined had ordinary line shapes. In the case of FDS and DF, however, the half-widths of H_{min} lines (8~9 G) were narrower than the ones in the case of the other dyes (16~26G). It will be noted that the half-widths in the case of EY and EB derivated from FDS by means of the replacement of four hydrogen atoms in the chromophore by Br atoms and NO_2 groups were about three times as wide as the one in the case of FDS. The half-width of the dye possessing the same chromophoric structure as that of type F dye is considered to be fairly narrow by nature in comparison with those of the other types of dyes, but the half-width of the derivative with Br substituent may be broader owing to the hyperfine interaction between π-electrons and replaced heavy atoms in the chromophore.

The weak ESR spectra of $\Delta M_S = \pm 1$ transitions in rigid ethanolic solutions were also recorded for RS, RB and R6G (type R), AO (type A), and FDS (type F) during laser excitation at 77 K. As to the $\Delta M_S = \pm 1$ ESR spectra, all the type R dyes disclosed only one observable pair of rather broad signals (43~71 G), AO did three pairs of narrow signals (27~44 G), and FDS, two pairs of still narrower signals (15~25 G), as shown in **Fig. 2-4.** These results suggest that the dyes of the same chromophoric structure show similar triplet spectra. Therefore, in the theoretical analyses of the triplet ESR spectra of xanthene and acridine laser dyes, we consider only the spin-spin interaction between π-electrons themselves and the hyperfine interaction between π-electrons and heavy atoms

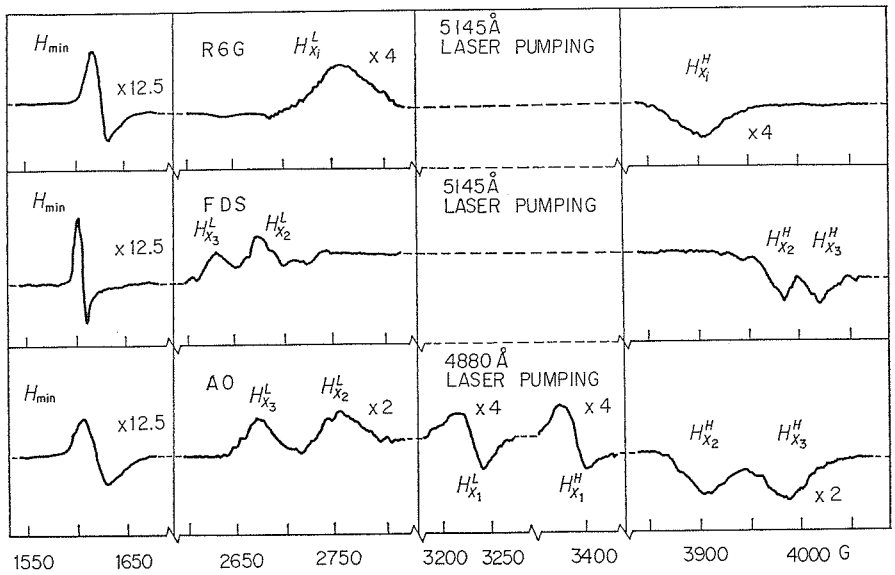

Fig. 2-4 The experimentally observed laser-pumped frequency derivative ESR spectra for rhodamine 6 G (R6G), fluorescein disodium salt (FDS), and acridine orange (AO) in ethanol at 9.359 GHz and 77 K.

in the chromophoric structure (not the total molecular structure). In this case, we do not need to consider the spin-orbit interaction which exerts important influence on the triplet-state lifetime and the intersystem crossing rate, as described in the next chapter.

In addition to the $\Delta M_S = \pm 2$ and $\Delta M_S = \pm 1$ signals, another microwave-absorption line (designated by H_d line) during laser irradiation was observed around 3187 G in the R6G solution at 8.984 GHz microwave-frequency. The applied microwave power dependence of the peak-to-peak height of the H_d line, given by curve A in **Fig. 2-5**, indicates that the relative heights increase approximately as the square of the power. Furthermore, the ratio of the height of the H_d line to that of the H_{min} line due to microwave-one-photon absorption (curve B in Fig. 2-5), shows similar behaviors to the ratio in case of the two-quantum transition of phenanthrene, as given by curve C in Fig. 2-5[54].

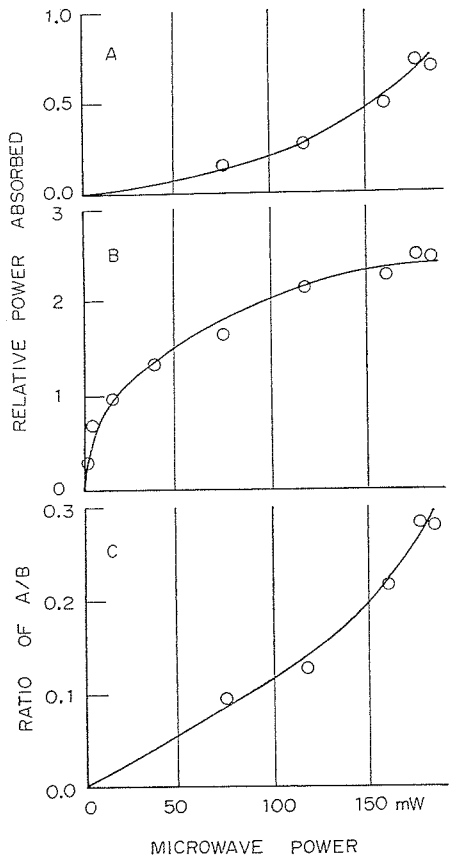

Fig. 2-5

A Microwave power dependence of the absorption intensities of H_d lines.

B Microwave saturation curve of H_{min} lines.

C Ratio of the absorption intensities of H_d lines and H_{min} lines versus the microwave power dissipated in the cavity. The pumping laser power of 4880 Å is 170 mW.

Therefore, we find that the $H_{\bar{a}}$ line is due to the simultaneous absorption of two photons. In order to observe the two-quantum transition, we had to take the spectrum as quickly as possible after the onset of irradiation, because the signal is swamped by that of free radicals generated by the exciting light after laser irradiation for several ten minutes with several hundreds milliwatts of power.

2-4-2 Resonance fields and ZFS parameters

At first, we will determine the principal values X_i of the spin-spin interaction hamiltonian for all the dyes where not only the $H_{\min}$ line but also the H_{X_i} lines were observed, by substituting the resonance fields experimentally obtained into the Eq. (2-25) derived in the previous section under resonance conditions in the randomly oriented triplet state. We do this under the condition that the principal values satisfy the inequalities (2-26). These inequalities do not express any restriction in the treatment, as the spectrum of randomly oriented molecules is unsensive to a permutation of X_1, X_2, and X_3 and to a simultaneous change of their signs. The determined values are given in **Table 2-2** where those values for AO dye having three pair of H_{X_i} lines were calculated from Eq. (2-25), those for FDS dye having two pair of H_{X_i} lines from Eqs. (2-25) and (2-12b), those for type R dyes having only one pair of H_{X_i} lines calculated by combining Eqs. (2-25), (2-12a) and (2-23b) with D_2^* from $\Delta M_S=\pm 2$ signals, as to satisfy the inequalities (2-26). These results show that, in the case of xanthene and acridine dyes unlike the other aromatic molecules, the value of $|X_1|$ is very small and $|X_2|$ is almost the same value as $|X_3|$. In this case, according to the detail calculation of the ESR absorption pattern[43], the ordering of the absorption line appearing with increasing the magnetic field is

$$0<H_{\min}<H_{X_1}{}''<H_{X_2}{}''<H_{X_3}{}''<H_{X_3}{}^L<H_{X_2}{}^L<H_{X_1}{}^L$$
$$<H_{X_1}{}^H<H_{X_2}{}^H<H_{X_3}{}^H, \qquad (2\text{-}36)$$

as $1/\lambda_m=0.31\ \mathrm{cm}^{-1}$ (corresponding to a microwave frequency of $\nu=9.3$ GHz), and some

Table 2-2 Magnetic principal values (cm^{-1}) of a spin-spin interaction tensor of π-electrons in laser-dyes dissolved in ethanol at 77 K.

DYES		X_1	X_2	X_3
R	RS	0.002 c	0.036 c	−0.038 c
	RB	0.002 c	0.037 c	−0.938 c
	R 6 G	0.001 c	0.036 c	−0.037 c
F	FDS	0.003 d	0.041 d	−0.044 d
A	AO	0.005 e	0.036 e	−0.041 e

c Calculated by combining Eqs. (2-12a), (2-12b), (2-23b), (2-25) and (2-26) with D_2^* from the $\Delta M_S=\pm 2$ signal.
d Calculated using $X_1+X_2+X_3=0$.
e Calculated from $\Delta M_S=\pm 1$ resonance fields.

absorption peaks may sometimes coalesce. But, the H_{X_1}'', H_{X_2}'', and H_{X_3}'' lines of their resonance lines appear only when $H_{rf}//H$, owing to the transition probability between Zeeman levels.

Using the obtained values X_1, X_2, and X_3, we can examine graphically the solution of resonance conditions Eqs. (2-17) or (2-18) which determine H for a given $1/\lambda_m$ and a given orientation. For example, **Fig. 2-6** presents the function $F(H, h\nu)$ with H as the variable for an FDS molecule, with $1/\lambda_m = 0.312\,\mathrm{cm}^{-1}$. From the graph it is clear that there are three resonance fields for any canonical orientation. That is, the abscissas of the two intersections in the higher field for $f(\theta=0, \phi)=X_3$, $f(\theta=\pi/2, \phi=\pi/2)=X_2$, or $f(\theta=\pi/2, \phi=0)=X_1$ give $H_{X_3}{}^L$ and $H_{X_3}{}^H$, $H_{X_2}{}^L$ and $H_{X_2}{}^H$, or $H_{X_1}{}^L$ and $H_{X_1}{}^H$ resonance fields, respectively, in the $\Delta M_S=\pm1$ region when $\vec{H}\perp\vec{H}_{rf}$, and the one of another intersection in the lower field gives H_{X_3}'', H_{X_2}'', or H_{X_1}'' resonance fields in the $\Delta M_S=\pm2$ region when $\vec{H}//\vec{H}_{rf}$. In addition, the $H_{\min}$ line which is the lowest possible resonance field is given at the field where $F(H, h\nu)$ ceases to be real function. These values for the molecule are also given in **Fig. 2-6**. In the case of type R dyes, the values indicate that $H_{X_3}{}^L$ and $H_{X_2}{}^L$ lines (or $H_{X_3}{}^H$ and $H_{X_2}{}^H$ lines) unlike the other types of dyes almost coalesce and $H_{X_1}{}^L$ and $H_{X_1}{}^H$ lines are covered by a free radical signal.

Furthermore, for three types of dyes, the values of ZFS parameters D and E can be determined by substituting the principal values into Eq. (2-12a), and the root-mean-square values of ZFS parameters $D_1{}^*$ and $D_2{}^*$ can be determined by substituting the values of D and E into Eq. (2-23b) and by combining Eqs. (2-28) and (2-23a) with the $\Delta M_S=\pm2$ signal, respectively. Those values are also given in **Table 2-3.** The value of $D_1{}^*$ calculated from the $\Delta M_S=\pm1$ signal agrees well with that of $D_2{}^*$ from the $\Delta M_S=\pm2$ signal.

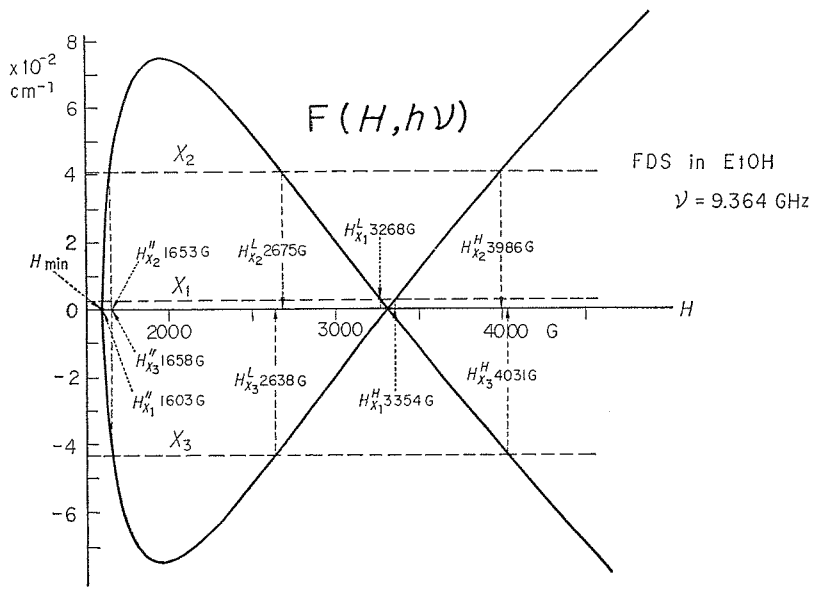

Fig. 2-6 The resonance magnetic field function $F(H,h\nu)$ for fluorescein disodium salt (FDS) laser-dye in ethanol at 9.364 GHz and 77 K.

Table 2-3 Zero-field splitting parameters (cm^{-1}) of laser-dyes in ethanol at 77K.

DYES		D_2* [a]	D_1* [b]	D	E
R	AR	0.068	—	—	—
	RS	0.064	—	0.057 [c]	0.017 [c]
	RB	0.065	—	0.058 [c]	0.017 [c]
	R6G	0.063	—	0.055 [c]	0.018 [c]
F	FDS	0.075	0.073	0.065 [d]	0.019 [d]
	DE	0.075	—	—	—
	EY	0.081	—	—	—
	EB	0.082	—	—	—
A	AO	0.069	0.067	0.061 [e]	0.015 [e]
	AY	0.071	—	—	—

a Calculated from the $\Delta M_S = \pm 2$ signal.
b Calculated from $D^* = (D^2 + 3E^2)^{1/2}$.
c Calculated by combining Eqs. (2-12a), (2-12b), (2-23b), (2-25), and (2-26) with D_2* from the $\Delta M_S = \pm 2$ signal.
d Calculated using $X_1 + X_2 + X_3 = 0$.
e Calculated from the $\Delta M_S = \pm 1$ resonance fields.

These values are also almost in agreement with the value of D^* obtained from the substitution of the values of ν and H_d in the two-quantum transition experiment into Eq. (2-29). Among the dyes examined, the values of D_2* of AR, RB, and R6G do not agree with the values already obtained in experiments conducted at high concentration in an ethanol-methanol glassy solution under mercury lamp excitation[58]. As for the values of D and D^*, the same type of dyes has almost the same values, both increasing in the order of types R, A, and F, as shown in Table 2-3. Even the largest of the values of D^* of these dyes is somewhat smaller than that of anthracene of three benzen rings. The already known fact that D^* is relatively insensitive to the replacement of hydrogen atoms in the aromatic ring[62] also suggests that the evaluated values of ZFS parameters are resonable. As to aromatic heterocycles and substituted hydrocarbons, substrituents affect to E most and to D least, but the effects are small, and usually can be attributed to increased delocalization[61]. As mentioned in subsection 2-2-1, the value of D decreases as the space available to the two π-electrons in the triplet state increases in size. Therefore, the result that the value of D^* of type R dyes is the smallest indicates that π-electrons in the T_1 state of the dyes are spatially distributed most broadly in the chromophore. As is understood from Eq. (2-13), the higher the distribution symmetry of two π-electrons along the symmetry axes perpendicular to the chromophoric plane is, the smaller the value of the parameter E is. From the result that type A dyes have the smallest value of E among the three types of dyes, π-electrons of this type of dyes are considered to have more symmetrical distribution than those of the others. This is also deduced from the fact that this type of dyes has the most symmetrical molecular structure among all the types of dyes examined.

2-4-3 Laser pumped magnetophotoselection

Experiments on the rotatable linear-polarized laser-pumped magnetophotoselection with several hundred milliwatts of power were performed for three pairs of the $\Delta M_S = \pm 1$ ESR signals that appeared in 3×10^{-4} M AO, two pairs of the signals in 1×10^{-3} M FDS, and a pair of the signals in 5×10^{-3} M RS, RB, and R6G.

The AO having the peak of the absorption band at 4900 Å was excited by the linear-polarized 4880-Å laser beam, and the FDS having the peak at 5000 Å excited by the 5145-Å one[21]. Both of these absorption bands correspond to the $S_0 \rightarrow S_1$ transitions possessing long-axis (X axis in Fig. 1-6) polarized moments. The behaviors of the low-field $H_{X_3}{}^L$, $H_{X_2}{}^L$, and $H_{X_1}{}^L$ lines corresponding to $\Delta M_S = \pm 1$ transitions were examined in the following two different cases: (a) the exciting laser beam was polarized parallel to the static magnetic field $\vec{H}$, and (b) the beam was polarized perpendicular to the field $\vec{H}$. As given in **Fig. 2-7**, the analysis of the experimental results indidates that the H_{X_2} and H_{X_3} lines in both low and high fields in the two dyes are very sensitive to the

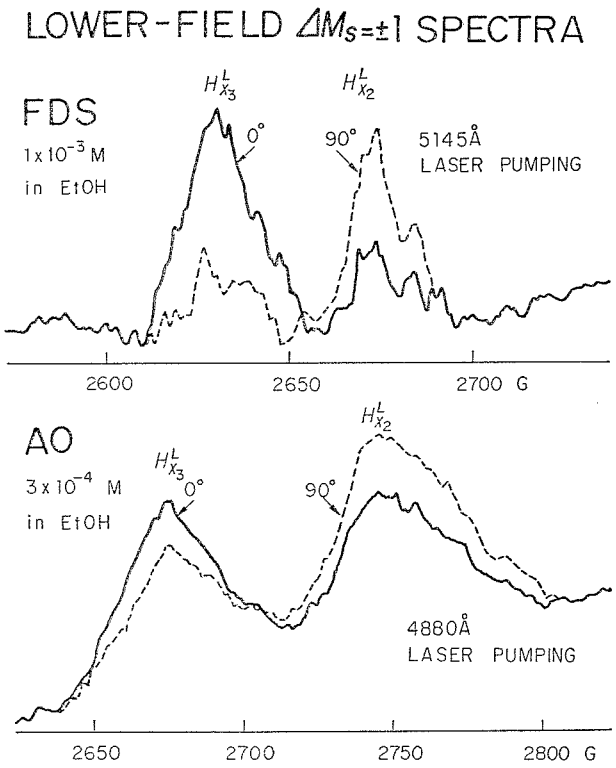

Fig. 2-7 The low-field signals $\Delta M_S = \pm 1$ ($H_{X_3}{}^L$ and $H_{X_2}{}^L$ lines) of 1×10^{-3} M FDS (5145-Å pumping) and 3×10^{-4} M AO dyes (4880-Å pumping) in ethanol with polarized excitation beam at 77 K. The solid and broken lines represent the cases of the pumping laser beams polarized parallel and perpendicular to the static magnetic field, respectively.

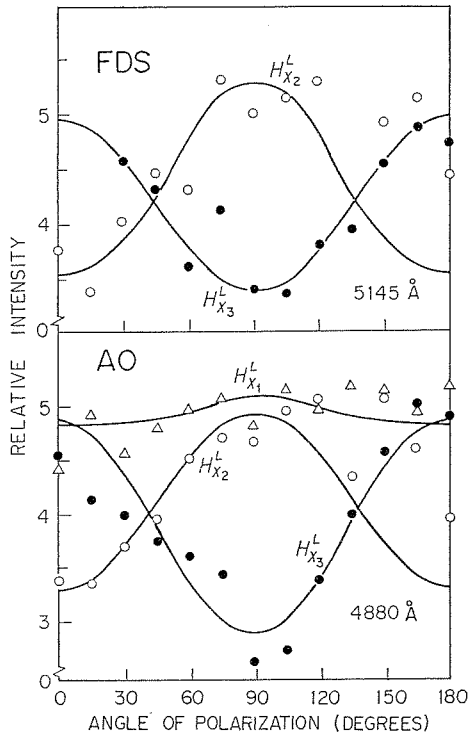

Fig. 2-8 Dependences of the relative height of the canonical peaks ($H_{X_3}{}^L$, $H_{X_2}{}^L$, and $H_{X_1}{}^L$ lines) appearing in the $\Delta M_S = \pm 1$ ESR frequency-derivative absorption lines of photo-selected FDS (5145-Å pumping) and AO (4880-Å pumping) triplet-dyes on the exciting beam polarization. The horizontal axis represents the angle between the electric field $\vec{E}$ of the incident laser beam and the applied magnetic field $\vec{H}$.

polarization directions of the exciting beam, and the H_{X_1} lines in AO are rather insensitive. When $\vec{H}$ and $\vec{E}$ (the electric field of the polarized laser beam) are parallel to each other, the H_{X_3} lines are relatively strong and the H_{X_2} lines are weak. The reverse is true when $\vec{H}$ and $\vec{E}$ are perpendicular to each other. Moreover, the variation of the signal intensity of the H_{X_3} and H_{X_2} lines with the direction of the beam polarization fits nearly to sine-sequared curves[56], and the intensities of the H_{X_3} and H_{X_2} lines show the maximum when $\vec{H} // \vec{E}$ and $\vec{H} \perp \vec{E}$, respectively, as shown in **Fig. 2-8.** These results indicate that three molecular structure symmetric axes (Fig. 1-6), one of which (X axis) the first electronic transition moments of the dyes lie along, coincide with, one another, three principal axes of the tensor describing the spin-spin interaction within 15 degrees. It is also concluded that the H_{X_3} lines appear due to the microwave absorption of the dyes having the orientation in which the X axis is parallel to the static magnetic field.

Table 2-4 Polarization ratios R_i and components r_i of the first singlet absorption bands of the FDS and AO dyes.

DYES	$H_{X_3(X)}$		$H_{X_2(Z)}$		$H_{X_1(Y)}$	
	R_{X_3}	r_{X_3}	R_{X_2}	r_{X_2}	R_{X_1}	r_{X_1}
FDS	0.50±0.04	0.95±0.14	−0.36±0.06	0	—	—
AO	0.19±0.03	0.76±0.14	−0.16±0.03	0	−0.11±0.03	0.10±0.10

The H_{X_2} lines appear due to the absorption of the dyes having the Z axis oriented along the magnetic field. Namely, H_{X_1} is assigned as H_Y, H_{X_2} as H_Z, and H_{X_3} as H_X.

Next we will obtain the component of polarization of the optical absorption transition moment r_i at 4880 Å for AO and at 5145 Å for FDS, using Eq. (2-35). It is assumed that only π-π^* transitions are involved in the absorption bands of the dyes. If we substitute the experimental values of polarization ratio R_Z (R_{X_2} given in **Table 2-4**) along the Z axis into the equation and set r_Z (r_{X_2}) equal to zero, approximate values of k_p for AO and FDS are 3.87±0.74 and 1.33±0.35, respectively. The large value of k_p for AO is considered to be mainly ascribed to the intramolecular depolarization by the vibrational relaxation and the state mixing rather than to the unexact polarized exciting beam. Furthermore, the values of the other r_i, which are calculated through the values of the other R_i and a modified form of Eq. (2-35), are given in Table 2-4. From the comparison of the values of r_X (r_{X_3}) of the two dyes, it is concluded that the polarization of the transition moment to the S_1 state along the X axis is stronger in the case of type F dyes than in the case of type A dyes. This probably corresponds to the conclusion in the previous subsection, deduced from the experimental results on ZFS parameters, that π-electrons in the T_1 state of type A dyes are spatially distributed in the chromophoric plane more broadly and symmetrically than those of type F dyes. This is also related to the simple rule, found by Drexhage in research for high efficient laser dyes, that the triplet-yield in a dye where π-electrons can make a loop when oscillating between the end groups will be higher than in a related compound where this loop is blocked[14].

Simillar experiments on the magnetophotoselection at 5145 Å were carried out for the pair of $\Delta M_S = \pm 1$ ESR signals of the three of type R dyes. But the intensity of these relatively broad signals changed hardly with the direction of the exciting beam polarization. This is possibly due to the fact that the $\Delta M_S \pm 1$ signal consists of the overlapping of the H_{X_2} and H_{X_3} lines.

2-5 Conclusions

It has been shown that the first application of a laser as a pumping source to the triplet-state ESR spectroscopy has enabled us to observe the randomly oriented triplet-state ESR spectra including weak signals such as of $\Delta M_S = \pm 1$ and double-quantum transitions and to perform the magnetophotoselection experiments of their $\Delta M_S = \pm 1$ signals in ten dyes of rhodamine (type R), fluorescein (type F), and acridine (type A). From the

observations, the dyes of the same chromophoric structure were found to have similar triplet spectra to one another in the position, width, and shape of the absorption lines, except the case of the line width affected by heavy atoms attached to the chromophore. As for the principal values X_i and the ZFS parameters D^*, D, and E, therefore, the same type of dyes have almost the same values, as shown in Tables 2-2 and 2-3. It is sufficient for theoretical analysis on the triplet ESR spectra in xanthene and acridin laser dyes to consider only the spin-spin magnetic dipole interaction between two π-electrons in the chromophore of the molecule (not those in the total moleculer structure), but as to the line width the hyperfine interaction between the π-electrons and the heavy atoms in the chromophore must be also considered.

It was also found that, the values of the ZFS parameter D and of its root-mean-spuare D^* increased in the order of types R, A and F, even the largest value of which was somewhat smaller than that of anthrancene of only three benzene rings, and in R type dyes the $H_{X_3}{}^L$ (or $H_{X_3}{}^H$) line was nearly overlapping with the $H_{X_2}{}^L$ (or $H_{X_2}{}^H$) line so that the two principal absolute values $|X_3|$ and $|X_2|$ were almost equal. Furthermore, the method of laser pumped magnetophotoselection for FDS and AO dyes showed that the principal molecular axes of the spin interaction tensor coincide with the chromophoric structural symmetric axes, one another, so that the H_{X_1} line was assigned as the H_Y line, the H_{X_2} as the H_Z, and the H_{X_3} as the H_X, and also that the polarization of the electric dipole transition moment to the S_1 state along the X axis of type F dyes was stronger than that of type A dyes. From these physical quantities concerning π-electron distribution in the excited state it can be concluded that π-electrons in the chromophore of type F dyes are the most unsymmetrically distributed and polarized along the long X axis but delocalization of π-electrons is the smallest among the three types of dyes. Those of type A dyes are the most symmetrically distributed among them and the delocalization is larger than that of type F dyes, and those of type R dyes are the most broadly distributed in the X-Y plane and the delocalization is the largest, which corresponds to the description of π-electrons in terms of mesomeric resonance structures by Drexhage[14].

Chapter 3 Relaxation Processes Related to First Excited Triplet States (T_1 States)

As for the T_1 state in laser dye molecules, we discuss the population dynamics and its relaxation processes, that is, an intersystem crossing process, triplet-to-singlet radiative and nonradiative transition processes, and an energy transfer process by a quencher. A novel and convenient method for measuring directly an intersystem crossing rate is presented. The principle of the method is based on the optical saturation of dye molecules in the T_1 state which is obtained at 77 K by using a laser excitation ESR technique. The effects of the molecular structure of dyes, of the temperature of dye solutions, and of the phase of solvents in which they are dissolved on triplet-state lifetimes are examined. Furthermore, the triplet-state quenching of rhodamine 6 G (R6G) molecules by cyclo-octatetraene (COT) molecules is indicated by direct detection of the decrease in the former molecular concentration in the T_1 state by addition of the latter molecules. Using Perrin's model it is explained in terms of triplet-triplet energy transfer by an electron exchange process.

3-1 Introduction

The main purpose of early studies on the triplet-state of organic molecules is to make clear theoretically the emmison mechanism of phosphorescence. In 1937, Jablonski suggested an energy-level scheme where three molecular states were involved, to explain phosphoresrence[63]. During the years 1943–1944 Terenin[64,65], and Lewis and Kasha[66] identified phosphorescence as radiative intercombination between the lowest excited triplet state and the singlet ground state, and shortly thereafter Lewis and Calvin[67,68] demonstrated the existence of unpaired electrons in the phosporescent state. In 1952, that a spin-orbital coupling process is responsible for intercombinations involving the metastable state was shown by the heavy-atom substituent perturbation experiments of McClue[69]. Hutchison and Mangum's characterization of the triplet state of naphthalene by first ESR studies in 1960 provided a final answer to the question[51,70].

After that, two theories of triplet-to-singlet radiationless transition which competes with phosphorescence were independently developed. Gouterman treated semiclassically the problem in which the vibrational-electronic excited molecule interacts with the time dependent oscillatory phonon field[71]. On the other hand, Robinson and Frosch developed a theory in which time-independent perturbations, caused by the relatively small Coulombic terms such as spin-orbit interaction, connect zero-order nonstationary states of the molecular system[72,73]. The two proposals stimulated further experiments on phosphorescent quantum yields and activation energies, as well as the effects of solvent-phase, inter- and intra-

molecular heavy atoms, hydrogen isotope, and temperature on triplet-state lifetimes of some polyacene molecules, using phosphorescence and ESR spectroscopy methods[10]. The relation between the radiationless transition rate and the energy separation of the zero-point vibrational levels of S_1 and T_1 states in unsubstituted hydrocarbons was explained using the latter theory[47,48,74]. But there is not yet any generally accepted interpretation of temperature effects on triplet-state lifetimes in different solvent phases such as glass, fluid, mixed crystal, and plastics[75].

Not only those unimolecular processes but also bimolecular processes which deactivate the triplet state were studied. In 1956 triplet-triplet energy transfer was first clearly demonstrated by Terenin and Ermolaev[76,77], who excited the phosphorescence of an acceptor (naphthalene) by triplet transfer from a donor (benzophenone) in rigid solution at 77 K and discussed using the model of F. Perrin[49]. Since that, energy tranfer has been theoretically discussed by Förster[78,79], Dexter[80], and Inokuti[81], and has been experimentally examined for some molecular pairs in the gas phase, in liquid and solid solutions, and in crystals by phosphorescence and ESR methods.

As it has been found out that the triplet state plays a important role in the photochemical reaction[12] because of the relatively long triplet-state lifetimes and the presence of the two unpaired electrons, the determination of the intersystem crossing rate or the triplet quantum yield has been tried by flash photolysis, chemical reaction, optical quenching and sensitizing, and ESR methods[82~88]. But their methods have some disadvantages which will be stated in the section 3-4. The variation of the intersystem crossing rate of several polyacene molectles at low temperature versus the S_1-T_1 energy gap was also theoretically discussed by applying the radiationless transition theory of Robinson and Frosch[10,47,48,74]. For laser materials such as xanthene and acridine dyes, however, the investigation on the relaxation and energy transfer processes of the triplet state and the determination of the intersystem crossing rate have been scarcely performed systematically[14,75].

On the other hand, in 1966 the first successful stimulated emmision at 7555 Å from an organic compound (chloroalminum-phthalocyanine) was obtained accidentally by Sorokin and Lankard in the experiment of the resonance Raman effect under giant-pulse ruby laser excitation[3]. In the following year, visible coherent radiation was produced by pumping a large number of dyes, among them several xanthene dyes, with the second harmonic output of ruby and neodymium lasers or short risetime flashlamps[33,89]. It was necessary to use a short risetime flashlamp because the rapid accmulation of dye molecules in the metastable triplet state presents a loss mechanism that soon prevents lasing from occurring. In 1969, Snavely and Schäfer[34] noticed that triplet-quenching by oxygen decreases the steady-state population of the triplet state in methanol solution of R6G for enough to permit lasing for over 100 μsec. In 1970 the findings were confirmed and extended by Marling[90] and Pappalardo[35], who also used unsaturated hydrocarbons, cyclooctatetraene (COT) is a typical one, as triplet quenchers.

Furthermore, CW operation was achieved by Peterson and his coworkers, by using an

Ar ion laser at 5145 Å to pump a solution of R6G in water with some detergent added[91]. In addition, ultrashort pulses were obtained in a mode-locked solid-state-laser pumped or self-mode-locking of flashlamp pumped dye-lasers[92,93].

Several hundreds of dyes today operate as laser active materials, whose wavelengths cover the whole visible spectrum with extensions into the near-ultraviolet (3400 Å) and infrared (1.175 μm)[14]. Among them, rhodamine and fluorescein types belonging to the class of xanthene dyes are the most efficient and photochemically stable which cover the wavelength region from 5000 to 7000 Å.

Dye lasers have some distinctive features in comparison with the other gas, inorganic liquid, solid-state, and semiconductor lasers. Namely, 1) It is easily tunable over a wide range frequencies and wavelengths. 2) The frequency stability of cw dye lasers is very good ($6/10^{13}$ for 25 sec.)[94]. The generation of ultrashot pulsese of unprecendentedely small pulse-widths is possible (1.5 psec)[95]. 4) Dyes can be used in the solid, liquid, or gas phases at a wanted concentration, and hence their absorption and laser gain are readily controlled. 5) The cost of organic dyes is negligibly small compared to that of solid-state lasers.

But the efficiency and the lifetime of dye lasers are limited by the triplet state and the photodegradation of dye molecules, respectively[5,6]. In this chapter we describe only the loss mechanisms due to the triplet state, while as for the poor photochemical stability we shall discuss in the next chapter. The population of T_1 state is increased at the expense of the molecules in the S_1 state that contribute to the laser action, which is called intersystem crossing loss. Furthermore, the dye molecules in T_1 states are excited to higher energy triplet-state by absorbing the pumping laser power, which is called optical losses[5,29,30]. It is necessary for us to find out the dye lasere materials where the values of the intersystem crossing rate and of the tiplet-state lifetime are so small that those losses are negligible. One of the most important developments in dye lasers now is to synthesize new laser dyes having good performance[14].

This chapter is intended to gain some insight into the relation between the molecular structure and the relaxation and quenching processes involving the triplet state of xanthene and acridine laser dyes[24~27]. In addition, a novel method for directly measuring the intersystem crossing rate of a molecule of high fluorescence and low triplet yield such as laser dyes is presented[24]. Those knowledges will be available for not only the planned syntheses of special laser dyes but also clarification of photochemical kinetics and of relaxation and quenching mechanisms of dye molecules in T_1 states.

3-2 Rate Equation Analysis of Population Dynamics in the T_1 State

A few of dye molecules excited to the S_1 state by laser light decay to the T_1 state by an intersystem crossing The molecules in the T_1 state return to the S_0 state at a rate very much smaller than that of the strong fluorescence transition. Therefore, as the power of the pumping laser light increases many dye molecules accumulate in this T_1

state and are at equilibrium.

The rate equation describing the population dynamics of the excited singlet S_1 stase[96] is

$$\frac{dN_1}{dt}=\frac{\sigma_p}{h\nu_p}N_0 I-\left(\frac{1}{\tau_S}+K_{IC}\right)N_1-K_{ST}N_1, \tag{3-1}$$

where $h\nu_p$ and σ_p are the quantum energies and the singlet absorption cross section at the pumping frequency ν_p, respectively, I is the power per unit area of the pumping laser light, N_1 and N_0 are the molecular concentrations of the lowest vibrational levels of the S_1 and S_0 states, respectively. The first term represents the number per unit time of the molecules excited to the S_1 state by the laser light. The second term represents the number per unit time of the molecules which return from the S_1 state to th S_0 state by fluorescence and internal conversion. The last term represnts the number per unit time of the molecules which which decay from the S_1 state to the T_1 state by an intersystem crossing. The rate equation for the T_1 state[96] is

$$\frac{dN_T}{dt}=K_{ST}N_1-(K_T{}^r+K_T{}^{nr})N_T, \tag{3-2}$$

where the effect of a T-T absorption is neglected. The first term is corresponding to the above mentioned last term, and the second term represents the number per unit time of the molecules which very slowly decay from the T_1 state to the S_0 state by phosphorescence and radiationless relaxation. The decay constant $\tau_T=1/(K_T{}^r+K_T{}^{nr})$ is a triplet-state lifetime. If suitable triplet-state quenchers are added to the dye solution at room temperature, the triplet-state lifetime τ_T in the last term are effectively shortened by a collisional energy-transfer from dye molecules in the T_1 state to the quenchers. Conservation of the number of molecules requires that

$$N_0+N_1+N_T=N, \tag{3-3}$$

where N is the total molecular concentration. Using Eqs. (3-1), (3-2), and (3-3) under steady-state conditions with continuous constant excitation, we obtain the following equation for the molecular concentratin in the T_1 state[24]

$$N_T=\frac{\tau_S\tau_T K_{ST}N(\sigma_p/h\nu_p)I}{1+\tau_S(\tau_T K_{ST}+1)(\sigma_p/h\nu_p)I}, \tag{3-4}$$

where we assume $1/\tau_S \gg K_{IC}$, which is reasonable in the case of the molecules such as laser dyes having a high fluorescent quantum yield. This equation shows that the population of T_1 state approaches the optical saturation region as pumping power of the laser is increased. This phenomena will be experimentally verified in the section 3-4.

In the next section we will try to describe theoretically each of the rate constants of the processes involving the triplet state.

3-3 Theories on Electronic Transitions and Energy Transfer Involving the T_1 state

3-3-1 Triplet-to-Singlet ($T_1 \rightarrow S_0$) Radiative Transitons

Triplet-singlet transitions are spin-forbidden, and the occurrence of the electric dipole transition moment is due to spin-orbit coupling between the wave functions of the singlet and triplet states. Due to such interactions triplet states acquire a small component of singlet character, and singlet states acquire a small component of triplet character. Then we will begin with to describe theoretically spin-orbit interactions in aromatic molecules, which were originally discussed by McClue[69] and were reviewed by Hameka[46,61,97]. A more detail treatment has been given recently by McGlynn, Azumi, and Kinoshita[22].

In the absence of an external field, the full form of the total spin-orbit Hamiltonian $\mathcal{H}_{so}$[61] is given by

$$\mathcal{H}_{so}=\frac{e^2}{2m^2c^2}\left[\sum_{K=1}^{N}\sum_{i=1}^{n}\frac{Z_K}{r_{iK}^3}(\vec{l}_i\cdot\vec{s}_i)\right.$$
$$\left.-\sum_{i=1}^{n}\sum_{j\neq i}^{n}\frac{1}{r_{ij}^3}(\vec{p}_i\times\vec{r}_{ij})\cdot\vec{s}_i+2\sum_{i=1}^{n}\sum_{j\neq i}^{n}(\vec{p}_j\times\vec{r}_{ij})\cdot\vec{s}_i,\right] \tag{3-5}$$

where l_i, s_i and p_i are the orbital, spin, and linear angular momentum operators of the i-th electron, r_{iK} and r_{ij} are the distances between the i-th electron and the K-th nucleus and between the i-th and j-th electrons, respectively, and eZ_K is the electric charge on the K-th nucleus. The first term in the bracket represents the coupling between orbital and spin motions of electron i caused by the nuclear attractive electrical field of Z_K; it is a one-electron operator. The second term represents the coupling between orbital and spin motions of electron i caused by the repulsive electical fields of all electrons other than i; it is a two-electron operator. The third term represents the coupling between the spin motion of one electron and the orbital motion of another electron caused by magnetic fields due to relative orbital motion of the two electrons, this is two-electron operator; it is called spin-other-orbit coupling and is normally very small. The first and second terms are usually lumped together by replacing the electic field of nucleus K at electron i by an effective electrical field of spherical symmetry Z_K(eff), where Z_K(eff) is supposed to be given by Slater's recipe[98]; namely, all electrons other than i are supposed to merely shield the centrosymmetric nuclear field from electron i. The third is neglected altogether[99]. With these suppositions and with extension to a polynuclear case, Eq. (3-5) reduces to the commonly used form

$$\mathcal{H}_{so}=\frac{e^2}{2m^2c^2}\sum_{K=1}^{N}\sum_{i=1}^{n}\frac{Z_K(\text{eff})}{r_{iK}^3}\vec{l}_i\cdot\vec{s}_i. \tag{3-6}$$

This equation shows that the larger the nuclear charge the larger is the magnetic field produced by its seeming orbital motion and hence also the larger is the spin-orbit coupling. This is called a heavy atom effect.

Secondly we describe the singlet and triplet electronic wavefunctions performed by

spin-orbit interactions, which is necessary for calculation of the electric dipole transition moment between T_1 and S_0 states. Let ${}^1\Psi_m{}^e$ be the unperturbed pure singlet electronic wavefunction of the S_m state in the absence of the spin-orbit coupling, and ${}^3\Psi_k{}^e$ that of the T_k state. Correspondingly, let $E_{1,m}{}^e$ and $E_{3,k}{}^e$ be the respective zero-point energies of the singlet and triplet states. According to the first-order perturbation theory, the wavefunctions are perturbed by the spin-orbit interaction $\mathcal{H}_{so}$ as follows:

$$ {}^1\Psi_0{}^{e\prime} = {}^1\Psi_0{}^e - \sum_{m>0} \frac{<{}^1\Psi_m{}^e|\mathcal{H}_{so}|{}^1\Psi_0{}^e>{}^1\Psi_m{}^e}{(E_{1,m}{}^e - E_{1,0}{}^e)} $$

$$ - \sum_k \frac{<{}^3\Psi_k{}^e|\mathcal{H}_{so}|{}^1\Psi_0{}^e>{}^3\Psi_k{}^e}{(E_{3,k}{}^e - E_{1,0}{}^e)}. \tag{3-7} $$

The second term, which does not affect the spin multiplicity, can be neglected in comparison with ${}^1\Psi_0{}^e$. The third term introduces a component of triplet character into the S_0 wavefunction, which can be written as

$$ {}^1\Psi_0{}^{e\prime} \cong {}^1\Psi_0{}^e - \sum_k c_k {}^3\Psi_k{}^e. \tag{3-8} $$

The magnitude of each c_k ${}^3\Psi_k{}^e$ term depends inversely on the energy gap $(E_{3,k}{}^e - E_{1,0}{}^e)$ and on the symmetry of ${}^3\Psi_k{}^e$ relative to ${}^1\Psi_0{}^e$. The perturbed wavefunctions of each of the three components of T_1 states are of the form

$$ {}^3\Psi_1{}^{e\prime} = {}^3\Psi_1{}^e - \sum_{k>1} \frac{<{}^3\Psi_k{}^e|\mathcal{H}_{so}|{}^3\Psi_1{}^e>{}^3\Psi_k{}^e}{(E_{3,k}{}^e - E_{3,1}{}^e)} $$

$$ - \sum_m \frac{<{}^1\Psi_m{}^e|\mathcal{H}_{so}|{}^3\Psi_1{}^e>{}^1\Psi_m{}^e}{(E_{1,m}{}^e - E_{3,1}{}^e)} \tag{3-9} $$

$$ \cong {}^3\Psi_1{}^e - \sum_m d_m {}^1\Psi_m{}^e. \tag{3-10} $$

The second term in Eq. (3-9), which does not change the spin multiplicity, can be neglected.

The $T_1 \rightarrow S_0$ phosphorescence transition probability $K_T{}^r$ is proportional to the square of the electric dipole transition moment $M_{T_1S_0}$, where

$$ \vec{M}_{T_1S_0} = <{}^3\Psi_1{}^{e\prime}\left|\sum_{i=1}^{n} \vec{er}_i\right|{}^1\Psi_0{}^{e\prime}> $$

$$ = -\sum_m d_m <{}^1\Psi_m{}^e\left|\sum_{i=1}^{n} \vec{er}_i\right|{}^1\Psi_0{}^e> - \sum_k c_k <{}^3\Psi_1{}^e\left|\sum_{i=1}^{n} \vec{er}_i\right|{}^3\Psi_k{}^e> $$

$$ = -\sum_m d_m \vec{M}_{S_mS_0} - \sum_k c_k \vec{M}_{T_1T_k}, \tag{3-11} $$

where the summation is carried out over all the electrons i. Terms like $<{}^3\Psi_1{}^e\left|\sum_{i=1}^{n} er_i\right|{}^1\Psi_0{}^e>$ vanish because of spin orthogonality. Eq. (3-11) gives rise to the following important conclusion: the phosphorescence is an emission having an energy equal to the difference in energy between the S_0 and T_1 states, but having polarization characteristics identical with those of the perturbing transition $S_m \leftrightarrow S_0$ and $T_k \leftrightarrow T_1$. In general, the effect of spin-orbit coupling is to introduce components of different spin-multiplicity and different

symmetry, but of the same parity as the original unperturbed wavefunctin because the space part of the spin-orbit coupling operator is of even parity.

In the molecular-orbital approximation[22] the spin-orbit matrix element $<{}^3\Psi_k^e|\mathcal{H}_{so}|{}^1\Psi_m^e>$ reduces to the evaluation of a *MO*-integral of the form $<\varphi_t|\mathcal{H}_{so}|\varphi_s>$ where φ_t and φ_s are the only two *MO*'s which are the two different configurational wavefunctions assumed representative of the states ${}^3\Psi_k^e$ and ${}^1\Psi_m^e$, because the matrix elements between the same *MO*'s are zero owing to the effect of the angular momentum operator on carbon *p*-atomic orbitals. Therefore, for example, the spin-orbit mixes ${}^3\Gamma_{\pi\pi^*}$ states (correspond to φ_t) with ${}^1\Gamma_{n\pi^*}$ states (correspond to φ_s) and vice versa, and ${}^3\Gamma_{n\pi^*}$ states with ${}^1\Gamma_{\pi\pi^*}$ states and vice versa. In dye molecules having nearly C_{2v} symmetry, the transition ${}^3\Gamma_{\pi\pi^*}$ (T_1) state $\leftrightarrow{}^1A_1$ (S_0) state steals transition probability from spin-allowed $\pi^*\leftrightarrow n$ transitions[22,23]. It is found experimentally that the transition probability of an allowed $\pi^*\leftrightarrow n$ excitation is roughly $10^2\sim10^3$ times less than that of an allowed $\pi^*\leftrightarrow\pi$ transition[22]. Consequently, if both triplet-states contain equal admixtures of singlet character, we can expect that the probability of the transition ${}^3\Gamma_{\pi\pi^*}\leftrightarrow{}^1A_1$ is approximately $10^2\sim10^3$ times less than the probability of the transition ${}^3\Gamma_{n\pi^*}\leftrightarrow{}^1A_1$. Taking the calculated radiative lifetime of the latter type of transitions to be 10^{-3} sec, we estimate the radiative lifetime of ${}^3\Gamma_{\pi\pi^*}$ states of dyes such as acridine and xanthene classes to be in the range 0.1$\sim$1 sec.

3-3-2 Radiationless Transitions

A. General theory

Various approaches have been made to the theory of radiationless transitions. In this thesis, however, we describe only the most popular theory developed by Robinson and Frosch[72,73] who have treated the case where the radiationless transition rate is determined by intramolecular interations, the role of the medium such as a solvent being restricted to that of a source or sink of thermal energy. The approach in which time-independent perturbations caused by the relatively small Coulombic terms such as spin-orbit interaction connect zero-order nonstationary states of the molecular system, is based on vibrational overlap or Franck-Condon factors.

In the Born-Oppenheimer approximation[22], the hamiltonian of a molecule is separated into an approximate electronic part $\mathcal{H}_o^e$ and a nuclear part $\mathcal{H}^N$, and the electronic energy levels $E_i^e(Q)$ and wavefunctions $\Psi_i^e(q,Q)$ corresponding to $\mathcal{H}_o^e(q,Q)$ are calculated assuming that the nuclei are stationary. Here, $\mathcal{H}_o^e(q,Q)$ represents kinetic energy of electrons and Coulomb's energies between electrons and nuclei and between electrons themselves, and $\mathcal{H}^N(Q)$ represents kinetic energy of nucleus and Coulomb's energy between nuclei themselves in a molecule[22]. And q and Q represent collections of electronic and nuclear coordinates, respectively, and were not explicitly considered in the previous chapter (Eq. (2-2)).

$$\mathcal{H}_o^e(q,Q)\Psi_i^e(q,Q)=E_i^e(Q)\Psi_i^e(q,Q). \tag{3-12}$$

The distances between nuclei and electrons can be varied in a manner consistent with

the maintainance of the symmetry of some symmetric vibrational mode of the molecule. Thus, the electronic levels and wavefunctions can be conputed at various value of Q. Then, corresponding to the total molecular hamiltonian $\mathscr{H}_o^e(q, Q)+\mathscr{H}^N(Q)$, one can write

$$\Psi_{ij}^T(q, Q)=V_{ij}(Q)\Psi_j^e(q, Q), \tag{3-13}$$

where the vibrational-electronic wavefunction $\Psi_{ij}^T(q, O)$ is a simple product of an electronic part, $\Psi_j^e(q, Q)$, and a nuclear part $V_{ij}(Q)$. The vibrational-electronic energies E_{ij} and vibrational wavefunctions $V_{ij}(Q)$ are obtained by solution of the hamiltonian

$$[\mathscr{H}^N(Q)+E_j^e(Q)]V_{ij}(Q)=E_{ij}V_{ij}(Q). \tag{3-14}$$

Even though the vibrational wavefunction $V_{ij}(Q)$ does not depend on the electronic coordinates, it is neverthless dependent on the electronic state—hence the subscript j on $V_{ij}(Q)$. In other words, each electronic state has its own set of vibrational energies and wavefunctions.

We consider a molecule interacting with a solvent at low temperatures. The electronic states of the system for fixed nuclei are Ψ_{lo}^e and Ψ_{up}^e with $E_{lo}^e<E_{up}^e$, and with corresponding vibrational states $V_{lo}(E_i)$ and $V_{up}(E_i')$, where E_i (or E_i') is the vibrational energy measured relative to the zero-point energy E_{lo}^e (or E_{up}^e), respectively. Initially the system is in the state $\Psi_{up}^eV_{up}(0)$, which is an exact eigenstate in the Born-Oppenheimer approximation. If we go beyond this approximation due to intramolecular or solute-solvent interactions, there is a non-zero matrix element of the form

$$H_{lo,up}=<\Psi_{lo}^eV_{lo}(E_i)|J_N|\Psi_{up}^eV_{up}(0)>, \tag{3-15}$$

where J_N is a nuclear kinetic energy operator (a perturbing hamiltonian). $H_{lo,up}$ is negligible, except when $E_i\cong E_{up}^e-E_{lo}^e$. The radiationless transition is envisioned to occur as a result of weak time-independent coupling of the initial level to a near-resonance band of strongly coupled final states. If the solvent causes rapid vibrational relaxation in Ψ_{lo}^e, the transition is irreversible. Once the transiton to the quasi-continuum of final states occurs, fast vibrational relaxation prevents the back transition to the initial state. In polyatomic molecules where one has a large number of states $\Psi_{lo}^eV_{lo}(E_i)$ and these are broadened by solvent interactions, they merge into a continuum of state density $\rho_{E_i}^s$. The radiationless transition probability per unit time is then given by

$$K_{lu}^{nr}=\frac{4\pi^2\rho_{E_i}^s}{h^2}|H_{lo,up}|^2. \tag{3-16}$$

$H_{lo,up}$ can be separated into electronic and vibrational components, by writing

$$\begin{aligned}
&H_{lo,up}=J_{lo,up}S_{lE_i,up}\\
&J_{lo,up}=<\Psi_{lo}^e|J_N|\Psi_{up}^e>\\
&S_{lE_i,uo}=<V_{lo}(E_i)|V_{up}(0)>.
\end{aligned} \tag{3-17}$$

Eq. (3-16) thus becomes

$$K_{lu}{}^{nr}=\frac{4\pi^2\rho_{Ei}{}^{s}}{h^2}|J_{lo,up}|^2|S_{lEi,uo}|^2=P_d\,C_{lu}F_{lu}, \tag{3-18}$$

where $P_d=4\pi^2\rho_{Ei}{}^{s}/h^2$ is the density of state factor, $C_{lu}=|J_{lo,up}|^2$ is the electronic factor, and F_{lu} is the Franck-Condon factor describing the overlap of the continuum of vibrational states $V_{lo}(E_i)$ with $V_{up}(0)$. This vibrational overlap factor is generally much smaller than unity except in the region of crossing of the potential energy surfaces where it is equal to unity. Such overlap is favored by high-amplitude vibrational manifolds associated with the molecule itself (the intramolecular vibrational relaxation) or the system of molecule-puls-environment (the intermolecular relaxation including structure mobility). Intramolecular vibrations involving hydrogen atoms are predicted to be especially active in high-amplitude vibrations, and the lower-amplitude vibrations of the heavior deuterium atoms should be less effective in facilitating radiationless decay. The hydrogen vibrational relaxation is, in a first approximation, independent of temperature and solvent viscosity.

B. Singlet-to-triplet ($S_1 \rightarrow T_1$) intersystem crossing[10]

Singlet-to-triplet intersystem crossing can occur either from the zero-point vibrational level of the S_1 state or from thermally-populated vibrational levels of the S_1 state. It may occur either into an excited vibrational level of the T_1 state or into a higher excited triplet state T_m which is closer in energy to the S_1 state.

We consider the case where there is no intermediate triplet state T_m between the S_1 and T_1 states. If we apply the above-mentioned radiationless transition theory to the intersystem crossing from the S_1 states to the T_1 states, from Eq. (3-18) the intersystem crossing rate $K_{ST}{}^{\circ}$ is

$$K_{ST}{}^{\circ}=P_d C_{ST}F_{ST}. \tag{3-19}$$

The electronic factor C_{ST} for the spin-forbidden intersystem crossing arises from spin-orbit coupling. The spin-orbit coupling of the S_1 states to the T_1 states is greater than that of the S_0 state because of the reduction in the inter-state energy gaps. For a series of aromatic hydrocarbons $K_{ST}{}^{\circ}$ decreases rapidly with increase in the S_1-T_1 energy separation i. e. with increase in the vibrational quantum number n of an excited vibrational level of the T_1 state which has the same energy as the zero-point vibrational level of the S_1 state. But, $K_{ST}{}^{\circ}$ is increased by introducing an atom of sufficiently high atomic number for the spin-orbit coupling to become important (heavy atom effect), or by intro ducing a paramagnetic molecule into the system. Furthermore, perdeuteration of the molecule reduces $K_{ST}{}^{\circ}$ due to the reduction of the Franck-Condon factor F_{ST}.

The temperature-independent parameter $K_{ST}{}^{\circ}$ is the rate of intersystem crossing from the zero-point vibronic level of the S_1 state. The intersystem crossing rate above a critical temperature K_{ST} increases with temperature, and is described by the frequency factor $K_{ST}{}'$ and the active energy W_{ST}

$$K_{ST}=K_{ST}{}^{\circ}+K_{ST}{}'\exp(-W_{ST}/kT). \tag{3-20}$$

The simplest model of this behavior is to assume a higher triplet state, T_m, at an energy

of W_{ST} above the S_1 state. Thermal activation of the molecule through the energy gap W_{ST} brings the molecule to a vibronic level of the S_1 state which is isoenergetic with the T_m state. Then, intersystem crossing from the vibronic level of the S_1 state to the T_m state occurs at a rate of K_{ST}. The temperature-dependent component is due to solvent collisional perturbation, and its magnitude depends on both the solute and solvent molecules.

C. Triplet-to-singlet ($T_1 \rightarrow S_0$) nonradiative transitions

The T_1–S_0 radiationless transition occurs from the zero-point vibrational state of T_1 state to isoenergetic vibrational states of S_0 state; in many cases at room temperasure the T_1–S_0 nonradiative rate $K_T{}^{nr} \gg K_T{}^r$ the competing radiative phosphorescent rate.

According to the Siebrand analysis[47,48,74] where the above-mentioned radiationless transition theory was applied to the $T_1 \rightarrow S_0$ nonradiative rate, from Eq. (3-13) the rate in unsubstituted hydrocarbons can be written as

$$K_T{}^{nr} = P_d C_{T_1} F_{T_1}. \tag{3-21}$$

Assuming that $P_d C_{T_1}$ is constant for this class of compounds under common conditions of solvent and temperature, we find that the relative values of $K_T{}^{nr}$ are determined solely by the Franck-Condon factor F_{T_1}. In the general case where there are N normal modes, the Franck-Condon factor is

$$F_{T_1} = \sum_P P\left[\prod_{n=1}^{N_m} |\langle V_{lo,n}(v_n) | V_{up,n}(0)\rangle|\right]^2, \tag{3-22}$$

where $V_{lo,n}$ and $V_{up,n}$ are the vibrational wavefunctions of mode n in the final and initial states, respectively, and v_n is the vibrational quantum number of mode n. The operator $\sum_P P$ permutes the vibrational quanta v_n among the N_m normal modes, subject to the energy-conservation condition

$$\sum_n v_n \hbar\omega_{lo,n} = E_{T_1} \pm \rho_E{}^s/2, \tag{3-23}$$

where $\omega_{lo,n}$ is the angular frequency of mode n in the final vibrational state, E_{T_1} is the energy separation of the zero-point levels of S_0 and T_1 states, and $\rho_E{}^s$ is the state density, defined as the reciprocal width of a single vibrational level. The density of states is sufficiently large that F_{T_1} has no vibrational structure for large $\sum_n v_n$, so that under these conditions F_{T_1} is a monotonically decreasing function of the energy E_{T_1}. As observed experimentally for both the protonated and deuterated compounds, evaluation of this factor $F_{T_1}(E)$ for a non-degenerate harmonic oscillator which is displaced and distorted gives exponentially decreasing dependence of $K_T{}^{nr}$ on E_{T_1}/η, where η is the relative number of hydrogen atoms in the compound to take account of structural differences. $F_{T_1}(E)$ at $E > E_{oc}$ is dominated by anharmonic distortions of CH- (or CD-) streching modes of the ground-state molecule, and it at $E < E_{oc}$ is mainly due to totally symmetric CC-streching vibrations of the ground state, where E_{oc} represents the crossing-point determined by the relation $v\hbar\omega_{lo} = E - E_{oc}$.

Like the case of temperature dependence of an intersystem crossing rate, when the environment seen by a molecule is changed by varing the temperature of a glassy solvent in which it is dissolved, it has been found that the triplet-state lifetime $\tau_T=1/(K_T^r+K_T^{nr})$ is constant until a critical temperature is reached at which τ_T decreases exponentially. The observed lifetime can be expressed in the form,

$$1/\tau_T=1/\tau_T^\circ+A\exp(-\Delta E_T/kT). \qquad (3\text{-}24)^{75)}$$

By contrast, in a plastic medium over the same temperature region the lifetime decreases only slowly with increasing temperature[62]. An entirely satisfactory theory on the temperature effect of triplet-state lifetimes of organic molecules in solvent is not yet established[101].

3-3-3 Triplet-Triplet Energy Transfer in Rigid Solutions

The term energy transfer is used to describe the transfer of the electronic excitation energy of an aromatic molecule to another molecule of a different species. We consider only intermolecular energy transfer occurring by a radiationless process, due to interaction between the donor and acceptor molecules during excitation lifetime of the donor, prior to its emission of a photon. Radiationless transfer due to Coulombic dipole-dipole interaction takes place over intermolecular distances (20~60 Å) which are large compared with the molecular diameter (~6 Å), and that due to electron exchange interaction over distances (6~15 Å) somewhat larger than the molecular diameter. Singlet-triplet and triplet-triplet transfers due to the former are normally negligible, because of the low S_0-T_1 transition moment of the acceptor. The latter transfer also can be distinguished from collisional processes, when their processes are inhibited in rigid or viscous systems. But, the conditions for electron-exchange transfer are similar to those for collisional transfer, namely short-range interaction between the donor and acceptor molecules and spin conservation in the transition. Triplet-triplet transfer can occur collisionally or by electron exchange intraction.

Triplet-triplet energy transfer was first clearly demonstrated by Terenin and Ermolaev[76, 77], who excited the phosphorescence of an acceptor (naphthalene) by triplet transfer from a donor (benzophenone) in rigid solution at 77 K. The energy E_{ex} of the exciting light and the S_1 states energies, $E_{S_1}{}^D$ and $E_{S_1}{}^A$, of the donor D_0 and acceptor A_0 molecules were chosen such that

$$E_{S_1}{}^A>E_{ex}>E_{S_1}{}^D. \qquad (3\text{-}25)$$

So that only the donor molecules were excited initially. The triplet excitation energies, $E_{T_1}{}^D$ and $E_{T_1}{}^A$, of D_0 and A_0 were such that

$$E_{T_1}{}^D-E_{T_1}{}^A=\Delta_{T_1}>0, \qquad (3\text{-}26)$$

thus providing the energy condition for triplet-triplet transfer following $D_{S_1}\rightarrow D_{T_1}$ intersystem crossing. The observed increase in the A_{T_1} phosphorescence intensity with acceptor concentration N_A and the simultaneous quenching of the D_{T_1} phosphorescence

intensity gave clear evidence for the process,

$$D_{T_1}+A_0 \rightarrow D_0+A_{T_1}. \tag{3-27}$$

After that, Smaller and his coworkers[102] studied triplet-triplet transfer from phenanthrene $-d_{10}$ to naphthalene-d_8 by observing the decrease of the donor triplet concentration $N_T{}^C$ and the increase and decrease of the acceptor triplet concentration, by th ESR technique after flash excitation.

The static quenching of the donor triplet concentration by triplet-triplet energy transfer is described by the active sphere model. In 1924 Parrin[49], in discussing concentration quenching, introduced the concept of the "active sphere", a volume of interaction around a quencher molecule A_0 such that a triplet-molecule D_{T_1} excited within this volume is quenched instantaneously, while triplet-molecules excited outside this volume are unquenched. This provides a model of static quenching which does not require the formation of a bound complex between D_0 and A_0 in ground state. If v is the volume (in cm^3) of the active sphere of each quencher molecule and $n_A=N_A\times N_{AV}\times 10^{-3}$ is the number of quencher molecules in unit volume ($1\,cm^3$), the probability that a triplet-molecule D_{T_1} will lie within an active sphere is

$$\rho=e^{-n_A v} \tag{3-28},$$

where N_A is the molecular concentration of quenchers, and N_{AV} is an Avogadoro number (6.02×10^{-23}). Hence on excitation the static quenching of the triplet-molecule is

$$N_T{}^C/N_T=\exp\left[-\frac{4}{3}\pi R_0{}^3 N_{AV}{}' N_A\right] \tag{3-29},$$

where R_0 is the critical radius in ångströms of the active sphere v and $N_{AV}{}'=6.02\times 10^{-4}$. The electron-exchange tranfer distance R_0 is of the order of the van der Waals' dimensions of the molecule (12~13 Å).

The magnitude of the electron-exchange interaction depends on the overlap of the vibronic wavefunction, $V_D(E_i)$ and $V_A(E_i')$, of the donor and acceptor molecules. The transfer probability by electron-exchange interaction was expressed by Dexter[80] in the form

$$K_{AD}\propto\frac{2\pi}{\hbar}L^2\int_0^\infty P_D(\nu)\varepsilon_A(\nu)d\nu, \tag{3-30}$$

where $P_D(\nu)$ is the donor emission spectrum, $\varepsilon_A(\nu)$ is the acceptor absorption spectrum, and L^2 is a parameter which cannot be directly related to optical parameters. Although electron-exchange interaction depends on overlap of spectrum or wavefunction, it differs from Coulombic interaction and radiative transfer in that it is independent of the optical transition moments.

3-4 A Novel Method for Measuring Intersystem Crossing Rates

3-4-1 Principle of the Method

Betides the nonradiative decay directly to the ground state, a dye molecule excited to the S_1 state relaxes to the lowest T_1 state. This process proceeds at a rate designated as an intersystem crossing rate constant K_{ST}, which is comparatively slow considering the small energy gap between S_1 and T_1 states, being a spin-forbidden process. We define the triplet quantum yield q_{ST} as the ratio of the number of molecules excited into the T_1 state to the number of molecules excited into the S_1 state (the number of absorbed photons), and it is given by

$$q_{ST}=K_{ST}/(1/\tau_S+K_{ST}+K_{IC}). \tag{3-31}$$

The determination of the intersystem crossing rate constant or the triplet quantum yield is important not only in evaluation of many of the other rate constants for the compex photochemical processes[12], but also in the study to improve the performance of dye lasers. But, its experimental determination has been difficult because of the so-called "dark" process.

Several techniques have been developed to determine the quantum yields for population of the T_1 state or the intersystem crossing rate, but most of them are indirect ones. That is, the triplet-yield of a molecule-solution system was determined by measuring the amount of products produced due to the chemical reaction between the molecules in the T_1 state and additives[83,85], or by measuring the change of a rate of an optical transition process occurring in additives due to the interaction between their molecules and the additives[84,86] when the additives were added to the system. So long as one uses the indirect methods, he has to always rely at any stage on knowledges of a rate constant in a related but low-fluorescence-yield additive and he cannot determine the triplet-yield of such a molecule that the molecules in the T_1 state does not interact with the additives. Because of such disadvantages in spite of many efforts, only a very limited number of molecules having a high triplet-yield or a low fluorescence-yield have been examined[10].

Recently, Webb and his coworkers have determined directly the intersystem crossing rate constant of R6G in an air saturated ethanol solution during laser action, by comparison between flashlamp-excitation threshold-energies measured as a function of lasing wavelength and an equation describing their relation[10]. But, this method also has the faults that it cannot be applied to any molecules except dye molecules as laser media and needs the informations of the wavelcngth-dependence of T-T absorption extinction and of stimulated emission cross sections which are not easily obtained.

Now we will describe a new method[24] for measuring directly the intersystem crossing rate using a laser excited ESR technique. This method can be applied to any molecules, only if the $H_{\min}$ line in the T_1 state of the molecules, whose signal is in general strong, is observed. The Eq. (3-4) derived in the section 3-2 describes the relation between the concentration of molecules excited to the T_1 state by the laser light and its excitation

power. Multiplying the terms in both sides of the equation by a constant number a, we obtain the modified equation under the assumption $\tau_T K_{ST} \gg 1$

$$N_T' = \frac{a\tau_S \tau_T K_{ST} N(\sigma_P/h\nu_P)I}{1+\tau_S \tau_T K_{ST}(\sigma_P/h\nu_P)I}, \tag{3-32}$$

where $N_T' = aN_T$. As was pointed out earlier, this equation shows that the molecules from the S_1 state begin to be saturated in the metastable T_1 state by an intersystem crossing process as the pumping laser power is increased. The reciprocal of this equation as a function of the pumping laser power I is as follows

$$1/N'_T = A/I + B, \tag{3-33}$$

where $A = 1/[\tau_S \tau_T K_{ST}(\sigma_P/h\nu_P)aN]$ and $B = 1/aN$. Then, the investigation on the variation of $1/N_T'$ as a function of $1/I$ enables us to determine the values of A and B from the slope and the intercept in its linealy plotted graph, respectively. Therefore, the intersystem crossing rate constant K_{ST} is given by the equation

$$K_{ST} = B/[\tau_S \tau_T(\sigma_P/h\nu_P)A]. \tag{3-34}$$

The N'_T is experimentally obtained by measuring the intensity of the $H_{\min}$ line, corresponding to the $\Delta M_S = \pm 2$ ESR transition in the T_1 state[41], during laser excitation with the power I per unit area. Now we will describe the experimental procedure for measuring the intersystem crossing rate constant of R6G molecules which are a typical dye laser medium.

3-4-2 Experimental Procedure and Results

The preparation of the sample solution and the experimental arrangement to examine the dependence of the signal intensity of the $H_{\min}$ line in the T_1 state of R6G molecules on the pumping laser power, are nearly indentical to those we described in the previous chapter. The dependence under excitation by an unfocused and circular polarized 5145-Å beam of the Ar ion laser was examined at 77 K for different concentrations (4×10^{-5}, 1×10^{-4}, 4×10^{-4}, 1×10^{-3}, and 5×10^{-3} M) of R6G molecules in ethanol and for the sample tubes with different diameters (2.5 and 4.5 mm i.d.). The observed saturation curves for the concentration of the R6G molecules in the T_1 state, which is proportional to the absorption intensity of the $H_{\min}$ line, are shown in **Fig. 3-1 a~c.** From these curves we find that the molecular concentration in the T_1 state for R6G solutions from 4×10^{-5} to 1×10^{-3} M in 2.5 mm i.d. tubes begins to be saturated above 1.5 W/cm², but for the highly concentrated 5×10^{-3} M solution the triplet concentration begins to be saturated above 6 W/cm². The difference is possibly caused by the fact that in the latter case not all the R6G molecules are homogeneously excited by the laser light since only some molecules near the irradiated surface of the sample tube absorb most of the laser power. Therefore, we should use the sample solution of lower concentration than that of the 5×10^{-3} M concentration to examine the optical saturation curve. In Fig. (3-1c), the saturation curve for 5×10^{-3} M R6G samples in the quartz tubes with different diameters

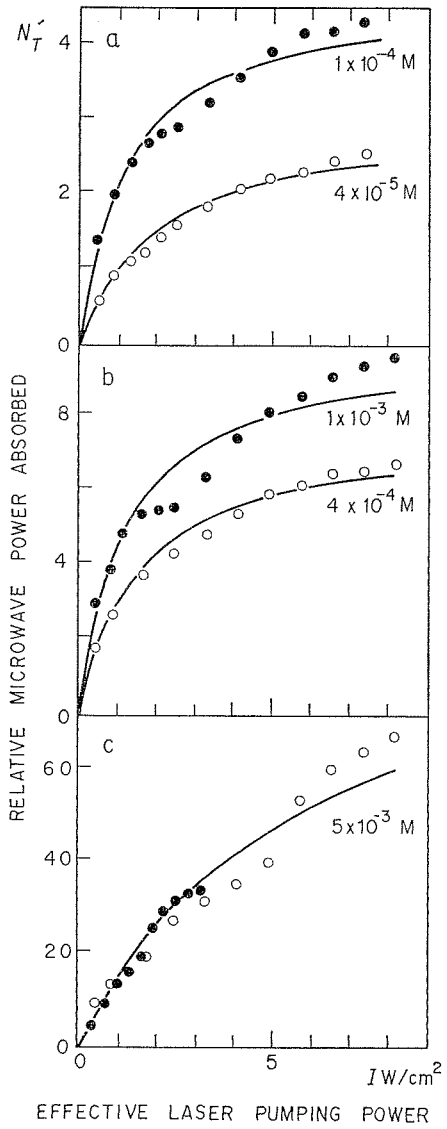

Fig. 3-1 Dependence of the relative intensities of the H_{min} lines of R6G molecules in the T_1 state on the effective laser pumping power. The a, b, and c show the optical saturation curves at 77 K for R6G concentrations 4×10^{-5} and 1×10^{-4} M, 4×10^{-4} and 1×10^{-3} M, and 5×10^{-3} M, respectively. Open and closed points in c represent the saturation curves for 5×10^{-3} M solution in 2.5- and 4.5- mm i.d. tubes, respectively. The curves calculated from a rate-equation analysis using values K_{ST} obtained in our method are shown by solid lines. Concentrations are values measured at room temperature.

is shown (the results for 2.5 and 4.5 mm i. d. tubes are corresponding to open and closed points in the figure, respectively). The curve hardly depends on the tube diameter. The pumping laser power was attenuated about 60 and 50% of the output power for the 2.5 and 4.5 mm i. d. tubes, respectiveiy, when the laser light reached the surface of the rigid solution. It is assumed that the laser beam diameter at the surface matches the diameter of the tube.

The triplet-state lifetime τ_T of the R6G molecule at 77 K are 1.7 ± 0.1 sec, which was determined from the decay curve of the $H_{\min}$ line after the cut-off of laser excitation[27]. The measurement and discussion of the triplet-state lifetime for different dye molecules will be in detail described in the next section.

For measuring fluorescence lifetimes at 77 K, the R6G-ethanol solution inserted in a liquid nitrogen Dewar was pumped by an Avco C950 pulsed N_2 gas laser operating at 3371 Å with the pulse width of about 5 nsec. After passing through an Optic Co. F-11-20 monochrometer, the decay of fluorescence of R6G molecules was detected by an RCA 8645 photomultiplier with the rise time of 1 nsec and was displayed on a Tektronix 7904 oscilloscope with the rise time of 500 psec. As a result the fluorescence lifetime τ_S of the molecule at 77 K was 8.3 ± 0.3 nsec[24].

Optical absorption spectra of 5×10^{-4} M R6G molecules in ethanol were measured at 77 K using a Cary Model 14 spectrometer with a sample-cell length of 0.1 cm. The result indicated that the singlet absorption cross section of the molecule at 5145 Å was 1.5×10^{-16} cm^2.

These lifetime and optical parameters of the molecule in ethanol at 77 K for calculation of an intersystem crossing rate constant are summarized in **Table 3-1**[24].

Table 3-1 Optical and lifetime parameters of R6G molecules in ethanol at 77 K used for calculation of K_{ST}.

Dye	ν_p sec^{-1}	τ_S nsec	τ_T sec	σ_p cm^2
R6G in EtOH	5.827×10^{14}	8.3 ± 0.3	1.7 ± 0.1	1.5×10^{-16}

3-4-3 Discussion

Now, we will determine the intersystem crossing rate constant K_{ST} of the R6G molecule at 77 K by obtaining the values of A and B from the saturation curve in **Fig. 3-1**, which are related to K_{ST} by Eq. (3-34). The variation of the reciprocal of the signal intensity of a $H_{\min}$ line versus the one of the effective pumping laser power is plotted in **Fig. 3-2** for the 4×10^{-5} M solution. The slope and intercept in the straight line give $A=0.688$ and $B=0.331$, respectively. Substituting these values and the measured values of the optical and lifetime parameters into Eq. (3-34), we can determine $K_{ST}=0.9\times10^5$ sec^{-1}. In much the same way the values of K_{ST} were determined for the solutions of different concentrations, which are given in **Table 3-2.** From the results we find that the average of their values K_{ST} is 1.1×10^5 sec^{-1}. The reason why the value K_{ST} in the case of the high concentration of 5×10^{-3} M is less than the lower concentration is

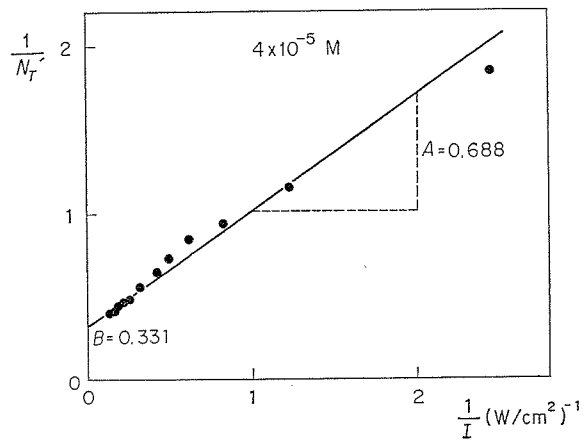

Fig. 3-2 The reciprocal of the relative triplet-concentration $1/N_T'$ as a function of $1/I$ in the case of the 4×10^{-5} M R6G rigid-solution.

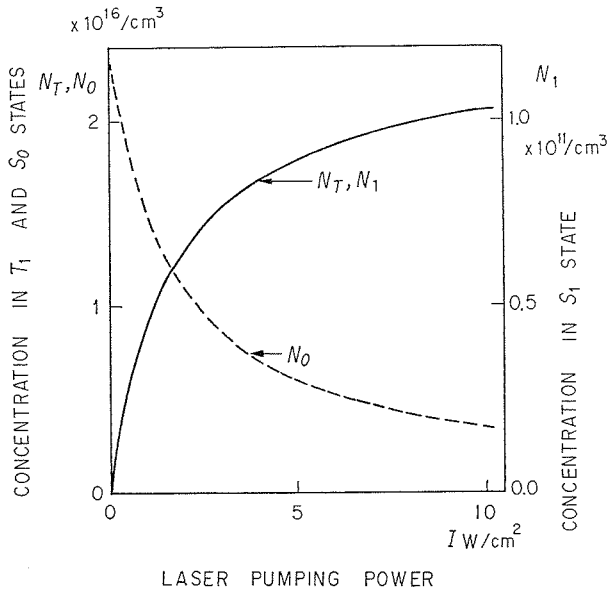

Fig. 3-3 Dependence of the concentration of R6G molecules in the T_1, S_1 (solid line), and S_0 (dotted line) states on the effective laser pumping power for the molecule in ethanol of 4×10^{-5} M concentration at 77 K.

Table 3-2 Intersystem crossing rate constants K_{ST} at 77 K obtained from R6G optical saturation curves for different concentrations.

N, M	4×10^{-5}	1×10^{-4}	4×10^{-4}	1×10^{-3}	5×10^{-3}
K_{ST}, sec^{-1}	0.9×10^5	1.6×10^5	1.1×10^5	1.5×10^5	0.3×10^5

probably that, as mentioned previously, the concentration is too high for all R6G molecules in an ethanol solution to be homogeneously excited by the laser light. The saturation curves calculated by substituting these values of K_{ST} into Eq. (3-32) are shown as solid lines in Fig. 3-1. Furthermore, the concentration in the T_1 state of R6G moleculees excited by a given laser power can be calculated by substituting these optical and lifetime parameters including the value of K_{ST} into Eq. (3-4), which is shown in **Fig. 3-3.** For example, the figure shows that at the pumping laser power of 8 W/cm² the molecules of 83 percent among the total ones are excited to T_1 state at 77 K. In spite that the dye molecule has the small S_1-T_1 energy separation ($\cong$4000 cm^{-1}) the value of K_{ST} is small. Also, the comparison of our value with that of $K_{ST}=3.4\times10^6$ sec^{-1} obtained at room temperature by Webb and his coworkers[103] indicates that the temperature dependence of the rate constant of the molecule is not so remarkable. These facts suggest that no higher triplet state exists between the S_1 and T_1 states of the molecule. For lack of informations available for different dyes we cannot discuss the relation between the molecular structure and the rate constant of laser dyes at present.

3-5 Lifetime Measurement and Quenching Experiment of the T_1 State

3-5-1 Experimental Procedures

As described in the chapter 2, the H_{min} line in the randomly oriented triplet states of dye molecules in rigid glassy and plastic solutions appears at the lowest magnetic field among several ESR absorption lines, and its intensity is proportional to the concentration of the molecules in the T_1 state. Therefore, the lifetime of the triplet state can be determined from the decay characteristics of the intensity of the H_{min} line after the cut-off of laser excitation.

Furthermore, quenching mechanisms in the T_1 state of a dye molecule by an additive molecule can be made clear by examining the variations of the peak-to-peak heights of the H_{min} line and of the triplet-state lifetimes versus the concentration of 1,3,5,7 cyclo-octatetraene (COT) molecules which are a typical triplet-state quencher of laser dyes. In that case the peak-to-peak height of the the H_{min} line is used in a first approximation to calculate the concentration of the dye molecule in the T_1 state.

The preparation of the sample solution is nearly identical to that described in the chapter 2. The COT obtained from Aldrich Chemical and Tokyo Kasei Kogyo Cos. was added as a quencher to a dye ethanol solution at a given concentration. The 5×5×2 mm plastic R6G in polymethylmethacrylate (PMMA) at 4×10^{-4} M concentration was offered by the Mitsubishi Electric Co[104].

The ESR spectrometer, the Ar ion laser, and the Dewar vessel used for observing the frequency-derivative spectrum of the H_{min} in dye molecules at 77 K were described in the chapter 2. After the cut-off of laser excitation, the decay curve of the derivative H_{min} line was recorded to determine the triplet-state lifetime. For some dyes possessing relatively short triplet-state lifetime, approximately 0.1 sec, the curve was recorded through

a PAR model 160 boxcar integrator which the out-put of the lock-in-amplifier of its spectrometer was connected into, with the use of an optical chopper and a triggering photodiode. In the case of the experiment on temperature dependences of the triplet-state lifetime and of the intensity of the H_{min} line, sample temperatures were regulated from 110 K to 240 K by a Varian cooled N_2 gas flow through system. The temperature increase of the sample due to the pumping laser light was calibrated against a Cu-constantan thermocouple. Optical absorption spectra of a COT-ethanol solution and of a COT added R6G-ethanol solution were measured by using the same spectrophotometer as that we have described in the section 3-4.

3-5-2 Experimental Results and Discussions

A. Triplet-state lifetimes[26,27]

Hitherto there has scarcely been any investigation on the relaxation processes of dye molecules in the T_1 state, which are of the utmost importance to dye lasers as pointed out in the section 3-1. It has been theoretically described in the sections 3-3-1 and 3-3-2 that three decaying processes are relevant to organic molecules in the T_1 state in a solvent and the reciprocal of the sum of the three decay constants is a triplet-state lifetime τ_T. One of those processes is the phosphorescence transition caused by spin-orbit coupling between the wavefunctions of the singlet and triplet states. Another is the nonradiative transition due to the intramolecular vibrational relaxation from the zero-point vibrational state of the T_1 state to isoenergitic vibrational states of the S_0 state. The rest is the intermolecular radiationless transition due to the solute-solvent collisional interaction affected directly by the temperature and the geometry of the solvent cage in which the bulkier molecule is situated.

A-1 Several dye molecules at 77 K

Triplet-state lifetimes obtained from the ESR signal decay curves, which are all exponential for ethanol or PMMA solvents[105], are given in **Table 3-3**. The values of lifetimes of AO and EY agree well with those already obtained[75,106]. The values nearly exist within the range 0.1~1 sec, which were theoretically estimated under the assumption that the wavefunction of ${}^3\Gamma_{\pi\pi^*}$ triplet state of dye moleculs containes equal admixture of singlet character to that of ${}^3\Gamma_{n\pi^*}$ triplet state due to spin-orbit interaction. And, they clearly differs according to the difference of the type of dyes molecule, increasing by a few times in the order of types F (FDS, DF, EY, and EB), R (AR, RS, RB, and R6G), and A (AO and AY). Therefore, the T_1 states of the three types of dyes are considered to contain different degrees of admixture of singlet character according to the chromophoric

Table 3-3 Triplet-state lifetimes (sec) of laser-dyes in ethanol at 77 K

DYES	R				F				A	
	AR	RS	RB	R6G	FDS	DF	EY	EB	AO	AY
τ_T	1.5	1.6	1.0	1.7	0.29	0.18	0.10	0.09	2.0	3.1

structure different among those types, which is produced by the difference in the strength of spin-orbit coupling among such types. Then the difference in the value of lifetimes among those types is possibly ascribed to the difference in the probability of radiative transition from the T_1 state to the S_0 state according to the difference of the types. Also, the fact that triplet-state lifetimes of type A of dyes are longer than those of the other types of dyes is possibly one of the reasons why cw laser oscillation is not yet realized in the former dye solutions unlike the latter dye solutions. Furthermore, the reason why EY and EB have the smallest values of lifetimes among the dyes examined is that the spin-orbit coupling is strengthened owing to the replacement of hydrogen atoms by heavy Br atoms in the chromophores. Namely, the internal heavy-atom effects in the chromophores are primarily caused by spin-vibronic interaction. The lifetime of RB is relatively short in comparison with those of other rhodamine dyes. This may be attributed to the above-mentioned third process, i. e., to the mobility of the diethyl-amino groups attached to the chromophore[14].

A-2 Temperature and solvent effects

Temperature dependences of the triplet-state lifetime and the relative intensity of microwave absoption due to ESR are shown in **Figs. 3-4** and **3-5**, respectively, for R6G molecules in ethanol or PMMA. These two dependences showed approximately the same changes with temperature. In the higher temperature region, however, the latter decreased more remarkably than the former with increasing the sample temperature. The reason is that the ESR signal intensity is reduced on account of the increase of microwave absorption losses in the solvent at high temperature. In the case of the ethanol solution, their temperature dependences in the case of the temperature decrease showed quite dif-

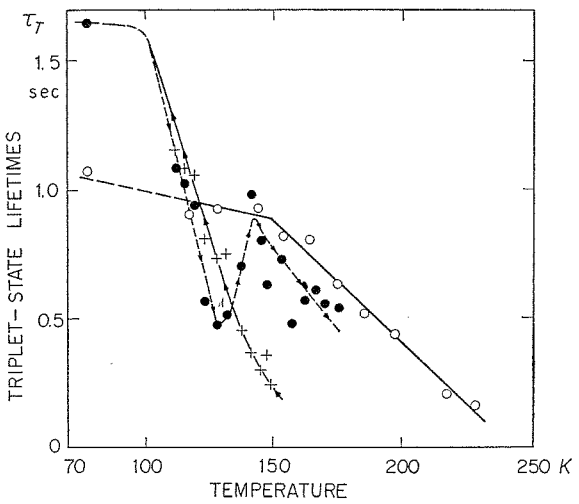

Fig. 3-4 Temperature dependence of the triplet-state lifetime of R6G molecules in ethanol (solid + and dotted ● lines correspond to the cases of temperature down and up, respectively) and PMMA (narrow solid ○ line).

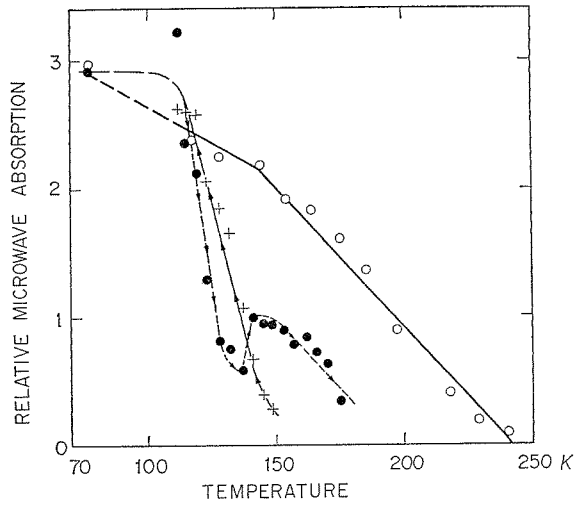

Fig. 3-5 Temperature dependences of the relative intensity of the H_{min} line of R6G molecules in ethanol and PMMA. The marks +, ●, and ○ correspond to those in Fig. 3-4.

ferent behaviors from those of the increase in the temperature region above 130 K. That is, when the temperature of the solution was decreased from 150 K, the lifetime τ_T increased according to the previously described Eq. (3-24), where $\tau_T^\circ = 1.70$ sec and the thermal activation energy ΔE_T was 1.0×10^3 sec^{-1}. The experimental errors of τ_T were about 15 percent. On the other hand, when the temperature was increased from 110 K, at first τ_T decreased. Then, τ_T began to increase near 130 K, reached the peak around 145 K, and again decreased with the further increase of the temperature. We consider that this difference is caused by the phase change of ethanol near 130 K from the glassy solution to the crystallization in the case of the temperature increase[75].

On the contrary, the triplet lifetime of R6G molecules in PMMA, behaved in the same manner for both cases of temperature up and down, varying relatively slowly as a function of temperature[62]. These provide a strong evidence of the dominant effect of solvent structure on the behavior of the triplet-state. We interpret that the relaxation from the T_1 state to the S_0 state of R6G molecules in an ethanol solution begins to significantly depend on the radiationless transition due to the solute-solvent interaction with the increase of the temperature. From the difference between the temperature effect on R6G molecules in ethanol and that in PMMA, we also suppose that the triplet-state lifetime in PMMA is still far longer than that in ethanol at room temperature. This effect is possibly one of the reasons why the threshold of the laser oscillation in plastic dyes is high in comparison with that in ethanolic dyes.

B. Triplet-state quenching by energy transfer to additive molecules[24]

COT molecules are known as a typical triplet-state quencher of laser dyes, but the quenching mechanism is not yet well understood. Then the effects of the COT molecular

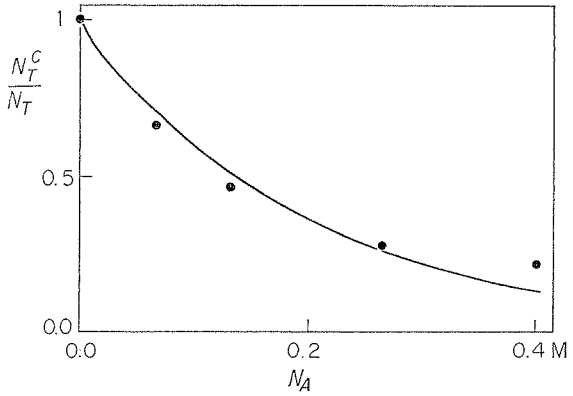

Fig. 3-6 Dependence on COT concentration N_A of the ratio of the R6G triplet-population at COT concentration N_A to that at zero COT concentration. The solid line is the curve calculated from Perrin's model. The COT concentrations are corrected for the shrinkage of the solution on freezing.

concentration on the signal intensity of the triplet-state ESR (H_{min} line) were examined at 77 K for 5×10^{-3} M R6G ethanolic solutions with different concentrations of COT molecules. The average values of the ratio of population of R6G molecules in the T_1 state at COT molecular concentration N_A to that at zero COT concentration are plotted as a function of N_A in **Fig. 3-6.** Population of the T_1 state decreased with the addition of COT molecules to the R6G solution and could not be detected at COT concentrations greater than 0.5 M. On the other hand, in spite of the addition of 0.3 M COT molecules to the solution, the triplet-state lifetime hardly changed at 77 K.

The fluorescence lifetime and singlet absorption cross section in the visible region of R6G molecules were independent of the concentration of COT molecules. From the measurements of the absorption spectra, we found that the absorption peaks of R6G and COT molecules lay at 5280 and 3620 Å, respectively, and the energy levels of the S_1 state of the latter molecule lay above that of the former.

As for this experimental results the concentrations measured at room temperature were always corrected for about 25 percent reduction in the volume of ethanol on freezing to 77 K[107].

From the fact that the concentration of R6G molecules in the T_1 state decreases exponentially with increasing the concentration of COT molecules at 77 K, as shown in Fig. 3-6, we find that COT molecules clearly play the role as a quencher of R6G molecules in the T_1 state. Since the energy of COT molecules in the S_1 state is greater than that of R6G molecules in the S_1 state, COT molecules cannot be directly excited to the S_1 state or the T_1 state by absorption of the pumping laser light at 5145 Å, which is satisfied the condition of Eq. (3-25). Then, the quenching of R6G molecules in the T_1 state is considered to be due to energy tranfer from the molecules in the T_1 state (donor) to COT molecules in the T_1 state (acceptor), where the energy level of the former T_1 state

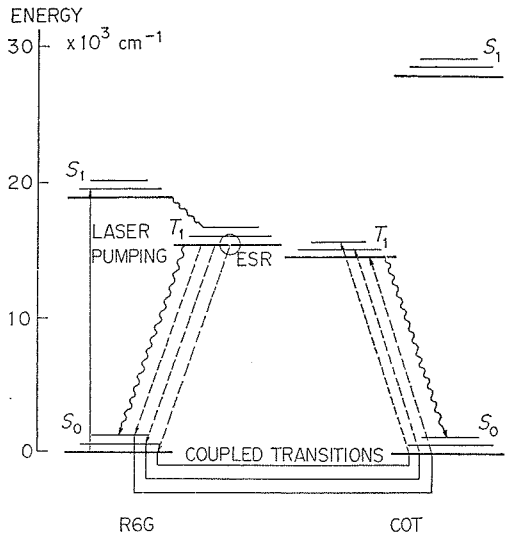

Fig. 3-7 Energy diagram for triplet-triplet excitation transfer in R6G-COT pair.

($E_{T_1}=15.3\times10^3\,cm^{-1}$) probably lies above that of the latter[20,108,109]. The occurrence of triplet-triplet energy transfer is described by Eq. (3-29), whose energy diagram for R6G-COT pair is given in **Fig. 3-7**. As pointed out in the section 3-3, triplet-triplet transfer in rigid media is considered to be due to an electron exchange mechanism on the basis of spin allowedness, long triplet-state lifetime of donor, and no diffusion in rigid media. The exchange mechanism occurs only when the donor in the T_1 state and the acceptor in the S_0 state are essentially in molecular contact. According to a model suggested by Perrin[49], the quenching of donor in the T_1 state obeys Eq. (3-29), where the radius of a quenching sphere R_0 depends only on the donor-acceptor pair but not on their concentrations. The experimental value of R_0 obtained from the plot in Fig. 3-6 is 13 Å, which agrees approximately with the order of the van der Waals dimensions of the molecule.

The donor lifetime in the rigid solution in our experiments hardly changed in spite of the increase of the acceptor concentration, in contrast to the case of fluid solutions at room temperature where the transfer rate constant depended noticeably on the rate of molecular diffusion, and a shortening of the lifetime apparently occurred[20]. The slight shortening of the mean lifetime may be ascribed to poor solubility and no diffusion of R6G-COT pair in the frozen ethanol solution[77,81].

3-6 Conclusin

The analysis of the rate equations for laser-dye molecules has shown that an intersystem crossing rate is determined directly from an optical saturation curve for the molecules in the T_1 state. Using a laser excitation ESR technique we experimentally obtained at 77 K

the saturation curve for R6G molecules, a typical laser dye, in ethanol of different concentrations. The results showed that the population of the molecules in the T_1 state at 77 K began to be saturated at an excitation power of about 1.5 w/cm^2, and that the intersystem crossing rate at 77 K was 1.1×10^5 sec^{-1}. This novel method for measuring directlly the intersystem crossing rate would be applied to any molecules only if relatively strong ESR spectra corresponding to the $\Delta M_S=\pm2$ transition in the T_1 state are observed.

The experimental result of triplet-state lifetimes of xanthene and acridine dyes in glassy ethanol solutions showed that the values of the lifetimes of each type of dyes differs according to the difference of the chromophoric structure of the dyes, increasing by a few times in the order of fluorescein (0.1～0.3 sec), rhodamine (1.0～1.7 sec), and acridine (2.0～3.1 sec) types. It was pointed out that the result possibly gives one of the reasons why cw laser operation is not yet realized in acridine dye solutions unlike xanthene dye solutions. Temperature dependences of triplet-state lifetimes of R6G molecules from 77 to 240 K indicated quite differet behaviors depending on the difference of the phase of solvents, glassy, crystal, and plastics, in which the molecules were dissolved. It was noted that the fact follows that the threshold of the laser oscillation in plastic dyes is high in comparison with that in ethanolic dyes. On the basis of the two experimental results concerning triplet-state lifetimes it was interpreted that the relaxation from the T_1 state to the S_0 state of R6G molecules in an ethanol solution mainly depends on the radiative transition due to the spin-orbit interaction near liquid nitrogen temperature, but with increasing temperature it begins to significantly depend on the radiationless transition due to the solute-solvent interaction. Furthermore, it was verified that the lifetimes of EB and EY dyes which were derivated from FDS dye by means of the replacement of four hydrogen atoms in the chromophore by Br atoms and NO_2 groups were shortened by the heavy atom effect in spin-orbit interactions.

The dependence of R6G molecules in the T_1 state on the concentration of COT molecules was monitored directly by an ESR technique during Ar ion laser excitation at 5145 Å. The result showed that the laser dye molecules in the T_1 state are clearly quenched by COT molecules at 77 K, and it was well explained in terms of triplet-triplet energy transfer by an electron exchange mechanism using Perrin's model.

Chapter 4 Laser Induced Photodegradation of Laser Dyes

It is necessary for preventing or diminishing the photodegradation of laser dyes and for increasing the lifetime of the laser to perform systematic studies in order to make clear photodegradation mechanisms in the laser dyes. In this chapter, a first laser irradiated ESR study on photodegradation in a rhodamine 6G (R6G) laser dye solution is described in detail. We first show that two kinds of different free radicals are induced in the solution by the irradiation of lasers with different wavelengths of UV and visible beams. The dependence of the radical concentration on the irradiation time and power, the effects of molecular structures of some laser dyes and solvents on the producing processes of radicales, and the role of dye molecules in the T_1 state are experimentally investigated. On the basis of those results the laser-induced reaction sequences in the cases of the UV laser irradiation and the visible laser irradiation are proposed. Finally, the rate-equation analysis for the photodegradation processes is presented by means of the reaction sequences, and the number of degradation molecules per absorbed photon is calculated from the decrease of dye molecules in the T_1 state after photodegradation.

4-1 Introduction

In the field of photochemistry it is known that organic dyes are a very important class of compounds which can usually undergo both oxidative and reductive processes, and hence many investigations were preformed to disclose the photochemical reaction processes by using steady-state irradiation or flash photolysis techniques.[8] Above all, Oster and his coworkers during their studies on the photodegradation of dyes in solution got convincing hints that the chemically reactive state in many photochemical reactions of dyes is a long-lived triplet state[111]. Soon afterwords, the epochmaking flash photolysis technique of Norrish and Porter gave this conclusion a direct evidence on the basis of the production of triplet state of dyes in solution by observation of triplet-triplet absorptions[12,110]. For example, for eosin and fluorescein disodium salt (=uranine) dyes in aqueous and ethanolic solutions with or without oxygen which were recently reported as laser active media[14], Koizumi and his coworkers investigated in detail the processes of the reductive photodegradation by observing changes in the absorption spectra and coefficients at room temperature after irradiation of a tungsten lamp or of one-pulse of a low-pressure argon flashlamp[111~116]. The results indicated that no degradation of xanthene dyes occurred in ethanolic solution in the presence of oxygen and in degassed agueous solution but it occurred in degassed ethanolic solution and in aqueous solution in the presence of oxygen. And for the reductive photodegradation of eosin the following reaction scheme was proposed,

$$S_0 \xrightarrow{h\nu_P} S_1 \xrightarrow{K_{ST}} T_1$$
$$\rightarrow T_1 + \mathrm{SolH} \rightarrow X \rightarrow \mathrm{DyeH}\cdot + \mathrm{Sol}\cdot \qquad (4\text{-}1)$$
$$\rightarrow 2\,\mathrm{DyeH}\cdot \rightarrow S_0 + \mathrm{DyeH_2},$$

and in the presence of air

$$X + O_2 \rightarrow S_0 + \mathrm{SolH} + O_2, \qquad (4\text{-}1)'$$

where S_0, S_1, and T_1 represent the ground singlet, the first excited singlet, and the first excited triplet states of eosin dyes, respectively, SolH is ethanol, DyeH· is a semiquinone radical of eosin, Sol· is a radical produced from ethanol, X is a molecular complex between triplet-state eosin and ethanol, and $\mathrm{DyeH_2}$ is a leuco compound of eosin. It appears that the validity of this proposal is now established.

It 1962 Smaller first applied an ESR technique, where free radicals and triplet-state molecules induced by excitation of a white light were detected directly at 77 K, to the investigation of photochemical reaction involving the triplet-state of an indole molecule in a methanolic rigid solution[117]. He suggested that the process is biphotonic, that is, the T_1 state of the solute is generated first; this is followed by a further excitation from the T_1 to the T_j states; energy is transferred from the T_j state of solute to a solvent molecule; this final localization of energy in the solvent causes bond rapture and produces radicals. Such ESR studies of sensitized solvent decomposition, after that, were performed for some polyacenes and their derivatives in organic solvents[118~121]. However, unfortunately no photochemical reaction occurring in alchohlic or aqueous solutions of rhodamine type of dyes had been ivestigated, till they were found to be typical good laser-materials[14].

Since Sorokin and Lankard successfuly obtained stimulated emission from an organic compound[3], several hundreds of organic laser-active materials have already been found[14]. The usefulness of the organic dye lasers are now amply demonstrated in a number of areas including spectroscopy, photochemistry, integrated optics, and isotopic separation by making use of some features of the lasers which have been described in the introduction of the previous chapter[4,122]. But it is also known that the performance is limitted not only by the metastable triplet state which has already been discussed, but also by photodegradation (which is also called photobleaching or photodeterioration) of the dye laser solution.

In 1971, a problem that photodegradation of rhodamine 6G (R6G) presents a severe limitation to the operation of nonflowing continuously excited dye lasers was first pointed out by Ippen and his coworkers[36]. They indicated that R6G molecules in ethanol, when optically pumped at 5145 Å and intensities required for laser threshold, had a usable lifetime of only 41 msec, and calculated the rate of degradation of the dye from change in extinction coefficient by continuous irradiation for 30 min. by an Ar ion laser operating at a laser power of 1 watt. In addition, as a result of extension of this type of investigation to several pH values, it was indicated that the adjustment of pH to minimize

potodegradation was useful for R6G in ethanol[123]. Recently, on the basis of the change in the fluorescence of R6G methanolic solution during the irradiation of a low-pressure mecury-argon discharge lamp with wavelength in the UV and visible region it was pointed out that oxygen dissolved in the solution made the degradation slow but the oxygen is soon spent in the photochemical reaction of methanol[124].

Weber showed that photodegradation of R6G in methanol and water by flashlamp-excitation induced a decrease of the quantum yield by fluorescence quenching and increases of the transmission at 5300 Å and of the laser-threshold energy, and calculated the number of degradation molecules from the change in the transmission by excitation with 80 pulses[6]. The smallest degradation rate was obtained by exciting without the UV (shorter than 3500 Å) light of the flashlamp. In addition, slight changes in the absorption spectrum of R6G in methanol after degradation by excitation with 60 pulses were obtained[37]. Also, the degradation rate of R6G in dimethylsulfoxide (DMSO) after pulse excitation was shown to depend on the triplet-state population by adding cyclooctatetraene (COT) molecules as a triplet-state quencher[38]. Recently, the photodegradation processes occurring in a flashlamp-pumped 7-diethylamino-4-methylcoumarin in ethanol were analyzed by using thin-layer chromatography which showed the presence of five compounds besides the original one[125].

As for plastic dyes in solid matrices, studies of R6G in polymethylmethacrylate (PM MA) using an Ar ion laser at 5145 Å or a pulsed frequency-doubled Nd YAG laser at 5310 Å indicated that cooling the matrix reduced photodegradation significantly[126]. As a result of the similar experiment for R6G in PMMA or epoxy resin it was shown that the degradation rate is linearly propotional to the intensity of incident radiation and the degradation is a one-photon process[127]. In addition, Reich and Neumann found that R6G dissolved in block-polymerized polyacrylonitrile has a smaller potodegradation rate at room temperature than in PMMA[126].

Thus several investigations of the photodegradation of the R6G solution, which is the most widely employed laser dye at the present time, have been carried out by observing changes in absorption and fluorescence spectra after optical excitation, but the reaction mechanism is not yet well understood systematically. Besides, the method for measuring optical spectra has some weak points that one is not able to detect directly the products after degradation and to monitor directly excited-state reactions. In this chapter we will make clear systematically the photodegradation mechanisms in an R6G ethanolic solution at 77 K by the first application of UV or visible laser-irradiation ESR methods which will overcome those weak points[39,40].

4-2 Application of a Laser Irradiation ESR Method to Photodegradation Investigation

4-2-1 Advantages and Procedure of the Method

As mentioned in the previous section, free radicals are produced in the processes of

photodegradation of an eosin molecule which belongs to the same class as an R6G molecule and is called xanthene class. In addition, Porter's group pointed out that any discussion of photochemical reactions in organic dyes involves the T_1 state[12,110]. Then we may infer from those facts that, in the photodegradation processes in the R6G which is the most popular laser dye, free radicals will be produced and the T_1 state will play the important role, too. In this chapter the photodegradation mechanism of the R6G laser dye in ethanol is investigated by a new method in which the behaviors of the laser-induced free radicals and dye molecules in the lowest excited triplet state (T_1 state) at 77 K are monitored directly, using an ESR technique during and after UV (3511+3638 Å) or visible (5145 Å) laser irradiations[41]. This method has the following advantages over the traditional methods measuring for optical spectra: 1) the dye molecules in the T_1 state and the free radicals produced photochemically after degradation are detected directly; 2) the sensitivity to detect the paramagnetic products induced by laser irradiations is much higher; 3) as a result of cooling the ethanolic dye solution to 77 K, the solution becomes glassy[27,75] and the products are stabilized at the irradiation point, trapped in the rigid glass. Furthermore, such studies on the laser-induced photochemical reaction will be performed very often in the future and will exert significant influence on the field of photochemical physics because of the high intensity, wide tunability and narrow spectral-width of the pumping laser light.

The preparation of the dye solution and the experimental arrangement are nearly identical to the one we have described in the chapters 2 and 3. Each dye was dissolved in ethanol, methanol, or dimethylsulfoxide (DMSO) at 1×10^{-3} M concentration. In order to determine the photodegradation mechanism easily, the oxygen-free solution outgassed by a freeze-thaw process, was sealed in a 4 mm-o.d. quartz tube. The peak-to-peak heights of the radical signal and of the $H_{\min}$ line corresponding to $\Delta M_S=\pm2$ transitions of dye molecules in the T_1 state, which were induced by laser light, were used in a first approximation to calculate the concentrations of the radicals and of the dye molecules in the T_1 state[24], respectively. The $H_{\min}$ line was recorded with an ESR spectrometer by using such a low power 5145-Å laser beam (0.29 W/cm^2) that no measurable amount of radicals occurred. The solution, cooled by inserting it into liquid nitrogen in a quartz Dewar, was irradiated by an unfocused beam consisting of UV (3511+3638 Å) light or 5145-Å light of an Ar ion laser (except for the acridine orange (AO) dye solution, which was irradiated by a 4880-Å beam). The transmittances of the quartz tube without a dye solution, which was inserted into the Dewar vessel containing liquid nitrogen, were measured for UV and 5145-Å laser beams. The results indicated the attenuations of the laser irradiation power due to the air, the liquid nitrogen, and the cylindrical quartz sheets of the Dewar vessel and the sample tube were about 35 and 45 percent, and the beam diameters were about 3.2 and 3.5 mm for the UV and 5145-Å laser beams, respectively.

4-2-2 Experimental Results and Interpretation

A. Observation of laser induced free radicals

In both cases -UV (3511+3638 Å) and 5145-Å laser irradiations to the R6G in an ethanol solution at 77 K - an ESR spectrum in the free-radical region was observed, which grew in intensity while the $\Delta M_S = \pm 2$ spectrum of the dye molecule in the T_1 state decreased in intensity. The spectral shape of the radical (denoted by FRI) which appeared in the dye solution during or after the UV laser irradiation for 8 min with 0.33 W/cm² power, was the same as that appearing during or after irradiation by a high pressure mercury lamp. But the shape of the FRI was quite different from that of the radical (denoted by FR2) which appeared during or after the 5145-Å laser irradiation for

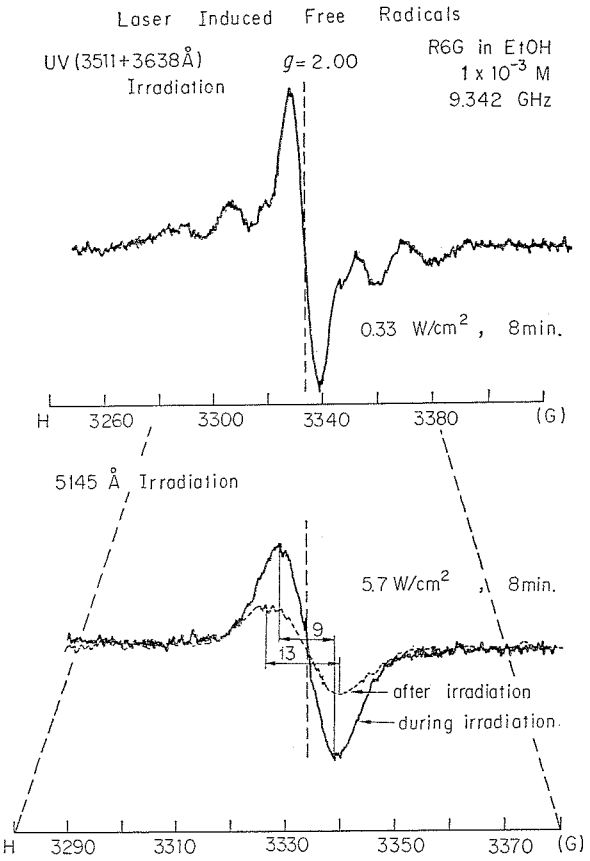

Fig. 4-1 Observed frequency-derivative ESR spectra of the free radical FR1 in a 1×10^{-3}M R6G-ethanol solution at 77K after UV laser irradiation (upper spectrum) and of the free radical FR2 during (solid line of the lower spectra) or after (dotted line of the lower ones) 5145-Å laser irradiation. The UV and 5145-Å laser irradiation time and power are 8 min. and 0.33 W/cm², and 8 min. and 5.7 W/cm², respectively.

8 min with 5.7 W/cm² power, as shown in **Fig. 4-1.** In the case of an Ar ion laser irradiation in the blue-green region (from 5145 to 4545 Å) with a shorter wavelength than 5145 Å, the same spectral shape as that of the FR 2 was always obtained. The ESR spectrum of the FR 1 obtained in the R6G-ethanol solution is quite good in comparison with that obtained in a hydrogen-peroxide ethanol solution by Gibson and his coworkers[129] using a photolysis method with a low peressure mercury lamp. They assigned the hyperfine pattern to the ethanol radical, $CH_3\dot{C}HOH$, formed by an α-hydrogen abstraction from ethanol. Therefore, the FR 1 spectrum appearing in the oxygen-free solution is considered to be due to the $CH_3\dot{C}HOH$ radical which arises by the abstraction of a hydrogen atom of an ethanol molecule by the laser-excited R6G molecule. On the other hand, the precise origin of the FR 2 radical induced by the 5145-Å laser irradiation cannot be stated at present. However, there seems to be no doubt that the radical depends on the chromophoric structure of the R6G dye, which will be mentioned subsequently.

B. Irradiation time dependence

For the cases of UV and 5145-Å laser irradiations to the R6G-ethanol solution, the dependence of the peak-to-peak heights of the radical and triplet signals on the increase of the repetation number of the irradiation using a constant time (2 min) and a constant power (0.53 W/cm² for UV and 3.4 W/cm² for 5145-Å) was examined. The spectra of the FR 1 or FR 2 with the corresponding wavelengths were first recorded, and afterwards

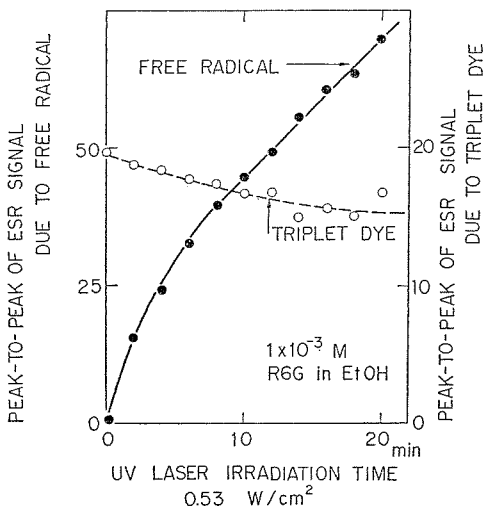

Fig. 4-2 Peak-to-peak heights of the FR 1 radical spectrum (symbol ●) induced after an UV laser irradiation and of the H_{min} line (symbol ○) in an R6G-ethanol solution versus the repetition number ($2 \times n$ min.) of the irradiation using a fixed power (0.53 W/cm²) for 2 min. The H_{min} line corresponding to $\Delta M_S = \pm 2$ transitions in the T_1 state was recorded during a 5145-Å laser irradiation such a low power (0.29 W/cm²) that no radical was produced.

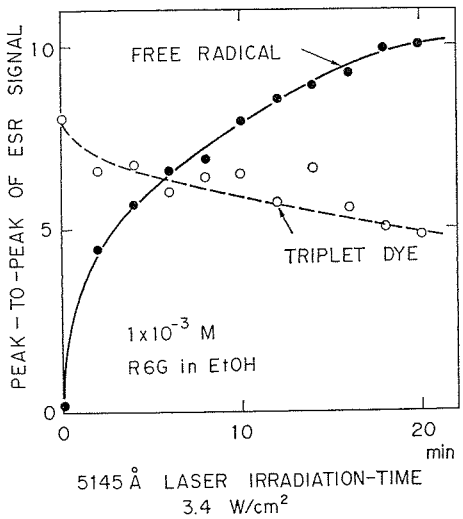

Fig. 4-3 Peak-to-peak heights of the FR2 radical spectrum induced after a 5145-Å laser irradiation and of the H_{min} line in an R6G-ethanol solution versus the repetition number ($2 \times n$ min.) of the irradiation using a fixed power (3.4 W/cm^2) for 2 min. The H_{min} line was recorded in the same way as in the case of Fig. 4-2. The symbols ● and ○ correspond to those in Fig. 4-2.

the H_{min} signal which was used to calculate the concentration of the dye molecules in the T_1 state was recorded during a 5145-Å laser irradiation with such a weak power that no FR2 could increase. From the results shown in **Figs. 4-2** and **4-3**, we find that the increase in the concentration of the radicals is correlative with the decrease in the concentration of dye molecules in the T_1 state in the cases of the FR1 and FR2. This is considered to be due to the following causes: 1) the shortening of the triplet-state lifetime is due to the paramagnetic interaction between the induced radicals and the dye molecules in the T_1 state; and 2) the decrease of the effective dye molecules is due to the change of its molecules into another compounds. But, on the basis of the experimental result that the triplet-state lifetime did not change significantly before and after UV or 5145-Å laser irradiations, it seems that the correlation between the increase of free radicals and the decrease of dye molecules in the T_1 state is mainly due to the last points.

C. Irradiation power dependence

The variation of the concenration of the radicals was examined by increasing the irradiation power with a constant time (2 min for UV and 5 min for 5145 Å). The dependences of the peak-to-peak heights of the FR1 and FR2 on the irradiation power are shown in **Fig. 4-4**. This figure shows that the curve of the FR1 induced by an UV laser irradiation increases with the square of the irradiation power, while that one of the FR2 induced by a 5145-Å laser irradiation starts to increase linearly and then begins

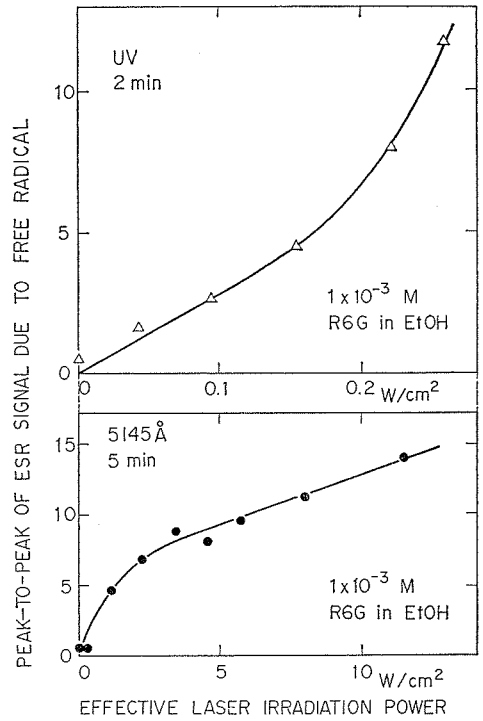

Fig. 4-4 Variation of the peak-to-peak heights of the FR1 and FR2 radical spectra induced in an R6G-ethanol solution after UV (upper curve) and 5145-Å (lower curve) laser irradiations as a function of the irradiation power for a constant time (2 and 5 min. for UV and 5145-Å laser irradiations, respectively).

to saturate with increasing the laser power. This saturation curve is similar to that of the concentration of dye molecules in the T_1 state depending on the pumping laser power[24]. Thus we can find that the FR1 and FR2 are produced by quite defferent optical processes, by two sequential single-photon absorptions including a T-T absorption and by a single-photon absorption, respectively. The fact that the T-T absorption is related to the producing process of the FR1 supports the foregoing assignment that the FR1 is a $CH_3\dot{C}HOH$ radical, because it is energetically sufficient to rupture the C-H bonds of ethanol by an energy transfer from the R6G molecules in a higher triplet state, which is produced by the stepwise single photon absorption or the T-T absorption of a dye molecule in the T_1 state, to ethanol molecules[117~121]. Furthermore, the comparison between the concentration dependence of the FR1 on the UV laser irradiation power and that of the FR2 on the 5145-Å laser irradiation power indicates that the FR1 is produced more easily by two orders of magnitude in the production rate per unit power and unit time. This corresponds to the experimental result that the smallest degradation rate of R6G in methanol at room temperature was obtained by exciting without the UV light (wavelengths shorter than 3500 Å) of a xenon flashlamp[6].

D. Dye molecular structure and organic solvent effects

In order to investigate more thoroughly the effect of dyes and organic solvents on the producing processes of free radicals, we recorded the ESR spectra of those radical occurring in dye-ethanol solutions for different dyes (R6G, RB, RS, AR, AO, and FDS) and occurring in R6G-organic solvents for different organic solvents (EtOH, MeOH, and DMSO). As shown in **Figs. 4-5** and **4-6**, the spectral shapes of the FR 1 induced by the UV laser irradiation depend remarkably on the molecular structure of the solvents but only a little on that of the laser dyes. This also supports the previously mentioned conclusion that the FR 1 is due to the solvent decomposition by the laser-excited dye molecule. On the other hand, the spectral shapes of the FR 2 induced by the 5145-Å laser irradiation (only

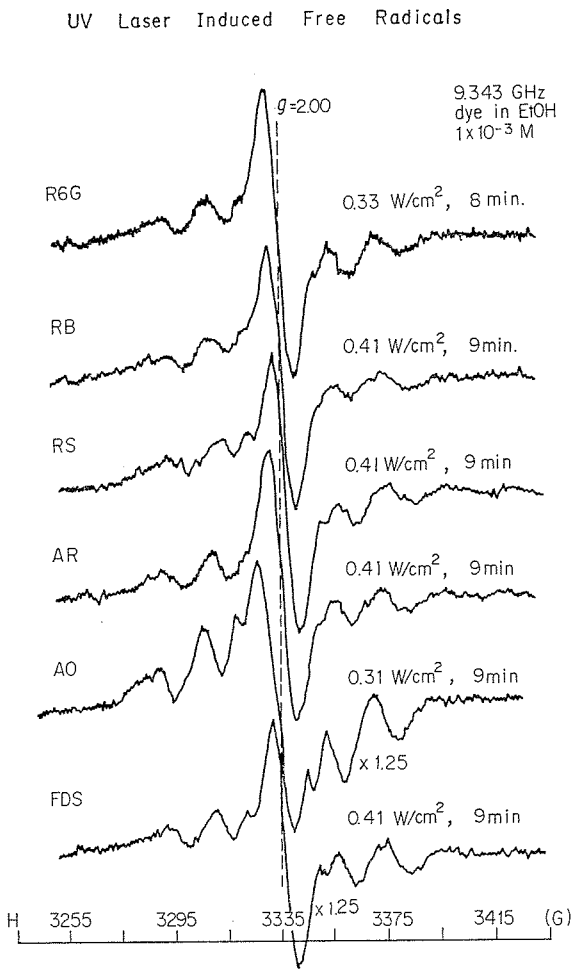

Fig. 4-5 Observed frequency-derivative ESR spectra of free radicals induced after an UV laser irradiation at 77K for different dyes dissolved in ethanol.

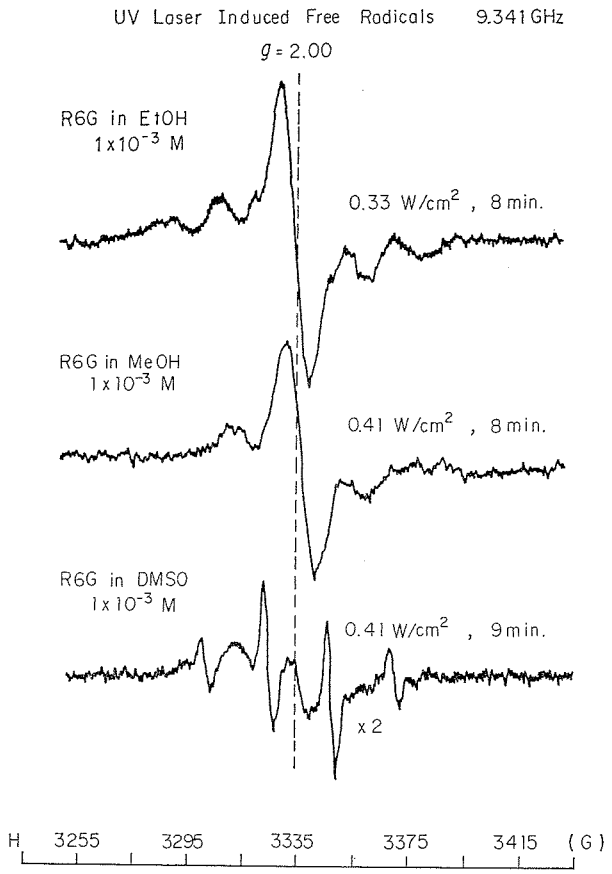

Fig. 4-6 Observed frequency-derivative ESR spectra of free radicals induced after an UV laser irradiation at 77 K for R6G in different solvents.

the AO dye solution was irradiated by a 4880-Å laser beam) depend more on the chromophoric structure of the dyes than on the molecular structure of the solvents, which is shown in **Figs. 4-7** and 4-8. In the case of the visible laser irradiation the FR2 radical spectra of the dye solutions differ in the half-width only if their chromophoric structure is different. All the radicals we obtained, however, have almost the same g-value of $g = 2.00$. It was also evident that the FR1 or the FR2 in the AO- and FDS- ethanol and in the R6G-dimethylsulfoxide solutions were easily induced compared with those radicals induced in the other dye-ethanol and R6G-solvent solutions, respectively. Furthermore, it was observed for all the examined dyes that the signal intensities of the FR2 after the cut-off of the irradiation rapidly decreased to constant intensities when we used the visible laser irradiation, while those of the FR1 using the UV laser irradiation did not change. The decay time of the signal intensities of the FR2 in the R6G-ethanol solution at 77K are about 1.0 sec, which is a little less than the triplet-state lifetime of the solution[26]. This suggests that the FR2 arises from a partially reversible change of a laser-excited dye molecule.

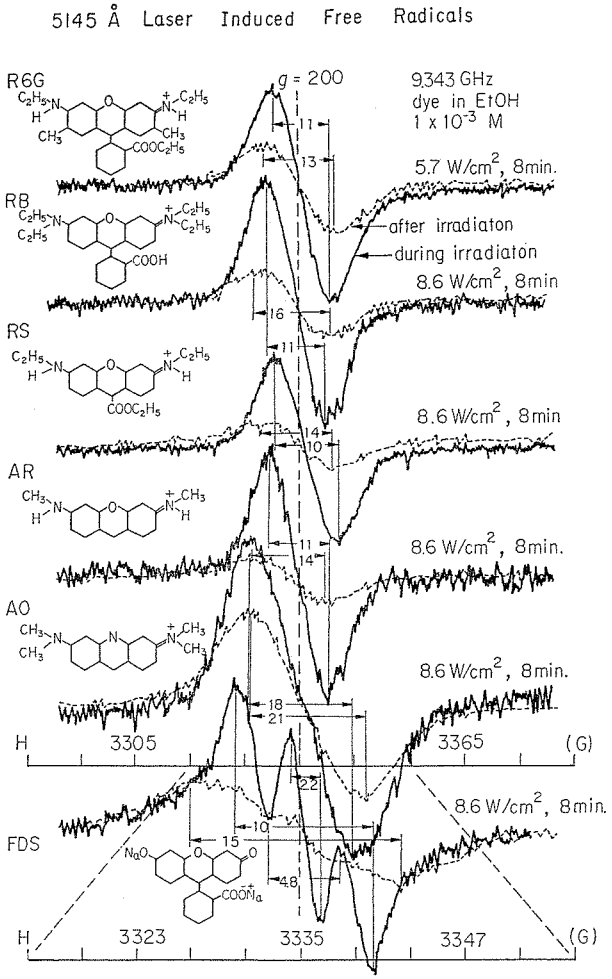

Fig. 4-7 Observed frequency-derivative ESR spectra of free radicals induced during (solid line) and after (dotted line) a 5145-Å laser irradiation at 77K for different dyes dissolved in ethanol. Spectral half-widths in gauss units and dye molecular structures are also noted.

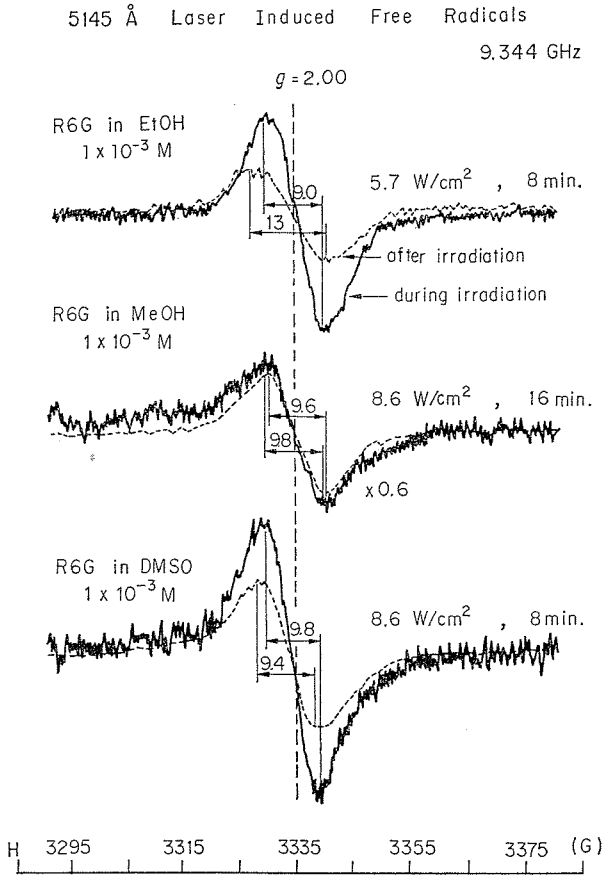

Fig. 4-8 Observed frequency-derivative ESR spectra of free radicals induced during (solid line) and after (dotted line) a 5145-Å laser irradiation at 77 K for R6G in different solvents. Spectral half-widths are again noted in gauss units.

E. Role of the T_1 state

Finally, in order to determine the connection of the amount of R6G molecules in the T_1 state with the producing processes of those radicals we examined the relation between the molecular concentration before the photochemical reaction and the radical concentration after the reaction for the R6G-ethanol solution, adding different amounts of a COT quencher. The results, which is shown in **Figs. 4-9** and **4-10**, is that the radical concentration (for the FR1 we got the same values during and after the UV laser irradiation and, for the FR2, different values during and after the 5145-Å laser irrcdiation) decreases as the concentration of the molecules in the T_1 state before the reaction decreases. This means that the molecules in the T_1 state have direct effects upon those two laser-induced chemical reactions, and corresponds to the already known fact that a small triplet-state population produces a small degradation rate of R6G in DMSO at room temperature under excitation of a xenon flashlamp without wavelengths shorter than 3200Å[38]. In particular, the FR2 appearing during or after the 5145-Å laser irradiation decreases even more rapidly than the decrease of the dye molecule in the T_1 state due to the quenching by an energy transfer to a COT molecule[24]. From this we conclude that the FR2, which depends on the chromophoric structure of the dye, is produced by a partially reversible change of one dye molecule in the T_1 state.

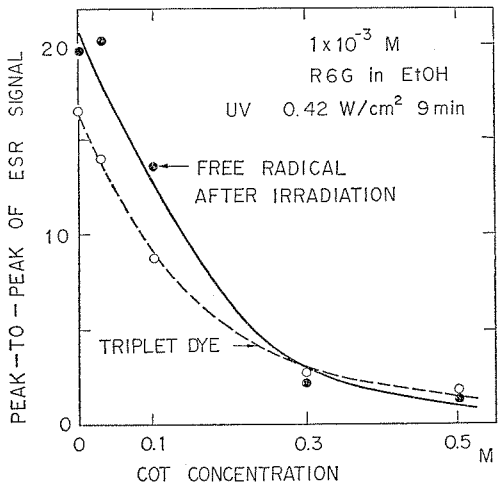

Fig. 4-9 Dependences of the peak-to-peak heights of the H_{min} line before the radicals occurred (symbol ○) and of the radical spectrum induced after an UV laser irradiation (symbol ●) on the COT concentration in an R6G-ethanol solution at 77K. The H_{min} line was in the same way as in the case of Fig. 4-2.

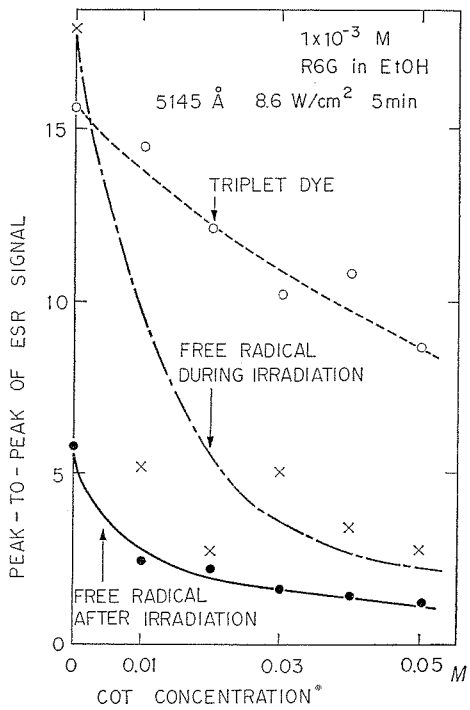

Fig. 4-10 Dependences of the peak-to-peak heights of the H_{min} line before the radicals occurred (symbol ○) and of the radical spectrum induced during (symbol ×) or after (symbol ●) a 5145-Å laser irradiation on the COT concentration in an R6G-ethanol solution at 77K. The H_{min} line was recorded in the same way as in the case of Fig. 4-2.

4-3 Photodegradation Mechanisms in Dye Laser Solutions

4-3-1 Reaction Schemes

Based on our considerations in the previous section, we find that the mechanisms of the photodegradation occurring in R6G-ethanol laser solutions at 77K are quite different for the two cases of UV and 5145-Å laser excitations, and the laser-induced photochemical reactions are explained in the following ways:

A) In the case of an UV laser irradiation including flashlamp excitation;

1) A few of the dye molecules excited to the S_1 state by the absorption of a photon decay to the T_1 state by an intersystem crossing process,
2) Some of them return to the S_0 state, but others absorb another photon to produce a higher excited triplet state (T-T absorption),
3) The C-H bonds of ethanol are ruptured by an energy transfer from a dye molecule in the higher triplet state to a solvent molecule, which results in the FR1 radical, and the dye molecule is finally reduced to a leuco compound[111~116]. That is, the molecule in the higher excited triplet state is reduced by ethanol and consequently

photodegradation of the dye occurs.

B) In the case of a 5145-Å laser irradiation;

1) Like A)-1), some dye molecules are excited to the T_1 state,

2) Except for decaying to the S_0 state, the dye molecule in the T_1 state changes into another radical, FR2, which is supposedly a semiquinone radical of the dye[111~116].

The schemes of the proposed reaction sequences in the two cases A) and B) are shown in **Fig. 4-11.** Then we consider that one of the most important procedures to increase the lifetime of R6G dye lasers is to use a triplet-quencher and an unreducible solvent. Finally, it should be pointed out that there are still some problems to be solved. Mainly, what is the exact nature of the second reaction, B), resulting in the FR2 radicals? But the informations necessary to answer this question are not yet available.

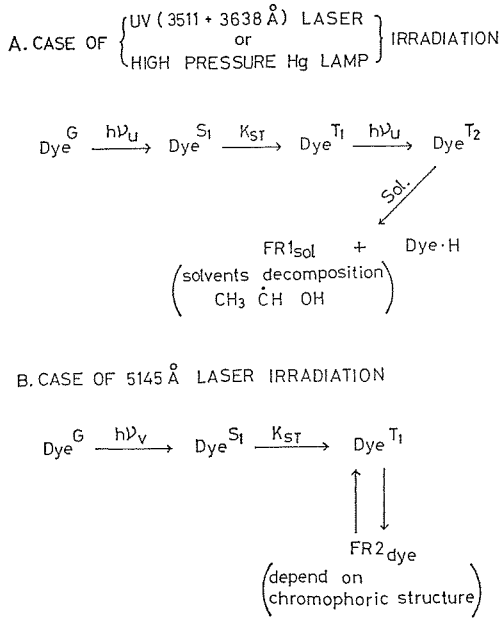

Fig. 4-11 Proposed photodegradation mechanisms occuring in a laser-dye solution under UV laser or flashlamp excitations (case A) and 5145-Å laser excitation (case B).

4-3-2 Reaction Kinetics and Quantum Efficiencies for Degradation

We will give the rate equations which describe the photodegradation processes of R6G molecules in ethanol by means of the reaction sequences proposed in the previous section. The behaviors of the S_1 state and some parts of the behaviors of the T_1 state can be described in the same manner as those of the rate equations presented in the chapter 2.

In the case of photochemical reactions under UV laser irradiation, the terms of a T-T absorption and of a quenching by COT molecules, and the terms of a T-T absorption and of the reaction due to energy-transfer from R6G molecules in the higher triplet state

to ethanol should be added for the T_1 state and the higher triplet state, respectively. The rate equations of each excited-state are related by Eqs. (4-2)

$$\begin{aligned}
\frac{dN_1}{dt} &= \frac{\sigma_P I}{h\nu_P} N_0 - \frac{N_1}{\tau_S} - K_{ST} N_1, \\
\frac{dN_T}{dt} &= K_{ST} N_1 - \frac{N_T}{\tau_T} - \frac{\sigma_T I}{h\nu_P} N_T + \frac{N_T{}^h}{\tau_T{}^h} - K_q N_A N_T, \\
\frac{dN_T{}^h}{dt} &= \frac{\sigma_T I}{h\nu_P} N_T - \frac{N_T{}^h}{\tau_T{}^h} - K_P{}^A n_S N_T{}^h,
\end{aligned} \tag{4-2}$$

where both photoreduction of the dye molecule by ethanol with a reaction rate constant $K_P{}^A$ and quenching by COT molecules (the concentration N_A) with a reaction rate constant $K_P{}^B$ are assumed to be second-order reaction[8], $N_T{}^h$ and $\tau_T{}^h$ represent the population and lifetime of the higher excited triplet state, respectively, and σ_T represents the cross section for the T-T absorption at UV wavelength. The total molecular concentration of the dye N is

$$N = N_0 + N_1 + N_T + N_T{}^h. \tag{4-3}$$

The producing rate of the free radical FR1 induced by the reaction between the dye and ethanol is given by

$$\frac{dn_{f1}}{dt} = K_P{}^A n_S N_T{}^h, \tag{4-4}$$

where n_{f1} and n_S represent the concentration of the FR1 and ethanol, respectively. We assume that the rate of attaining the steady-state concentration for each excited-state is fast compared with the rate of the photochemical reaction[8], which is possibly an adequate approximation for the results in its reaction. As a consequence of this steady-state approximation the reactive intermediates of excited states are treated as if they were in a steady state. Hence, the population of each exdited-state is constant during a uniform laser excitation :

$$\frac{dN_1}{dt} = \frac{dN_T}{dt} = \frac{dN_T{}^h}{dt} = 0. \tag{4-5}$$

By using Eqs. (4-2) and (4-3) under the condition of Eq. (4-5), Eq. (4-4) for the producing rate of the FR1 or the degradation rate of the R6G molecule becomes

$$\begin{aligned}
\frac{dn_{f1}}{dt} = K_P{}^A n_S K_{ST} N \sigma_T \sigma_P \left(\frac{I}{h\nu_P}\right)^2 \Big/ \Big\{ & \frac{1}{\tau_T{}^h}\left(\frac{1}{\tau_T} + K_q N_A\right) \\
& \times \left(\frac{\sigma_P I}{h\nu_P} + \frac{1}{\tau_S} + K_{ST}\right) + \left(K_P{}^A n_S + \frac{1}{\tau_T{}^h}\right) K_{ST} \frac{\sigma_P I}{h\nu_P} \\
& + K_P{}^A n_S \left(\frac{1}{\tau_T} + \frac{\sigma_T I}{h\nu_P} + K_q N_A\right)\left(\frac{\sigma_P I}{h\nu_P} + \frac{1}{\tau_S} + K_{ST}\right) \\
& + K_{ST}\left(\frac{I}{h\nu_P}\right)^2 \sigma_T \sigma_P \Big\}.
\end{aligned} \tag{4-6}$$

It may be assumed that the cross sections of the $S_0 \rightarrow S_1$ absorption σ_P and of the $T_1 \rightarrow$

T_2 absorption σ_T of an R6G molecule are almost equal to 10^{-17}cm^2 and 10^{-19}cm^2, respectively, under excitation by an UV laser light with wavelengths from 3511 Å to 3638 Å[30,37,96], and the relaxation from the higher excited triplet state to the T_1 state is very fast, e.g. $1/\tau_T{}^h \cong 10^{12}\,\mathrm{sec}^{-1}$ [10]. Then, from some parts of the data already presented in the section 3-4, each rate constant (sec^{-1}) in Eq. (4-6) at the pumping laser power $I \cong 0.1$ W/cm^2 is considered to have the value with the following order;

$$\frac{1}{\tau_T{}^h} \cong 10^{12} \gg \frac{1}{\tau_S} \cong 10^8 \gg K_{ST} \cong 10^5 \gg \frac{\sigma_P I}{h\nu_P} \cong 10^0 \cong \frac{1}{\tau_T} \cong 10^0 \gg \frac{\sigma_T I}{h\nu_P} \cong 10^{-2}. \tag{4-7}$$

Therefore, Eq. (4-6) can be approximately simplified

$$\frac{dn_{f_1}}{dt} = \frac{K_P{}^A n_S K_{ST} N \sigma_P \sigma_T \left(\frac{I}{h\nu_P}\right)^2}{\frac{1}{\tau_S}\left(K_P{}^A n_S + \frac{1}{\tau_T{}^h}\right)\left(\frac{1}{\tau_T} + K_q N_A\right)}. \tag{4-8}$$

This equation explains the experimental result that the free radical FR1 increases with the square of the UV laser irradiation power, which is shown in Fig. (4-4) of the previous section. Besides, the result shown in Fig. (4-9), that the concentration of the FR1 decreases with the increase of the concentration of COT quenchers is also explained well.

Next we will consider the case of photochemical reactions after 5145-Å laser irradiation. Taking account of the effects of a T-T absorption and of the decrease of the triplet-state population due to change of the dye molecule into the free radical FR2 and due to quenching by COT molecules, we obtain the following equations for population of each excited-state.

$$\begin{aligned}
\frac{dN_1}{dt} &= \frac{\sigma_P I}{h\nu_P} N_0 - \frac{N_1}{\tau_S} - K_{ST} N_1, \\
\frac{dN_T}{dt} &= K_{ST} N_1 - \frac{N_T}{\tau_T} - \frac{\sigma_T I}{h\nu_P} + \frac{N_T{}^h}{\tau_T{}^h} - K_P{}^B N_T - K_q N_A N_T, \\
\frac{dN_T{}^h}{dt} &= \frac{\sigma_T I}{h\nu_P} N_T - \frac{N_T{}^h}{\tau_T{}^h},
\end{aligned} \tag{4-9}$$

where the reaction order for changes of the dye molecule in the T_1 state with a reaction rate constant $K_P{}^B$ is assumed to be first, and the other notations at 5145 Å correspond to those in Eq. (4-2). In the same manner as in the case of the FR1 the producing rate of the free radical FR2 is given by

$$\frac{dn_{f_2}}{dt} = K_P{}^B N_T, \tag{4-10}$$

where n_{f_2} represents the concentration of the FR2. The assumption of the steady-state approximation for populations of the excited-state also enable us to obtain Eq. (4-5) under a uniform 5145-Å laser irradiation. It seems that, however, in the case of the 5145-Å laser irradiation this approximation can be applied to the equations for production of

the FR2 after the irradiation but it cannot be applied to those under a partially reversible reaction during the irradiation, because it is surmised that the order of the latter reaction rate is comparable to that of the T_1 state decay rate. Correspondingly to Eq. (4-6), Eq. (4-10) for the producing rate of the FR2 under the assumption becomes

$$\frac{dn_{f_2}}{dt}=K_P{}^B K_{ST}\frac{1}{\tau_T{}^h}N\frac{\sigma_P I}{h\nu_P}\Big/\left\{\frac{1}{\tau_T{}^h}\left(\frac{1}{\tau_T}+K_P{}^B+K_q N_A\right)\right.$$
$$\left.\times\left(\frac{\sigma_P I}{h\nu_P}+\frac{1}{\tau_S}+K_{ST}\right)+K_{ST}\frac{\sigma_P I}{h\nu_P}\left(\frac{1}{\tau_T{}^h}+\frac{\sigma_T I}{h\nu_P}\right)\right\} \tag{4-11}$$

From the data already presented in the section 3-4 under the 5145-Å laser excitation with the power of $I\cong 10\,\mathrm{W/cm^2}$, we find that each rate constant ($\mathrm{sec^{-1}}$) in Eq. (4-11) has the approximate value as follows;

$$\frac{1}{\tau_T{}^h}\cong 10^{12}\gg\frac{1}{\tau_S}\cong 10^8\gg K_{ST}\cong 10^5\gg\frac{\sigma_P I}{h\nu_P}\cong 10^3\gg\frac{1}{\tau_T}\cong 10^0\cong\frac{\sigma_T I}{h\nu_P}\cong 10^0. \tag{4-12}$$

Therefore, Eq. (4-11) for the producing rate of the FR2 can be approximately simplified

$$\frac{dn_{f_2}}{dt}=\frac{K_P{}^B K_{ST}N\dfrac{\sigma_P I}{h\nu_p}}{\dfrac{1}{\tau_S}\left(\dfrac{1}{\tau_T}+K_P{}^B+K_q N_A\right)+K_{ST}\dfrac{\sigma_P I}{h\nu_P}}. \tag{4-13}$$

This equation has the same form as Eq. (3-35) representing the population of the triplet state, except for the constants $K_P{}^B$ and $K_p N_A$. This corresponds to the experimentally obtained result shown in Fig. (4-4), that the concentration of the FR2 increases linearly and begins to be saturated with increasing the laser power like the dependence of the triplet-stats population on the pumping laser power. In addition, the Eq. (4-13) also explains qualitatively the concentration dependence of the FR2 on the concentration of COT quenchers, which is shown in Fig. (4-10) of the previous section. But the transient behaviors of the FR2 during and after the laser irradiation cannot be described by Eq. (4-13).

Finally, we will estimate quantum efficiencies B for degradation of the R6G molecule in ethanol at 77K, using the experimental result that the molecular concentration in the T_1 state decreases with increasing the laser irradiation time, which is shown in Figs. (4-3) and (4-4). From the change of $N_T{}^0-N_T{}^b$ in the molecular concentration of the T_1 state, and from the known total concentration M and volume SD and the total irradiation energy absorbed, a value is approximately calculated for the number of degradation molecules per absorbed photon, B,

$$B=\frac{N_T{}^0-N_T{}^b}{N_T{}^0}MN_{AV}\times 10^{-3}\times SD\Big/\frac{IST_i}{h\nu_P}, \tag{4-14}$$

where $N_T{}^0$ and $N_T{}^b$ represent the molecular concentration in the T_1 state before and after the laser irradiation with a time T_i at a power I, respectively, S is the irradiation area of the sample, D is the inner diameter of the sample tube which is about 0.22cm, and N_{AV} is an Avogadoro number. The average value of the number of degradation

molecules per absorbed photon under the UV laser irradiation and that under the 5145-Å laser irradiation are 42×10^{-6} and 9.7×10^{-6} for R6G dyes in ethanol at 77K, respectively. The latter value is almost equal to that (8.1×10^{-6}) obtained from the optical absorption changes in the same laser dye solution under a 5145-Å laser irradiation at room temperature[123]. Those two values mean that the R6G solution under the UV laser irradiation is photochemically degraded more easily than that under the 5145 Å laser irradiation[6]. In the calculation, the averaged frequency $\nu_P=8.39\times10^{14}$ Hz between the wavelengths 3511 and 3638 Å in the case of the UV laser irradiation was used, and the total molecular concentration measured at room temperature was corrected for about 25 percent reduction in the volume of ethanol on freezing to 77K[107]. The values of the quantum efficiency are higher for short time of the irradiation[128], and they are in the range from 2.1×10^{-5} to 6.6×10^{-5} molecules/photon and from 3.9×10^{-6} to 2.7×10^{-5} molecules/photon for the UV and 5145-Å laser irradiations, respectively.

4-4 Conclusions

Photodegradation mechanisms in an R6G laser dye in ethanol was systematically investigated by a new method where behaviors of laser-induced free radicals and dye molecules in the T_1 state at 77K were monitored directly using an ESR technique during and after UV (3511+3638Å) or visible (5145Å) laser irradiations. It was shown that the ESR spectral shape of the radicals induced by an UV laser beam is quite different from that of those induced by a 5145-Å laser beam and the former radicals were produced more easily by two orders of magnitude in the production rate. For those radicals the irradiation time and power dependences, the effects of dye and solvent molecular structures, and the role of the T_1 state by addition of COT quenchers were examined in some detail. As the result the two following laser-induced chemical reaction sequences were proposed: in UV laser- or flashlamp-pumped dye lasers, the *C-H* bond rupture of a solvent molecule due to the energy transfer of a dye molecnle in a higher triplet state excited by a *T-T* absorption of the dye molecule in the T_1 state, produces a radical and a leuco compound of the dye. On the other hand, in the case of the 5145-Å laser excitation, a partially reversible change of a dye molecule in the T_1 state by only a one-photon absorption produces another radical which depends on the chromophoric structure of the dye. On the basis of this proposal it was pointed out that one of the important procedures to increase the lifetime of R6G dye lasers is to use an efficient triplet-state quencher and an unreducible solvent.

Furthermore, under the steady-state approximation the rate-equation analysis for photodegradation processes in the dye laser solution was carried out by means of the reaction schemes with some rate constants experimentally obtained in the previous chapter. Equations deriven from the analysis well explained qualitatively the experimental results of the dependences of the concentration of the induced free radicals on the irradiation power and on the added amount of COT quenchers in both cases UV and 5145-Å laser

irradiations. Quantum efficiencies for the degradation were estimated from the decrease of R6G molecules in the T_1 state with increasing the irradiation time. The results indicated that photodegradation numbers for the R6G dye in ethanol at 77K are 42×10^{-6} and 7.9×10^{-6} molecules/photon for UV and visible laser irradiations, respectively.

Chapter 5 Summary and Conclusion

Recently organic dye lasers are widely utilized as a very important tunable source in the fields of isotopic separation, photochemistry, high-resolution spectroscopy, and so on. The performance of the laser, however, is limited by the accumulation of dye molecules in the T_1 state and the photodegradation of the dye laser solution. In order to select out or synthesize good laser dyes with a low triplet-yield and high photochemical-stability, the relation between the molecular structure and the properties of the T_1 state or the photodegradation mechanisms should be made clear. On the other hand, it is known that the T_1 state of dye molecules plays an important role to many kinds of photochemical reactions essential to most forms of life. Therefore, the investigation on behaviors of the molecules in the T_1 state is needed for the elucidation of detail mechanisms of the reactions. In particular, the determination of the intersystem crossing rate is the key to evaluate the molecular concentration in the T_1 state from which most of the photochemical reactions start to occur.

In this study it has been demonstrated that a first laser excited ESR technique enables us to reveal magnetic properties, relaxation and quenching mechanisms in the T_1 state, and processes of two kinds of photochemical reactions in the rhodamine (type R), fluorescein (type F), and acridine (type A) types of laser dye solutions, by utilizing several advantages of its technique. Furthermore, a novel method for determining the intersystem crossing rate of organic molecules with high luminescence and low triplet-yield at 77K has been established.

In Chapter 2, the randomly oriented triplet-state ESR spectra including weak signal such as of $\Delta M_S = \pm 1$ transitons and microwave-two-photon absorption have been observed for types R, F, and A of ten dyes in rigid glass. The observation has shown that the triplet ESR spectra depend not on the total molecular structure of the dyes but on only the chrmophoric structure, and hence the principal values of a π-electron spin-spin dipole interaction tensor and the ZFS parameters also do so. That is, the values of the ZFS parameter D and of its root-mean-square D^* increase in the order of type R, A, and F. Also, resonance magnetic fields $F(H, h\nu)$ have been calculated, from which one can know the positions of all the ESR spectra appearing in the T_1 state. For the $\Delta M_S = \pm 1$ transitions in FDS and AO dyes a further experiment on the magnetophotoselection has been carried out under laser excitation with a linearly polarized beam. It has been found that the principal molecular axes of the spin interaction tensor coincide with the chromophoric structural axes, one another, and those $\Delta M_S = \pm 1$ ESR spectra have been assigned. In addition, the polarizations of the π-electron distribution in the T_1 state and of the electric dipole transition moment to S_1 state have been discussed. It is concluded that π-electrons in the chromophore of type F dyes are the most unsymmetrically distributed and polarized along the long X axis but the delocalization of π-electrons is the

smallest among the three types of dyes, those of type A dyes are the most symmetrically distributed and those delocalization is larger than that of type F dyes, and those of type R dyes are the most broadly distributed in the X-Y plane and those delocalization is the largest.

In Chapter 3, we have determined the intersystem crossing rate of an R6G laser dye in ethanol with different concentrations (from 4×10^{-5} to 5×10^{-3} M) using a new method. The principle is based on the direct observation on the optical saturation of dye molecules in the T_1 state at 77 K during laser excitation at 5145 Å. The result has shown that population of the molecules in the T_1 state begins to be saturated at an excitation power of about 1.5 W/cm^2, and concequently the intersystem crossing rate is 1.1×10^5 sec^{-1}. This method will be applied to any organic molecules only if a relatively strong $H_{\min}$ line is observed. Substitution of the obtained value of the rate into the equation derived from the rate-equation analysis allows also the calculation of the absolute concentration of R6G molecules excited to the T_1 state by a given laser power. The concentration curve is necessary for not only the evaluation of dye-laser operating losses related to the T_1 state but also that of the other rate constants for the complex photochemical processes.

We have measured the triplet-state lifetime from the decay of the $H_{\min}$ line after the cut-off of laser excitation for different laser dyes, solvent phases (glass, crystal, or plastic), or under the variation of temperature (from 77 to 240 K). In glassy solutions, the value of the triplet-state lifetime of each type of dyes differs by the difference of the chromophoric structure of the dyes, increasing by a few time in the order of type F (0.1 ~0.3 sec), R (1.0~1.7 sec), and A (2.0~3.1 sec). This fact gives possibly one of the reasons why cw laser operation is not yet realized in acridine dye solutions unlike rhodamine and fluorescein dye solutions. Also, triplet-state lifetimes of R6G molecules have indicated quite different temperature-dependences according to the difference of the solvent phases in which the molecules are dissolved. It follows from this fact that the threshold of the laser oscillation in plastic dyes with a much longer triplet-state lifetime is higher than that in ethanolic dyes. Those two experimental results concerning triplet-state lifetimes enable us to conclude that the triplet-to-singlet relaxation ($T_1\rightarrow S_0$) of the three types of dyes in ethanol depends mainly on the radiative transition due to the spin-orbit interaction between π-electrons near liquid nitrogen temperature, but with increasing temperature it begins to depend significantly on the radiationless transition due to the solute-solvent interaction. In addition, the heavy atom effect predicted by the theory of the radiative transition has been verified by the following result. That is, the triplet-state lifetime of FDS dye is longer by three times than that of EB or EY dyes which are derivated from the former dye by means of replacement of hydrogen atoms by Br atoms in the chromophore.

The relative number of R6G molecules excited to the T_1 state by a 5145-Å laser beam has been obtained as a function of the concentration of COT molecules from the intensity variation of the $H_{\min}$ line. The result has shown that the laser dye molecules in the T_1 state are clearly quenched by COT molecules at 77 K, and it has been well

explained in terms of triplet-triplet energy transfer by an electron exchange mechanism using Perrin's model.

In Chapter 4, photodegradation mechanisms in an R6G laser dye in ethanol has been investigated systematically by a method where both laser-induced free radicals produced by the degradation and dye molecules in the T_1 state at 77 K have been monitored directly by using an ESR technique during and after UV (3511+3638 Å) or visible (5145 Å) laser irradiations. It has been found that the ESR spectral shape of the radicals induced by an UV laser beam is quite different from that of those induced by a 5145-Å laser beam and the former radicals were more easily produced. For those radicals the irradiation time and power dependences, the effects of dye and solvent molecular structures, and the role of the T_1 state have been studied in some detail. From the results we have proposed two different laser-induced chemical recation sequences, photoreduction by the solvent and intramolecular reaction, which are dependent on the wavelength of the irradiation beam. That is, in UV laser- or flashlamp-pumped dye laser, the C-H bond rupture of a solvent molecule by the energy transfer of a dye molecule excited from the T_1 state to a higher triplet state by a T-T absorption produces a radical due to the decomposition of the solvent and a leuco compound of the dye. On the other hand, in the case of the 5145-Å laser excitation, a partially reversible change of a dye molecule in the T_1 state excited only by a one-photon absorption produces another radical which depends on the chromophoric structure of the dye. On the basis of this proposal it has been pointed out that one of the important procedures to increase the lifetime of the R6G dye laser is to use an efficient triplet-state quencher and an unreducible solvent.

Furthermore, the rate-equation analysis for the photodegradation processes with the steady-state approximation has been performed by using some relaxation-rates experimentally obtained in Chapter 3. Equations derived from the analysis allow a qualitative explanation of the concentration dependences of the induced free radicals on the irradiation power and on the added amount of COT quenchers for both UV and 5145-Å laser irradiations. Quantum efficiencies for the degradation have been calculated from the decrease of R6G molecules in the T_1 state with increasing the irradiation time. Consequently, it has been indicated that photodegradation numbers of the R6G dye in ethanol at 77 K are 42×10^{-6} and 7.9×10^{-6} molecules/photon for UV and visible laser irradiations, respectively.

Finally we enumerate some possible extensions of this study;

(1) Applications of the laser excited ESR technique to determination of the intersystem crossing rate and the quantum efficiency for photodegradation of other laser dyes and important biomolecules such as chlorophyll, protein, and nucleic acids[9,50].

(2) Investigation on the effect of wavelengths of pumping lights on the producing rate and spectral shape of free radicals induced in an interesting molecule when a tunable dye laser is used as a pumping source. That is, study of laser-controlled chemical reaction.

(3) Possibility of triplet-state ESR during dye laser action in such solvents with a small microwave-absorption loss as vapor, crystal, or plastic.

Acknowledgements

The author would like to express his sincere gratitude to Dr. Kenjiro Sakurai, Chief of Radio- and Opto-Electronics Division, and Dr. Hiroshi Kashiwagi, Chief of Laser Research Section, for their continuous encouragement and support in this work. He extends equal thanks and appreciation to Professor Toru Ogawa of Kyoto University, who provided pertinent guidance and invaluable help in the structure of this manuscript.

The author wishes to express his gratitude to Mr. Takuzo Sato, Senior Research Scientist of Laser Research Section, for his many discussions and experimental advices. He is also very grateful to Assistant Professor Tsutomu Yabuzaki of Kyoto University for his careful reading of the manuscript.

A number of valuable discussions with all the staff members of Laser Research Section are also acknowledged with many thanks.

The author thanks Miss Noriko Kobayashi and Mrs. Hama Oshina for their enthusiastic cooperation in preparing this manuscript.

References

1) Maiman, T.H., Nature 187, 493 (1960), and Phys. Rev. Letters **4**, 564 (1960).
2) DeMaria, A.J. and Whitehouse, D.R., "1975 Conference on Laser Engineering and Applications, Washington D.C.", IEEE J. Quantum Electron. **QE-11**, No. 9 (1975).
3) Sorokin, P.P. and Lankard, J.R., IBM J. Res. Develop. **10**, 162 (1966).
4) Hänsch, T.W., in "Dye Lasers", Schäfer, F.P. Ed., Springer-Verlag, Berlin, 1973, p. 194.
5) Keller, R.A., IEEE J. Quantum Electron. **QE-6**, 411 (1970).
6) Weber, J., Phys. Letters **37A**. 179 (1971).
7) Gregg, D.W. and Thomas, S.J., IEEE J. Quantum Electron. **QE-5**, 302 (1969).
8) Meier, H., in "The Chemistry of Synthetic Dyes", K. Venkataraman, Ed., Academic Press, New York, N.Y. 1971, Vol. 4, p. 389.
9) Lhoste, J.M., Helene, C. and Ptak, M., in "The Triplet State", Zahlan, A.B. Ed., Cambridge Univ. Press, 1967, p. 479.
10) Birks, J.B., "Photophysics of Aromatic Molecules", John Wiley & Sons Ltd., New York, N.Y. 1970.
11) Oster, G., Sci. Am. **219**, 158 (1968).
12) Porter, G., Science **160**, 1299 (1968).
13) Turro, N.J., "Molecular Photochemistry", W.A. Benjamin, New York, N.Y. 1967.
14) Drexhage, K.H., in "Dye Lasers", Schäfer, F.P. Ed., Springer-Verlag, Berlin, 1973, p. 144.
15) Maeda, M. and Miyazoe, Y., Japan J. Appl. Phys. **11**, 692 (1972).
16) Maeda, M. and Miyazoe, Y., Japan J. Appl. Phys. **13**, 827 (1974).
17) Pavlopoulos, T.G., IEEE J. Quantum Electron. **QE-9**, 510 (1973).
18) Kuhn, H., Fortschr. Chem. Org. Naturstoffe **16**, 169 (1958).
19) Kuhn, H., Fortschr. Chem. Org. Naturstoffe **17**, 404 (1959).
20) Marling, J.B., Ph.D. Thesis, University of California, 1971.
21) Berlman, I.S., "Handbook of Fluorescence Spectra of Aromatic Molecules", Academic Press, New York, N.Y. 1971.
22) MaGlynn, S.P., Azumi, T. and Kinoshita, M., "Molecular Spectroscopy of the Triplet State", Prentice-Hall, Englewood Cliffs, N.J. 1969.
23) Hermann, J.P. and Ducuing, J., Opt. Commun. **6**, 101 (1972).
24) Yamashita, M. and Kashiwagi, H., J. Phys. Chem. **78**, 2006 (1974).
25) Yamashita, M. and Kashiwagi, H., "VIII. Int. Quant. Electro. Conf., San Francisco, California, 1974", IEEE J. Quantum Electron. **QE-10**, 770 (1974).
26) Yamashita, M., Ikeda, H. and Kashiwagi, H., J. Chem. Phys. **63**, 1127 (1975).
27) Yamashita, M. and Kashiwagi, H., Japan J. Appl. Phys. **14**, 421 (1975).
28) Schäfer, F.P., in "Dye Lasers", Schäfer, F.P. Ed. Springer-Verlag, Berlin, 1973, p. 1.

29) Snavely, B.B., Proc. of IEEE. **57**, 1374 (1969).
30) Buettner, A.V., Snavely, B.B. and Peterson, O.G., in "Molecular Luminescencs", Lim, E.C. Ed. W.A. Benjamin, New York, N.Y., 1969, p. 403.
31) Peterson, O.G., McColgin, W.C. and Eberly, J.H., Phys. Letters **29 A**, 399 (1969).
32) Furumoto, W.H. and Ceccon, H.L., IEEE I. Quantum Electron. **QE-6**, 262 (1970).
33) Sorokin, P.P., Lankard, J.R., Moruzzi, and Hammond, E.C., J. Chem. Phys. **48**, 4726 (1968).
34) Snavely, B.B. and Schäfer, F.P., Phys. Letters **28 A**, 728 (1969).
35) Pappalardo, R., Samelson, H. and Lampicki, A., Appl. Phys. Letters **16**, 267 (1970).
36) Ippen, E.P., Shank, C.V. and Dienes, A., IEEE J. Quantum Electron. **QE-7**, 178 (1971).
37) Beer, D. and Weber, J., Opt. Commun. **5**, 307 (1973).
38) Weber, J., Opt. Commun. **7**, 420 (1973).
39) Yamashita, M., Ikeda, H. and Kashiwagi, H., "1975 Conference on Laser Engineering and Applications, Washington D.C.", IEEE J. Quantum Electron. **QE-11**, No. 9, 3D (1975).
40) Yamashita M. and Kashiwagi, H., to be published in IEEE J. Quantum Electron. **QE-12**, No. 2 Part II (1976).
41) Yamashita, M. and Kashiwagi, H., J. Chem. Phys. **59**, 2156 (1973).
42) Kottis, P. and Lefebvre, R., J. Chem. Phys. **39**, 393 (1963).
43) Kottis, P. and Lefebvre, R., J. Chem. Phys. **41**, 379 (1964).
44) Kottis, P. and Lefebvre, R., J. Chem. Phys. **41**, 3660 (1964).
45) Siegel, S. and Judeikis, H.S., J. Phys. Chem. **70**, 2205 (1966).
46) Hameka, H.F., "Advanced Quantum Chemistry", Addison-Wesley Publishing Co. Massachusetts, 1965.
47) Siebrand, W., J. Chem. Phys. **47**, 2411 (1967).
48) Siebrand, W., in "The Triplet Stete", Zahlan, A.B., Cambridge Univ. Press, 1967, p. 31.
49) Perrin, F., Acad, C.R., Sci. Paris **178**, 1978 (1924).
50) Gueron, M., Shulman, R.G. and Eisinger, J., in "The Triplet State", Zahlan, A.B. Ed., Cambridge Univ. Press, 1967, p. 505.
51) Hutchison, C.A. and Mangum, B.W., J. Chem. Phys. **29**, 952 (1958), and **34**, 908 (1961).
52) van der Waals J.H. and de Groot, M.S., Mol. Phys. **2**, 333 (1959) and **3**, 190 (1960).
53) Yarger, W.A., Wasserman, E. and Cramer, R.M.S., J. Chem. Phys. **37**, 1148 (1962).
54) de Groot, M.S. and van der Waals, J.H., Physica **29**, 1128 (1963).
55) Boorstein, S.A. and Gouterman, M., J. Chem. Phys. **39**, 2443 (1963).
56) El-Sayed, M.A. and Siegel, S., J. Chem. Phys. **44**, 1416 (1966).
57) Lhoste, J.M., Haug, A. and Ptak, M., J. Chem. Phys. **44**, 654 (1966).
58) Antonucci, F.R. and Tolley, L.G., J. Phys. Chem. **77**, 2712 (1973).
59) Thomson, C., Quart. Rev. **122**, 45 (1968).
60) Heisenberg, W.Z., Physik **39**, 499 (1926).

61) Hameka, H.F. and Oosterhoff, L.J., Mol. Phys. **1**, 358 (1958).
62) Thomson, C., J. Chem. Phys. **41**, 1 (1964).
63) Jablonski, A., Z. Physik **94**, 38 (1935).
64) Terenin, A., Acta Physicochim. URSS, **18**, 210 (1943).
65) Terenin, A., Zh. Fiz. Khim. **18**, 1 (1944).
66) Lewis, G. and Kasha, M., J. Am. Chem. Soc. **66**, 2100 (1944).
67) Lewis, G. and Calvin, M., J. Am. Chem. Soc. **67**, 1232 (1945).
68) Lewis, G., Calvin, M. and Kasha, M., J. Chem. Phys. **17**, 804 (1949).
69) McClure, D., J. Chem. Phys. **17**, 905 (1949).
70) Hutchison, C.A. and Mangun, B.W., J. Chem. Phys. **32**, 1261 (1960).
71) Gouterman, M., J. Chem. Phys. **36**, 2846 (1962).
72) Robinson, G.W. and Frosch, R.P., J. Chem. Phys. **37**, 1962 (1962).
73) Robinson, G.W. and Frosch, R.P., J. Chem. Phys. **38**, 1187 (1963).
74) Siebrand, W., J. Chem. Phys. **46**, 440 (1967).
75) Berg, R.A. and Ron, A., J. Chem. Phys. **59**, 3289 (1973).
76) Terenin, A. and Ermolaev, V., Dokl. Akad. Nauk. SSSR. **85**, 547 (1952).
77) Terenin, A. and Ermolaev, V., Trans. Faraday Soc. **52**, 1042 (1956).
78) Förster, T., Discussions Faraday Soc. **27**, 7 (1959).
79) Förster, T., "Fluoreszenz Organishe Verbindungen", Vandenhoek and Ruprecht, Göttingen, 1951.
80) Dexter, D.L., J. Chem. Phys. **21**, 836 (1953).
81) Inokuti, M. and Hirayama, F., J. Chem. Phys. **43**, 1978 (1965).
82) Bowers, P.G. and Porter, G.' Proc. Roy. Soc. **A 299**, 348 (1967).
83) Nemoto, M., Kokubun, H. and Koizumi, M., Bull. Chem. Soc. Japan **42**, 1223 (1969).
84) Horrocks, A.R., Kearvell, A., Tickle, K. and Wilkinson, F., Trans. Faraday Soc. **62**, 3393 (1966).
85) Lamola, A.A. and Hammond, G.S., J. Chem. Phys. **43**, 2129 (1965).
86) Stevens, B. and Algar, B.E., Chem. Phys. Letters **1**, 219 (1967).
87) Parker, C.A. and Joyce, T.A., Chem. Comm., p. 108 and 234 (1966).
88) Brinen, J.S., J. Chem. Phys. **49**, 586 (1968).
89) Schäfer, F.P., Schmidt, W. and Marth, K. Phys. Letters **24 A**, 280 (1967).
90) Marling, J.B., Gregg, D.W. and Wood, L.L., Appl. Phys. Letters **17**, 527 (1970).
91) Peterson, O.G., Tuccio, S.A. and Snavely, B.B., Appl. Phys. Letters **17**, 245 (1970).
92) Glenn, W.H., Brienza, M.J. and DeMaria, A.J., Appl. Phys. Letter **12**, 54 (1968).
93) Schmidt, W. and Schäfer, F.P., Phys. Letters **26 A**, 558 (1968).
94) Wu, F.Y., Grove, R.E. and Ezekiel, S., Appl. Phys. Letters **25**, 73 (1974).
95) Schank, C.V. and Ippen, E.P., Appl. Phys. Letters **24**, 273 (1974).
96) Tuccio, S.A. and Strome, Jr. F.C., Appl. Opt. **11**, 64 (1972).
97) Hameka, H.F., in "The Triplet State", Zahlan, A.B. Ed., Cambridge Univ. Press, 1967, p. 1.
98) Slater, I.C., "Quantum Theory of Atnmic Structure", McGraw-Hill, New York, N.Y.

1960, Vol. II.
99) Clementi, E., J. Mol. Spectry. **6**, 497 (1961).
100) Birks, J.B. and Munro, I.H., in "Progress in Reaction Kinetics", Poter, G. Ed., Pergamon Press, Oxford, 1967, p. 239.
101) Kilmer, N.G. and Spangler, J.D., J. Chem. Phys. **54**, 604 (1971).
102) Smaller, B., Avery, E.C. and Remko, J.R., J. Chem. Phys. **43**, 922 (1965).
103) Webb, J.P., McCogin, W.C., Peterson, O.G., Stockman, D.L. and Eberly, J.H., J. Chem. Phys. **53**, 4227 (1970).
104) Ito, K., Kusakawa, H. and Takahashi, K., Oyo Butsuri **39**, 1067 (1970), [in Japanese].
105) Siegel, S. and Judeikis, H.S., J. Chem. Phys. **42**, 3060 (1965).
106) Parker, C.A., in "Advances Photochemistry", John Wiley & Sons Ltd., New York, N.Y. 1964, Vol. 2, p. 305.
107) Handbook, A.I.P., Coordinating 3rd ed., Gray, D.E. Ed., McGraw-Hill, New York, N.Y., 1972.
108) Drake, J.M., Thesis, Ph.D., Clark Uninersity, 1973.
109) Tanaka, I. and Okuda, M., J. Chem. Phys. **22**, 1780 (1954).
110) Porter, G. and Windsor, M.W., Nature **180**, 187 (1957).
111) Imamura, M. and Koizumi, M., Bull. Chem. Soc. Japan **28**, 117 (1955).
112) Imamura, M. and Koizumi, M., Bull. Chem. Soc. Japan **29**, 899 (1956).
113) Imamura, M. and Koizumi, M., Bull. Chem. Soc. Japan **29**, 913 (1956).
114) Uchida, K., Kato, S. and Koizumi, M., Bull. Chem. Soc. Japan **33**, 169 (1960).
115) Kato, S., Watanabe, T., Nagaki, S. and Koizumi, M., Bull. Chem. Soc. Japan **33**, 263 (1960).
116) Uchida, K., Kato, S. and Koizumi, M., Bull. Chem. Soc. Japan **35**, 16 (1962).
117) Smaller, B., Nature **195**, 593 (1962).
118) Siegel, S. and Eisenthal, K., J. Chem. Phys. **42**, 2949 (1965).
119) Judeikis, H.S. and Siegel, S., J. Chem. Phys. **43**, 3625 and 3638 (1965).
120) Terenin, A., Pylkov, V. and Kholmogorov, V., Photochem. Photobiol. **5**, 543 (1966).
121) Shimokoshi, K., Mori, Y. and Tanaka, I., Bull. Chem. Soc. Japan **40**, 302 (1967).
122) Tuccio, S.A., Dubrin, J.W., Peterson, O.G. and Snavely, B.B., IEEE J. Quantum Electron. **QE-10**, 796 (1974).
123) Britt, A.D. and Moniz, W.B., IEEE J. Quantum Electron. **QE-8**, 913 (1972).
124) Kato, D. and Sugimura, A., Opt. Commun. **10**, 327 (1974).
125) Winters, B.H., Mandelberg, H.I. and Mohr, W.B., Appl. Phys. Letters **25**, 723 (1974).
126) Fork, R.L. and Kaplan, Z., Appl. Phys. Letters **20**, 472 (1972).
127) Kaminow, I.P., Stulz, L.W., Chandross, E.A. and Pryde, C.A., Appl. Opt. **11**, 1563 (1972).
128) Reich, S. and Neumann, G., Adpl. Phys. Letters **25**, 119 (1974).
129) Gibson, J.F., Symons, M.C.R. and Townsend, M.G., J. Chem. Soc., 269 (1959).